RESPIRATORY MUSCLE OVERLOAD TRAINING AND DIAPHRAGM REMODELING

By

BARBARA KELLERMAN SMITH

A DISSERTATION PRESENTED TO THE GRADUATE SCHOOL
OF THE UNIVERSITY OF FLORIDA IN PARTIAL FULFILLMENT
OF THE REQUIREMENTS FOR THE DEGREE OF
DOCTOR OF PHILOSOPHY

UNIVERSITY OF FLORIDA

2010

To Gram

ACKNOWLEDGMENTS

This journey could not have begun without the assistance of my wonderful family, friends, and mentors. I thank my husband Brian and family for their immeasurable love, support and guidance. I sincerely appreciate the ongoing support of my doctoral committee, consisting of Drs. Paul Davenport, Orit Shechtman, Krista Vandenborne and chaired by Dr. Danny Martin, and value their patience and wisdom. Dr. Davenport personifies the enthusiasm of a scientist moved by the joy of discovery and continually motivates me. Dr. Shechtman's contributions to the exercise physiology background of my studies have been invaluable to me, and I appreciate her thoughtful questions and kindness. I admire Dr. Vandenborne's constructive suggestions for improving the design of this project as well as her vast wisdom and assistance with future planning. I cannot imagine a finer model of the clinician-scientist than Dr. Martin, and will always be grateful to him for his many years of support, patience and compassion. I am especially thankful to the patients who inspired my research pursuits and provide continued motivation to further the body of knowledge in cardiopulmonary rehabilitation.

Doctoral studies were supported by a research assistantship (January-July 2007, R01HD42705) and training fellowship (August 2007-August 2010 T32HD043730) from the National Institutes of Health. The author gratefully acknowledges the Foundation for Physical Therapy for their Promotion of Doctoral Studies (PODS I and II) awards, co-co-sponsored by the Cardiovascular and Pulmonary Section, APTA and endowed in honor of Scot C. Irwin, DPT, CCS, an educator, advocate, and true pioneer in cardiopulmonary physical therapy. Mentorship training and laboratory supplies were provided through the Group Advantaged Training of Research program, co-sponsored through University of Florida and Howard Hughes Medical Institute. Psalm 150:6.

TABLE OF CONTENTS

page

LIST OF TABLES

LIST OF FIGURES

LIST OF ABBREVIATIONS

A_A	Area fraction
C_{dyn}	Dynamic compliance
COPD	Chronic obstructive pulmonary disease
CPAP	Continuous positive airway pressure
CSA	Cross-sectional area
dP/dt	Rate of pressure development
FRC	Functional residual capacity
HR	Heart rate
IAA	Interrupted aortic arch
IGF-1	Insulin-like growth factor-1
IMST	Inspiratory muscle strength training
IMV	Intermittent mandatory ventilation
MAP	Mean arterial pressure
maxRPD	Maximal rate of pressure development
MHC	Myosin heavy chain
MIP	Maximal inspiratory pressure
MRF	Myogenic regulatory factor
MV	Mechanical ventilation
OCCL	Occlusion training
PBS	Phosphate-buffered saline
$PEEP_i$	Intrinsic positive end-expiratory pressure
PVR	Pulmonary vascular resistance
R_{awdyn}	Dynamic airway resistance (inspiratory or expiratory)
RIPA	Radio immunoprecipitation assay

RR	Respiratory rate
SBT	Spontaneous breathing trial
SDS-PAGE	Sodium dodecyl sufate polyacrylamide gel electrophoresis
SHAM	Sham training
SpO_2	Pulse oximetry saturation of oxygen
TA	Truncus arteriosus
TTI	Tension-time index
V_E	Minute ventilation
VIDD	Ventilator-induced diaphragm dysfunction
VSD	Ventricular septal defect
V_T	Tidal volume
ZAP	Zone of apposition

Abstract of Dissertation Presented to the Graduate School
of the University of Florida in Partial Fulfillment of the
Requirements for the Degree of Doctor of Philosophy

RESPIRATORY MUSCLE OVERLOAD TRAINING AND DIAPHRAGM FIBER REMODELING

By

Barbara Kellerman Smith

August 2010

Chair: Anatole D. Martin
Major: Rehabilitation Science

It is well-known that the diaphragm undergoes rapid atrophy and contractile dysfunction with inactivity, but the effect of overload training on the respiratory muscle pump is less understood. We investigated whether overload training produced by intermittent tracheal occlusion facilitated muscle fiber hypertrophy and regeneration, or whether the loads induced damage. Twelve animals underwent placement of a tracheal cuff and were randomly assigned to receive either ten sessions of brief occlusions (n=6, OCCL) or observation (n=6, SHAM). After the intervention, the costal diaphragm, third parasternal intercostal, and soleus muscles were examined for fiber morphology, myosin heavy chain isoform composition and cross-sectional area, and presence of embryonic myosin. In the OCCL animals, type IIx/b fibers were 27% larger in the medial costal diaphragm ($p<.05$) and 22% larger in the intercostals ($p<.01$). A modest yet significant increase in embryonic myosin occurred in the intercostals of OCCL animals ($p<.05$). These results indicate that tracheal occlusion may facilitate rapid, preferential type II fiber hypertrophy in the respiratory muscle pump. Additional study is suggested to determine whether the training offers a performance benefit.

CHAPTER 1
SPECIFIC AIMS

Mechanical ventilation (MV) is a medical therapy used to sustain alveolar ventilation and rest the inspiratory muscles of patients with respiratory failure. Paradoxically, this life-saving therapy can induce severe weakness and atrophy of the diaphragm, referred to as ventilator-induced diaphragm dysfunction (VIDD). While the median duration of MV is approximately 4 days, VIDD can make it progressively difficult to discontinue the use of MV, termed weaning. Nearly 20 percent of mechanically-ventilated adults will experience difficulty with weaning (1). In addition, 5 to 10% of ventilated patients develop chronic ventilator dependence (2). Because prolonged MV is associated with disproportionate healthcare costs and high mortality (3, 4), it is imperative to understand the mechanisms responsible for preventing or treating VIDD.

Animal studies have repeatedly demonstrated that MV elicits rapid diaphragm fiber dysfunction (5-9). Significant diaphragm atrophy occurs within six hours of controlled MV in small mammals, and contractile dysfunction increases in a dose-time response (10, 11). The inactive human diaphragm can also atrophy within three days of controlled MV (12). Less is known about respiratory responses to increased activity and rehabilitation. Inspiratory muscle strength training (IMST) has shown promise to prevent or reverse the effects of VIDD. A recent randomized, controlled clinical trial from our laboratory demonstrated that IMST increased maximal inspiratory pressure (MIP) and facilitated ventilator weaning in MV-dependent adults (13). Inspiratory exercises may promote intercostal muscle fiber hypertrophy in adults with chronic obstructive pulmonary disease (COPD), in conjunction with increased strength (14). It is unknown whether overload training can elicit significant diaphragm muscle fiber hypertrophy.

Animal models show that chronic respiratory loading increases slow fiber size and phenotype expression in the diaphragm, but the intense, prolonged loads also elicit significant muscle damage (15-17). However, the previous loading models did not resemble the intermittent, moderate loads used for rehabilitation. We employed a novel model of tracheal occlusion to transiently overload the respiratory pump. The overall objective of following experiments was to investigate whether tracheal occlusion elicits positive respiratory muscle fiber remodeling, including hypertrophy, or whether the overload generates fiber damage. The projects were designed to achieve the following specific aims.

Specific Aim #1: *To determine whether intermittent tracheal occlusion generates hypertrophy and phenotype remodeling of inspiratory muscle fibers.*

Sub-aim 1a: *To determine whether the fiber cross-sectional area of the diaphragm and third intercostal muscles differs in animals that receive tracheal occlusion.*

Sub-aim 1b: *To determine whether the expression of myosin heavy chain isoforms differs in the diaphragm and intercostal muscles of animals that undergo tracheal occlusion.*

Rationale: It has been suggested that the highly active respiratory muscles may be more susceptible to disuse atrophy (5, 18). Alternatively, mechanical loading activates protein synthesis and regeneration, and upregulates diaphragm myosin heavy chain (MHC) mRNA expression within hours (19). In the costal diaphragm, the baseline regional fiber composition is similar. It is not known whether occlusion training modifies the regional fiber size or phenotype of the diaphragm, due to varied biomechanics.

Hypothesis: The fiber cross-sectional area will be significantly greater in the medial costal diaphragm and intercostal muscles of animals that undergo ten sessions of tracheal occlusion, without evidence of a shift in MHC phenotype composition.

Specific Aim #2: To determine whether transient tracheal occlusion induces muscle fiber damage and regeneration in the respiratory muscles.

Sub-aim #2a: To determine whether cellular remodeling is more prevalent in the diaphragm and intercostal muscles of animals that receive tracheal occlusion.

Sub-aim #2b: To determine whether diaphragm expression of embryonic myosin heavy chain is greater in the respiratory muscles of occlusion-trained animals.

Rationale: Sustained overload produces diffuse injury to the diaphragm and intercostal muscles (20). However, intermittent occlusion could induce less secondary inflammation than prior models that imposed a constant load (21). The reports in the literature differ regarding regional costal diaphragm damage. The medial region undergoes the greatest shortening with ventilation and therefore may be more susceptible to remodeling (22).

Hypothesis: Respiratory muscle regeneration will significantly increase in animals that undergo ten sessions of tracheal occlusion, without a significant presence of damage in the respiratory muscles or costal diaphragm regions.

The following experiments were designed to increase the current understanding of respiratory strength training and muscle remodeling. Translational applications will be discussed in a case report of clinical inspiratory occlusion training. It is hoped that these findings will help advance our understanding of respiratory muscle plasticity, in order to promote motor recovery of the ventilatory muscle pump and facilitate ventilator weaning.

CHAPTER 2
REVIEW OF LITERATURE

The Respiratory Pump Generates the Work of Breathing

The Diaphragm Muscle

Ventilation is the passage of air from the atmosphere into the alveoli of the lungs, and represents the first step to supply oxygen to body tissues. The thin, elliptically-shaped diaphragm is the primary muscle of the inspiratory pump. This muscular membrane spans the internal diameter of the ribcage and separates the thoracic and abdominal body compartments. The diaphragm muscle consists of costal and crural segments which are thought to assume divergent secondary functions due to differences in muscular architecture. The bony origins of the costal diaphragm include the xiphoid process and the seventh through twelfth ribs and costal cartilages. The crural diaphragm arises from the transverse processes of the first three lumbar vertebrae, and this region contains a larger number of muscle spindles (23). Crural fibers differ from costal fibers in both anatomy and function. The crural diaphragm can act as an accessory esophageal sphincter and exerts considerable influence on non-ventilatory maneuvers such as coughing and emesis (24). Its non-ventilatory physiological functions are distinct from the costal diaphragm, despite similar timing of motor unit activation during inhalation (24, 25). The larger costal segment accounts for approximately 80% of the weight of diaphragm. Its greater oxidative capacity and mobile anatomical origins reflect the primary ventilatory function of the costal diaphragm (26).

The diaphragm is capped by a centrally-located tendon, which gives the muscle a dome-shaped appearance and acts as the muscular insertion for both the costal and crural segments. The fibers of the costal diaphragm fan out circumferentially around the

inner portion of the thoracic cage. The stiffness of the central tendon is much greater than that of muscle tissue (27), and thus muscular contraction results in a flattening of the diaphragm muscle tissue, similar to the movement of a piston. Because of the closed architecture of the thoracic cavity, fiber orientation can differ considerably at different regions of the costal diaphragm and influence the efficiency of contracting fibers. At its bony attachments, the crural diaphragm contractile forces yield no direct motion of the vertebral column. On the other hand, the costal diaphragm interacts with the thoracic cage at the zone of apposition, and the abdominal contents act as a fulcrum. Coordinated diaphragm contraction results in a decrease in intrathoracic pressure, descent of the abdominal contents accompanied by a rise in abdominal pressure, and expansion of the ribcage.

The architecture of the thoracic cage, fiber length, and fiber orientation differ between regions of the costal diaphragm, but regional myosin heavy chain (MHC) isoform proportions do not appear to vary (28). The diaphragm bears a mixed fiber composition, reflective of both its continuous ventilatory function and its intermittent roles in vocalization, expulsion, and protective reflexes. Sieck reported that the rodent diaphragm contains ~37% type I slow, oxidative fibers, 30% type IIa fast, oxidative fibers, 25% type IIx fast, intermediate fibers, and approximately 8% type IIb fast, fatigable fibers (29). Although 86% of rat diaphragm fibers express a single MHC isoform, type IIx and IIb MHC is co-expressed in approximately 12% of rat diaphragm myofibers (29). The MHC isoform composition of the diaphragm can be influenced by training. Aerobic conditioning results in a greater oxidative capacity and slow phenotype shift in the costal, but not the crural diaphragm (30). Although larger mammals including

humans do not express the type IIb MHC isoform, the human diaphragm metabolic, architectural and innervation properties are similar to those of the rodent.

Innervation of the diaphragm is organized somatotopcially. In the rat, the ventral costal and crural regions are innervated by C4 nerve segments, medial regions by C5, and dorsal regions by C6 nerve roots (31). Diaphragm muscle contractions follow a predictable order of motor unit recruitment, consistent with Henneman's size principle (32). In skeletal muscles, small motor units with high resistance and a low rheobase are recruited first, and small ventilatory demands result in the contraction of primarily slow motor units (33). Greater efferent drive results in rate modulation of active motor units as well as additional recruitment of larger motor units (34, 35). The neuromechanical efficiency of the diaphragm influences its rate modulation and motor unit recruitment, as well as the recruitment of accessory ventilatory muscles (36).

Form and Function of the Costal Diaphragm Regions

Although the diaphragm comprises less than 0.5% of body mass (37), it spans a large relative surface area, and its heterogeneous muscular attachments may yield regional differences in function. Scientists have delineated the diaphragm previously, based upon somatotopic innervations, anatomical origins, or functional properties. For the following experiments, the regions of the costal diaphragm have been differentiated according to the functional divisions described by Poole and colleagues (26) (Figure 2-1). Important regional distinctions for our experiments included the zone of apposition, metabolism, mechanical advantage, and eccentric contractions.

Zone of apposition: The portion of the diaphragm that is apposed to the thoracic cage extends from the bony origin of the diaphragm to the point where it begins to turn away from the chest wall. This zone of apposition (ZAP) couples the pressures exerted

through the ribcage and abdomen. Mechanical stress generated by the costal diaphragm varies regionally, because a larger ZAP permits contracting fibers to generate more stress (38). In other animal models, the length of the ZAP is greatest at the medial costal region of the diaphragm, and the ZAP is smallest in the ventral costal region (38). During contraction, fibers along the ZAP exert a cephalad force on the thoracic cage and facilitate expansion of the lower lung segments.

Bioenergetic considerations: Although MHC isoform expression does not differ substantially between diaphragm regions, the ventral costal segment exhibits a lower oxidative enzyme capacity (39). The magnitude of blood flow in the costal diaphragm may also account for regional differences in oxidative capacity (40). Medial costal segments appear to receive the greatest blood flow both at rest and with exercise, while dorsal segments receive the smallest flow rate (41). On the other hand, ventral-sternal diaphragm sections exhibit lower rates of glycogen depletion during aerobic exercise (42). The findings could indicate that the ventral regions relied less upon glycogen as an energy substrate, or instead, the region was recruited to a lower degree with exercise.

Mechanical advantage: In quadruped animals, the diaphragm generates ~40% of inspiratory pressure during quiet breathing (22). Inspiratory pressure generation can be influenced by the mechanical advantage (μ) of a given region as well as muscle tension (43, 44). The magnitude of μ depends upon mechanical strain and the change in lung volume: ($\mu = \Delta L/L_M \div \Delta V_L$). There are regional differences for μ in the costal diaphragm that are largely dictated by mass. Both the mass and the μ is greatest in the medial costal diaphragm and the lowest in dorsal regions (41). Regional differences in μ are preserved during passive shortening, quiet breathing and forceful ventilatory efforts

(22, 45). The ratios of passive to active muscle shortening are highly correlated and suggest that these regional variations serve to minimize the work of breathing (46).

Eccentric loading and injury: Inspiration is typically associated with shortening contractions of the diaphragm, but lengthening loads may be imposed under certain conditions. During expulsive reflexes and vigorous exhalation, diaphragm contractions stiffen the thoracic cage as the muscle is lengthened (47). Medial costal regions of the diaphragm may specifically contract in an eccentric fashion during obstructed inspiration (48). Eccentric contractions of skeletal muscles have been associated with a higher incidence of muscle fiber damage (49), but eccentric training may also yield greater fiber hypertrophy and strength gains, compared to concentric contractions (50). Thus, respiratory occlusion could potentially result in eccentric loading, damage, and hypertrophy. However, the diaphragm does not contract in isolation. Large respiratory efforts generate additional motor unit recruitment in accessory ventilatory muscles. Additionally, phasic activation of the abdominals can yield a pre-inspiratory diaphragmatic stretch (51). Therefore, accessory ventilatory muscles may influence the degree of diaphragm stress and remodeling.

Accessory Muscles of Inspiration

The diaphragm contracts the earliest among the muscles of inspiration (36), and its displacement accounts for approximately 70% of the change in resting tidal volume (52). Although the diaphragm is the primary muscle of the inspiratory pump, synergistic ventilatory muscles contract in a predictable fashion during breathing. The scalene and inspiratory intercostal muscles are also recruited during quiet inspiration in humans (36). The negative intrathoracic pressure generated by diaphragmatic descent is offset by stiffening and expansion of the ribcage by the intercostal muscles. This cooperation

prevents inefficient, paradoxical movements between the thorax and the abdomen. Without co-contraction of the accessory intercostal muscles, isolated diaphragm contractions result in inward displacement of the upper thoracic cage (53). On the other hand, accessory muscle contraction in the presence of diaphragm paresis results in expansion of the upper ribs and narrowing of the lower ribcage (53, 54).

Of the accessory inspiratory muscles, the human and canine intercostals are the best understood. The individual intercostals are heterogeneous muscles, and the ventilatory function of these muscles is specified to both its mechanical advantage and its distribution of neural drive (34, 55). The external intercostals originate at the costal tubercles and continue to the ventral costal cartilage. In each thoracic segment, fibers run from the lower margin of the upper ribs anteriorally and inferiorly to the lower rib. At most thoracic interspaces, the external intercostals primarily exert an inspiratory moment on the thoracic cage. In quadrupeds, the inspiratory mechanical advantage of the external intercostals increases from rostral to caudal segments (44).

In opposition to the external intercostals, the internal intercostal muscles originate ventrally at the sternocostal articulations, and each segment runs posteriorally and inferiorly from the lower margin of the upper rib to the lower rib. In the upper thoracic segments, the internal intercostals are functionally divided into dorsal (interosseus) and ventral, parasternal regions. Based upon the kinematics of the rostral thoracic cage and the neural drive, parasternal intercostals act as inspiratory muscles, and they are recruited within the first 10% of the inspiratory time (56). The inspiratory mechanical advantage of the parasternal intercostals is greatest at the second and third thoracic segments (57). After the first few costal segments, the mechanical advantage and drive

to the internal intercostal muscles transition rapidly from inspiratory to expiratory action (55, 56). (55)The timing and amplitude of motor unit recruitment in the accessory muscles match their mechanical advantage (34).

Contraction of the inspiratory muscle pump establishes a negative pressure gradient, which drives airflow into the lungs. The diaphragm contracts for ~30-40% of the life cycle of an organism in order to continually meet its ventilatory requirements (58). The ventilatory pump must be activated with sufficient timing, amplitude and coordination to meet ventilatory motor drive. With additional respiratory demands, the degree and intensity of accessory muscle recruitment increases to match the amplitude and timing of breathing (52). When ventilatory demand is unmet due to illness or injury, MV may be initiated to maintain the movement of air from the atmosphere to the alveoli.

The Effects of Mechanical Ventilation on the Diaphragm

Intensive care therapies, including mechanical ventilation (MV), can save many lives following a life-threatening injury or illness. MV attenuates the mechanical work of the inspiratory pump and results in decreased descending corticospinal drive to the diaphragm (59). Ventilatory support can be modified to regulate the number of assisted breaths, level of pressure and/or tidal volume support, or mode of control. Progressively higher levels of MV support can diminish or cease diaphragmatic electromyography (EMG) activity, enabling physicians to “rest” the diaphragms of critically ill patients (60). Paradoxically, MV can facilitate dysfunction of inactive diaphragm sarcomeres, termed ventilator-induced diaphragm dysfunction (VIDD), a condition identified clinically by progressive inspiratory weakness.

VIDD results in structural and functional changes to the diaphragm, manifested by atrophy and contractile dysfunction. Numerous animal models have confirmed that

periods of controlled MV between six and 48 hours result in diaphragmatic atrophy (61-64). Atrophy of the inactive diaphragm occurs in conjunction with rapidly down-regulated protein synthesis (5, 65), followed shortly by a heightened, sustained state of proteolysis (7, 65, 66). Initially, MV-induced diaphragm inactivity affects all muscle fiber types, but sustained ventilation appears to preferentially atrophy fast-fatigable fibers (62, 63, 67, 68). Controlled MV initiates atrophy signaling cascades in the diaphragm up to eight times faster than in the limb muscles (5, 18), suggesting that this chronically active muscle may be more susceptible to disuse atrophy (8). In humans, proteolytic gene expression significantly increases within the first several hours of MV (69).

Mechanisms of Ventilator-Induced Diaphragmatic Dysfunction

The diaphragm is an active muscle characterized by a high duty cycle, strong oxidative capacity and large number of mitochondria. Therefore, the inactive, ventilated diaphragm is vulnerable to damage from oxidative stress (Figure 2-2) (6, 9). Oxidative stress is thought to play a key role in disturbances of muscle ion channels, resulting in an influx of intracellular calcium and ineffective calcium sequestration by the sarcoplasmic reticulum (8). In addition, the antioxidant defenses of the ventilated diaphragm become less efficient, and mitochondria become particularly susceptible to damage (7, 70). Preliminary work from our collaborators indicates that 3-4 hours of controlled MV alters state 3 and 4 mitochondrial respiration in the human diaphragm by ~25% (unpublished pilot data). Oxidation of phospholipids, nucleic acids, and protein in the diaphragm may also activate apoptosis and proteolysis. Caspase signaling cascades in receptors, sarcoplasmic reticulum and mitochondria trigger apoptotic activity of myonuclei or myofibers (11). The rate of myonuclear apoptosis matches the rate of proteolysis, preserving the diaphragmatic myonuclear domain in VIDD (11).

Severe disturbance results in apoptosis of skeletal myocytes. Within several hours of controlled MV, gene expression of a number of apoptotic and proteolytic regulatory molecules becomes significantly upregulated (5).

Proteolysis can be mediated by lysosomal, calcium-regulated, and ubiquitin-proteosomal pathways. The myofibrillar proteins account for over 50% of muscle proteins (8), and ubiquitin-proteosomal pathways are primary mediators of atrophy in adult muscle fibers (71, 72). Ubiquitin-related proteolysis is activated by the forkhead box (Foxo) transcription factors and occurs through initiation (E1), elongation (E2), and ligation (E3) protein families Two atrophy-specific E3-ligases, atrogin-1 and muscle ring finger-1 (MuRF1), modulate the rate and extent of myofibrillar protein decomposition. The Foxo transcription factors also initiate lysosomally-mediated autophagy in specific cases of muscle atrophy (73). Although only a small portion of myofibrillar degradation occurs through autophagy, the lysosome may facilitate the breakdown of sarolemma, sarcoplasmic reticulum, and mitochondrial proteins (74). The calcium-mediated proteolytic molecules calpain and caspase-3 are thought to initiate myofibrillar deconstruction(10), because the E3 ubiquitin ligases cannot degrade intact contractile elements. Proteolytic drive is accompanied by down-regulation of key hypertrophic transcription factors within regenerative and protein synthesis signaling cascades (63, 64).

In addition to muscle fiber atrophy, the contractile function of the diaphragm is impaired by MV. Controlled MV induces rapid and profound decrements in specific twitch and tetanic isometric force in multiple animal models, in a time course that parallels the rate of diaphragm atrophy (10, 62, 67, 75-78). Significant reductions in

diaphragmatic force can be detected within 6 hours of controlled MV (10, 76, 78). The literature suggests that periods of 6 to 72 hours of controlled ventilation impair the specific tension of the diaphragm by 18 to 60% (10, 64, 76, 77, 79). Impairments in isometric and isotonic specific force can be detected throughout the physiological and supra-maximal ranges of the force-frequency curve (10, 64, 77), in proportion to MV duration (77, 78).

While a number of factors can accelerate diaphragm contractile dysfunction, other influences can be ruled out. Diaphragm force impairments not appear to result from a shift in relative fiber-type proportions within the first 72 hours of MV (64, 76, 77). In conjunction, MV does not alter phrenic nerve conduction latency or the duration of the compound muscle action potential (80), suggesting that nerve conduction and membrane inexcitability do not contribute substantially to VIDD. Additionally, repetitive passive shortening of the diaphragm by MV does not alter the length-tension properties of the muscle (67, 68, 77). However, some neuromuscular blocking medications can exacerbate diaphragm force impairments brought about by MV (81). Some scientists attribute diaphragm contractile dysfunction to reduced quantities of fast MHC protein and mRNA (65, 79), but these findings have not been universally reported (78). On the other hand, ultrastructural damage of the diaphragm and intercostals can be visualized within 2 days of MV, accompanied by reduced mitochondrial numbers and blunted mitochondrial respiration (82). Ion channel disruption and ultrastructural damage of the diaphragm likely contribute to excitation-contraction uncoupling (76, 78). In summary, diaphragm inactivity-induced oxidative stress rapidly promotes mitochondrial

dysfunction, proteolysis, and excitation-contraction uncoupling, resulting in atrophy and contractile dysfunction.

Evidence for Diaphragm Dysfunction in Ventilated Humans

Clinical research illustrates that diaphragm dysfunction also occurs in ventilated humans. The first evidence of VIDD in humans consisted of a post-mortem report of fiber atrophy in neonates who required extended periods of ventilation (83). More recently, research by Levine (12) illustrated that passively ventilated adults (age: 35±16 years), free from active pulmonary or infectious diseases, exhibited rapid and profound diaphragmatic atrophy. In this study, organ donors with terminal brain injuries experienced 57% atrophy of type I fibers and 53% atrophy in type II fibers within a median 34 hours of controlled MV, compared to the diaphragms of older adults who underwent thoracic surgeries (MV duration: 2.4±0.5 hours). Although MHC gene expression did not appear to change, patients expressed markedly elevated mRNA levels of atrogin-1 and MuRF1. These compelling data indicate that clinically meaningful proteolysis occurs in humans after short periods of controlled MV. Moreover, they indicate that VIDD can affect ventilated humans of any age.

Additional factors in critical care clinical practice influence the development of VIDD in humans. Neuromuscular blocking agents and corticosteroids medications may impair excitation-contraction coupling and accelerate the formation of critical illness myopathy (84). Hyperglycemia, systemic inflammatory response syndrome, and multiple-system organ failure each place patients at greater risk for ICU-acquired weakness of the diaphragm (85). Clinically meaningful decreases in inspiratory and limb muscle strength occur within one week of continuous MV, and inspiratory muscle weakness is

associated with delayed weaning (86). Scientists acknowledge that VIDD is a major clinical problem that can delay or prevent weaning (1, 87-89)

Inspiratory Weakness Reinforces Prolonged Mechanical Ventilation

To minimize the risk of VIDD, weaning efforts should begin as soon as possible (90, 91). Weaning readiness trials use short periods of unassisted breathing, termed spontaneous breathing trials, to test patients' readiness for extubation (92, 93). Even after short periods of MV, the ventilatory characteristics of patients who successfully wean from MV differ from those who fail (94-102). Patients who fail extubation often develop a rapid, shallow ventilatory pattern during a spontaneous breathing trial (102). However, many causes of early failed extubations do not necessarily predict weaning failure in patients who require prolonged MV (1). After longer periods of MV, the reasons for weaning failure are more complex and cannot be explained by weaning predictors based upon respiratory mechanics (1). Additional risk factors for prolonged weaning include cardiac insufficiency, use of myotoxic drugs, sepsis and advanced age, as well as inspiratory muscle dysfunction (87, 103). Of these factors, it is acknowledged that a principal reason for weaning failure in alert, difficult to wean patients is insufficient ventilatory capacity, in relation to required breathing loads (1, 101, 104-106).

Inspiratory weakness has been identified as a crucial contributor to ventilator dependence (97, 101, 107). Specifically, patients who repeatedly fail to wean require large pressures to generate a tidal breath, in comparison to the peak pressure capacity of the inspiratory pump (101). At rest, passive respiratory mechanics are unable to reliably differentiate patients who fail a weaning trial from those who pass (108). However, patients with respiratory muscle weakness often exhibit a deterioration of pulmonary mechanics during periods of unassisted breathing. Most notably, intrinsic

positive end-expiratory pressure ($PEEP_i$) increases, which may occur due to active expiratory muscle contractions and early termination of exhalation (109, 110). At end-expiration, lung volumes progressively expand, resulting in dynamic hyperinflation. Progressive hyperinflation is accompanied by increased airway resistance and decreased pulmonary compliance during failed breathing trials (100, 106).

In the presence of dynamic hyperinflation, tidal breathing occurs over a less-compliant region of the respiratory pressure-volume curve. As a result, the pressure load increases during a tidal inhalation (100). Excessive resistive ventilatory loads may occur due to airway obstruction by edema, bronchoconstriction, or mucus plugging, while pulmonary congestion, effusion, ascites, or skeletal injury can elevate elastic loading. Chronic co-morbid diseases such as COPD may exacerbate acute changes in resistive and elastic ventilatory loads. Patients with repeated weaning failure often experience tidal pressure loads (P_{di}/P_{dimax}) that approximate 40% of maximal transdiaphragmatic pressure (101). Workloads of this magnitude are unsustainable in healthy adults who undergo breathing or extremity loading tasks (101, 106, 111). Clinically, the pressure demands of inspiration and the timing of breaths have been integrated into a tension-time index, TTI ($TTI = P_{di}/P_{dimax} * T_i/T_{tot}$, where P_{di}/P_{dimax} = proportion of maximal transdiaphragmatic pressure required for tidal inhalation, and T_i/T_{tot} = duty cycle). Values of TTI that exceed 0.15 have been identified as a major pathophysiological characteristic of repeated weaning failure in infants, children and adults (101, 104, 106, 112). Moreover, TTI underscores the relationship between respiratory muscle weakness and breathing patterns during weaning failure.

In conjunction with altered mechanics and increased energetic requirements of breathing, accessory muscle recruitment may increase in patients who fail a weaning trial. Some prior investigators have interpreted accessory muscle use as a sign of diaphragmatic fatigue (97, 113). Indeed, accessory muscle use and increased diaphragmatic TTI frequently occur with weaning failure (104, 109). However, the evoked tension of the diaphragm does not deteriorate in patients who fail to wean, compared to successfully-weaned patients, indicating that inspiratory fatigue does not predicate weaning failure (114). Rather, clinical signs of physiological or psychological distress, each associated with recruitment of ventilatory accessory muscles, likely preceded the onset of diaphragm fatigue (100, 109, 115). Notably, the relationship between weaning failure and inspiratory weakness implies that two primary strategies may facilitate weaning. Clinical weaning success may be achieved by decreasing the loads which oppose breathing, or by increasing the strength of the ventilatory muscles.

Inspiratory Muscle Training Effects on the Ventilatory Pump

Evidence that Inspiratory Muscle Strength Training (IMST) Improves Inspiratory Muscle Strength

While diaphragmatic weakness is a well-recognized characteristic of prolonged MV (86, 104, 107), less is known about the role of inspiratory muscle strengthening to facilitate weaning. The first reports of concurrent respiratory muscle training and ventilator weaning were published nearly 30 years ago and consisted of isolated reports and case series (116-119). Early studies of inspiratory muscle training provided sustained breathing loads designed to improve ventilatory endurance. Patients received training with isocapnic hyperpnea (116, 117) or by alinear resisters that provided flow-dependent breathing loads (118, 119). In these reports, training produced

significant maximal inspiratory pressure (MIP) gains that were associated with weaning (116-119). However, not all reports have shown positive effects of inspiratory training. Light, sustained resistive breathing can be associated with hypoventilation and oxygen desaturation in patients, without an improvement in breathing performance (120). Others used the ventilator to “train” patients, by programming the ventilator to deliver MV-assisted breaths at higher pressure settings (121). Although patients needed to briefly generate greater pressures to trigger the ventilator, the elastic loads of inspiration were abolished by MV. Therefore, it is not surprising that respiratory muscle efficiency did not improve and this method of training did not accelerate weaning. Weaning success necessitates the prevention or reversal of respiratory weakness, particularly with extended MV (1, 105, 107, 109, 114, 122). Strengthening can be achieved with training overloads appropriate for the capacity of the patient.

Reliable inspiratory muscle strength training (IMST) loads can be provided by weighted plungers, occlusions, or commercially-available threshold trainers (123, 124). Conventional threshold IMST devices use a spring-loaded, one-way valve, and subjects must generate a minimum amount of inspiratory pressure, in order to overcome the tension of the spring (125-127). Below the threshold pressure value, the poppet valve of the training device remains closed, and patients do not receive any inspiratory tidal volume. During valve closure, small volume fluctuations occur due to gas compression and chest wall compliance, and the pressure effort of the inspiratory muscles is quasi-isometric. Once the target pressure has been reached, the poppet valve opens and the diaphragm contraction becomes isotonic in nature as airflow begins. Threshold IMST trainers deliver flow-independent loads under most airflow rates (123). While respiratory

endurance exercises require light, sustained loaded breaths, IMST typically provides moderate to high-intensity loads for brief durations, akin to limb strength training (125, 128).

The application of IMST to patient populations was based upon inspiratory performance benefits that were established in healthy human subjects. Studies in healthy adults consistently demonstrated that four to six weeks of moderate to high intensity IMST (50% to 100% of MIP, brief durations) yield an average 45% gain in MIP (69, 129-131). More intense training loads produced greater relative MIP improvements, and some of the highest relative pressure gains have occurred with training sets of 1-repetition maximal inspirations (131). In addition to improved strength, IMST decreased the inspiratory neural drive, in proportion to the MIP gain (69, 132). With improved MIP, subjects perceived standard inspiratory loads as smaller (129), and the detection of the smallest threshold pressure loads decreased (69). In conjunction, IMST appears to improve ventilatory performance. After training, subjects could maintain tidal volume with a faster airflow and produced greater power while breathing against inspiratory loads (69, 129, 131). Thus, moderate to high intensity IMST resulted in robust strength increases in that lowered drive, reduced load perception and improved ventilatory performance.

Just as IMST improved strength in healthy adults, it can facilitate recovery from respiratory muscle weakness, including VIDD. However, compared to their healthy counterparts, ventilated adults achieved a more modest strength benefit. MIP improvements between 16 and 140% (excluding the outlier, average gain 27%) have been reported after 2-4 weeks of IMST (13, 127, 133-135). A lower MIP gain in patients

may be due to a lower training intensity (between 30% and 50% of MIP). Short, intense IMST sessions appeared to elicit as large a strengthening effect as moderate, sustained training modes.

Clinical training studies show that many difficult to wean patients can achieve liberation from MV, when IMST accompanies the weaning efforts (125, 127). In clinical studies, the greatest rates of ventilator weaning occurred with higher training intensities. Moreover, trained patients exhibited improved MIP upon weaning (126, 127). Our laboratory recently completed a randomized, controlled trial of 69 ventilated adults and demonstrated a significant weaning benefit of IMST, compared to sham inspiratory training (128). After an average 44 continuous days of MV, 71% of IMST subjects weaned from MV, compared to 47% of sham-trained subjects ($p<.05$). Other medical co-morbidities, treatments or medications did not differ appreciably between the groups. The collective data imply that IMST can improve ventilatory performance and enhance weaning from MV, yet it is less understood how IMST remodels the inspiratory pump.

IMST and Diaphragm Fiber Remodeling

Although rapid strength and functional gains have been reported with IMST, fiber hypertrophy has not been traditionally considered to occur within the first 4 weeks of training (136). However, other physiological evidence indicates that strong overload training can elicit brisk muscle remodeling. In the limb muscles, expression of myogenic growth factors significantly increase within hours of single resistance training bouts, and adaptations are reinforced with repeated training sessions (72, 137). The evidence in extremity muscles suggests that IMST could facilitate rapid diaphragm remodeling.

Diaphragm fiber hypertrophy has been examined in animals, after sustained inspiratory loading. These efforts were largely unsuccessful due to the use of

experimental designs that did not implement high tension, low repetition contractions, in concordance with accepted principles of strength training. Early loading studies used bands to reduce the internal tracheal diameter of animals, creating a resistive load that was sustained for days to weeks (15, 16, 138). The continuous resistive loads expanded the proportion of slow oxidative fibers and oxidative activity in the diaphragm and increased diaphragm mass and fatigue resistance (15, 17). Although a chronic inspiratory overload appears to increase oxidative capacity, muscle growth and some components of contractile function, it produced a high rate of mortality (16). This suggests that the intervention elicited unsustainable physiological stresses (17, 139). Short yet physiologically challenging durations of inspiratory resistive breathing (2 continuous hours at 50% MIP) have been shown to increase slow MHC gene expression (19). However, this training duration has also been associated with plasma membrane damage and sarcomere disruption (140).

To minimize sarcomere damage, alternative animal training studies utilized alinear resistive masks to provide low intensity inspiratory training (21, 139). Eight weeks of light respiratory muscle conditioning induced type I and IIa hypertrophy (139), and moderate training increased type IIa and IIx/b cross-sectional area (CSA). In spite of the modest fiber hypertrophy, inspiratory training did not improve evoked tension of the diaphragm. Alternatively, the extent of the force adaptation may have been limited by a low training intensity (TTI = 0.05) (21, 139). Collectively, the animal training studies indicate that diaphragm fiber hypertrophy is possible, yet these studies cannot elucidate if or how the diaphragm remodels with strengthening, because they did not administer strength training. In contrast, this investigation employed a novel model of intermittent

tracheal occlusion that applied a high-intensity, brief strengthening stimulus to the inspiratory muscles. We postulated that the respiratory muscles would demonstrate robust histological plasticity, in the presence of this transient, intense pressure stimulus.

Mechanisms of myofiber hypertrophy

The primary histological outcome variable in this study was muscle fiber CSA, an estimate of fiber hypertrophy. Muscle hypertrophy ultimately results from a net increase in protein synthesis, in relation to protein degradation. Atrophy and hypertrophy function antagonistically to mediate muscle size, and these events share a number of key regulatory signaling mechanisms. Resistance training can mediate muscle fiber hypertrophy through a network of interrelated signal transduction pathways, resulting in elevated protein synthesis or myogenic activation (briefly summarized in Figure 2-3). Muscle fiber size, MHC isoform expression and regeneration adaptations may each be modified by changes in activity. Growth of mature, terminally differentiated myofibers is driven by an increase in synthesis and reduction in proteolysis (141). Myogenesis and protein synthesis can facilitate fiber hypertrophy independently (142, 143), yet activity-mediated hypertrophy in intact animals likely results from coordination of these events.

Protein synthesis is largely mediated by the PI3K-Akt-mTOR signaling pathway, and can be initiated by receptor-specific binding of insulin-like growth factor I (IGF-1) molecules (144, 145) and activation of PI3K. Downstream of IGF-1 and PI3K, Akt molecules influence protein turnover activity and muscle growth through a linkage to the Foxo transcription factors. Akt phosphorylation prevents nuclear translocation of phosphorylated Foxo, an action that inhibits expression of proteolytic regulatory genes such as atrogin-1 and Murf1. The Akt-Foxo interaction is a primary regulatory point for maintenance of muscle protein balance. Akt concurrently promotes downstream activity

of the mammalian target of rapamycin (mTOR) isoforms. In particular, mTORC1 is a potent stimulator of ribosomal translation and a crucial regulator of eukaryotic initiation and elongation factors (144). Mechanical strain alone is capable of inducing hypertrophy through Akt-mTOR signaling, independent of a functional IGF-1 receptor (146). The Akt-mTOR signaling proteins are integral modulators of protein synthesis, but it is not fully understood how these signals dictate the rate of ribosomal translation or specify protein synthesis (147).

While hypertrophy depends upon protein synthesis, the extent of mature fiber growth can be limited by the myonuclear domain when muscle regenerative pathways are inhibited (148-150). Research in limb muscle suggests that the extent of muscle fiber hypertrophy is restricted to a myonuclear domain approximating 2000 μm^2, without addition of myonuclei (151, 152). Regeneration can be promoted when mechanical strain deforms key cytoskeletal proteins and induces an inflammatory reaction. Pro-regenerative paracrine and autocrine molecules include hepatocyte growth factor, nitric oxide, IL-6, fibroblast growth factor, and IGF-1. Systemic and local growth factors and circulating cytokines bind to cell receptors, resulting in mechanical-chemical signal transduction (153, 154). Pro-regenerative signal transduction promotes activation of satellite cells, peripherally-located muscle fiber progenitors that can be anatomically and functionally differentiated from other myonuclei (155).

The fate of activated satellite cells, termed myoblasts, depends upon the environmental niche as well as the subsequent expression of influential myogenic regulatory transcriptional factors (MRFs). IGF-1 facilitates anti-apoptotic signaling through PI3K-Akt, and promotes ERK signaling, resulting in progression of the

mitogenic cycle (156). During proliferation, activated satellite cells express the Pax7, MyoD and Myf5 MRFs. Some proliferating myoblasts yield daughter cells responsible that renew the satellite cell pool. Other daughter cells undergo withdrawal from the cell cycle and subsequent differentiation.

The cyclin-dependent kinase inhibitor, p21 promotes cell cycle arrest and facilitates differentiation. During differentiation, Pax7 and MyoD downregulate, accompanied by the upregulation of Mrf4 and myogenin. In addition, anti-apoptotic Akt/PI3K/mTOR transcription factors module the rate and extent of differentiation (157, 158). Differentiating myoblasts can fuse to existing myofibers to promote repair and facilitate fiber growth, become myonuclei, or fuse together to create new, regenerating myotubes (Figure 2-4) (159, 160). Additional myonuclei are thought to preserve the myonuclear domain, to support hypertrophied muscle tissue (152, 161). With terminal differentiation, nascent and repaired myofibers express developmental MHC isoforms and subsequently mature into adult fibers. Together, signal transduction for myogenic activation and protein synthesis synergistically promote muscle growth in response to overload training.

Overload training and myofiber damage

In addition to CSA, our experiments analyzed diaphragm fiber damage and regeneration in an animal model of tracheal occlusion. Respiratory loads can induce widespread diaphragm injury (162). Myofibrillar damage can be influenced by the mode (stretch vs. contraction), intensity and duration of the mechanical stimulus, as well as the contractile state of the muscle (shortening vs. lengthening). Diaphragm damage has been found with both acute and chronic loads. To study acute muscle damage in the diaphragm, experimental designs typically delivered a single sustained, injurious

overload in an animal model. Damage responses differ in regions of the diaphragm and between accessory muscles. The costal diaphragm appears more susceptible to acute injury than the crural diaphragm or accessory muscles of respiration (162-165). The extent and timing of diaphragm damage responses occurs in proportion to the duration and intensity of the respiratory load. One day after a single, injurious load, significant proportions of injured myofibers and inflammatory cell infiltration become apparent with light microscopy and continue for three days (163, 166, 167). In contrast to severe sustained loads (~70% MIP), moderate loads (~45% MIP) do not induce significant diaphragm injury (163). With continuous load, damage is prolonged. Six days of continuous respiratory loading increased the pooled proportions of abnormal muscle fibers and connective tissue in the costal diaphragm (162). Substantial remodeled and inflamed diaphragm fibers persist after thirty days of chronic respiratory loading (17).

After a mechanical or chemical injury, muscle fiber remodeling occurs in four related, overlapping phases: degeneration, inflammation, regeneration, and fibrosis (Reviewed in (168)). Degeneration begins rapidly following mechanical overloads. Excessive mechanical strain disrupts the myofibrillar scaffolding and sarcolemma proteins, and elevates calcium influx, oxidative stress and proteolytic signaling (20, 169-172). Physiological strength training loads and damaging contractions trigger proportionate levels of oxidative stress and proteolysis (166, 173). Moderate to severe calcium ion influx can impair excitation-contraction uncoupling, leading to measureable decrements in evoked tension (174-176). Degeneration can be measured within five minutes of severe eccentric overloads in the limb muscles (177), and may continue for days. The activation of proteolytic pathways and fiber degeneration corresponds to a

rapid inflammatory response. Macrophages and lymphocytes migrate to injured tissue, and levels of local and circulating pro-inflammatory cytokines and growth factors increase (167). Pro-inflammatory molecules mediate the immune responses of remodeling dictate the outcome of subsequent fiber adaptations. Pro-regenerative molecules include macrophages, interleukin-6, hepatocyte growth factor, and IGF-1.

In human limb muscle, regenerative activity peaks approximately two weeks after introducing mechanical loads (168, 178). Rodent tissue may remodel more rapidly; expression of proliferation genes increases within 12 hours and peaks within three days (179, 180). Next, expression of immature myosin heavy chains increases in differentiated myotubes. In differentiated myotubes, gene expression of embryonic myosin increases approximately three to seven days and peaks within seven to ten days of a training load or damage stimulus (172, 180). Regenerative markers may be detected earlier into training, before measureable hypertrophy can be detected (159).

Alternatively, apoptotic dominance or elevated myostatin expression can inhibit regeneration and promote fibrosis (181). However, physiological strengthening loads typically inhibit myostatin gene expression, in the absence of muscular disease or myotoxic medications (182, 183). Force recovery accompanies muscle fiber regenerative and remodeling, but impaired evoked force may continue in the presence of fibrosis, due to decreased myofibrillar protein content (184).

The phases of muscle fiber remodeling can be characterized by specific histological adaptations. Connective tissue and changes in muscle fiber shape or size indicate the remodeling state of the muscle. Degeneration may be characterized by disruption of ultrasctuctural features or cellular incursion of plasma fibronectin, and

increased proportions of inflammatory cells within the interstitium characterize early remodeling (166, 167). Elevated ratios of inflamed or necrotic fibers occur during inflammation and can persist during regeneration and fibrosis (166, 184). Proportions of centrally-nucleated fibers and small fibers increase during myofiber regeneration (185). In contrast, incomplete or inhibited regeneration can be visualized by the replacement of myofibrillar tissue with excessive connective tissue and elevated presence of fibroblasts (168, 186). While histological assessments of muscle remodeling cannot identify the underlying causes of remodeling or whether they are beneficial or maladaptive, they provide valuable insight regarding the timing and degree of fiber remodeling.

Summary and Significance

This work is significant because the rate of ventilatory failure continues to increase, despite advancements in critical care medicine (187). Patients who require prolonged MV experience significant disability and risk additional medical co-morbidities and death (3, 188, 189). Despite improved critical care practices, incidence of weaning failure has increased at a rate five times faster than the incidence of hospital admissions, and chronic ventilator dependence is projected to grow ~250% by 2020 (187). VIDD remains a substantial problem and reflects a need to explore optimal respiratory muscle rehabilitation practices. The respiratory loading regime in this experimental design resembles brief airway occlusions utilized for clinical respiratory testing (190), and could also be adapted for training patients who cannot voluntarily participate in respiratory exercises. The experiments contribute novel information regarding the timing and extent of inspiratory muscle training responses. Results of this study may bear particular significance to the rehabilitation of patients with respiratory failure and diaphragm atrophy.

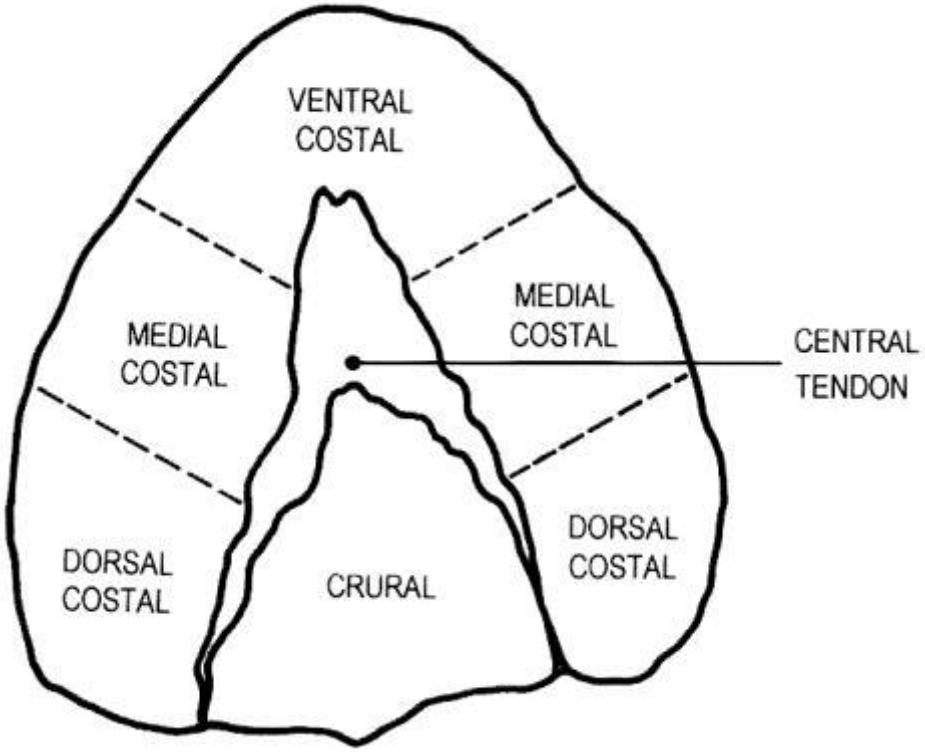

Figure 2-1. Regional architecture of the rodent diaphragm. Figure printed with permission from Poole et al, MSSE, 1997; 29(6): 740.

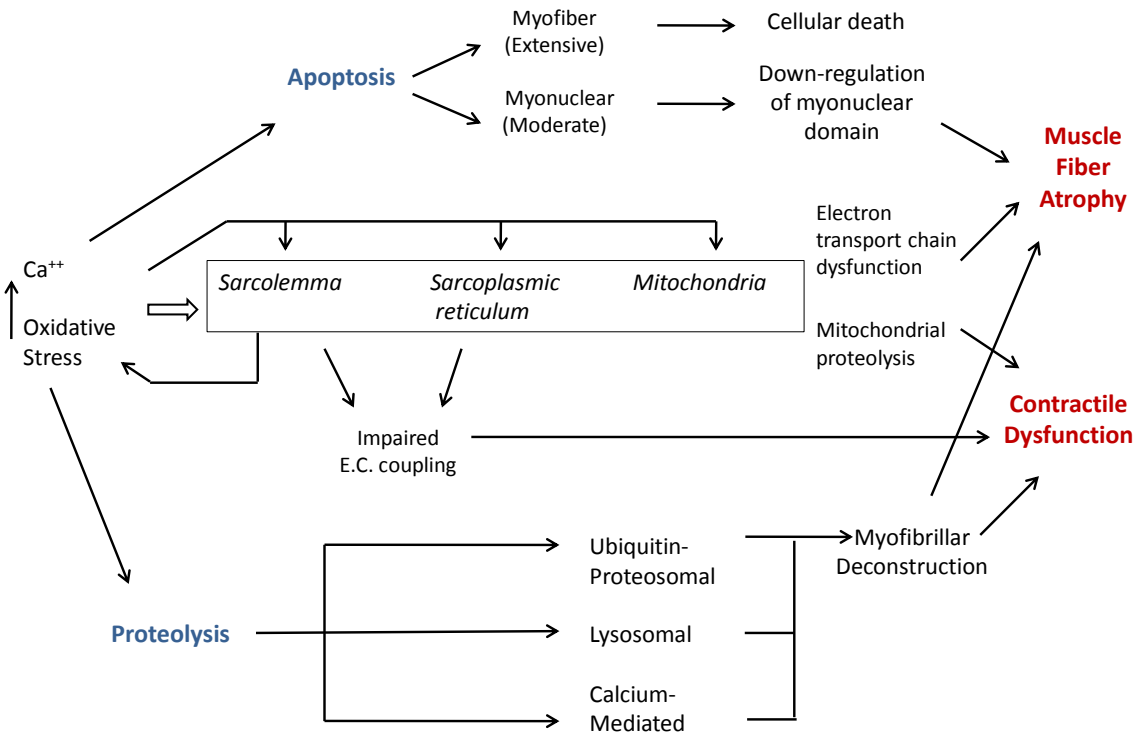

Figure 2-2. Summary of mechanical ventilation effects on atrophy and contractile dysfunction in the diaphragm.

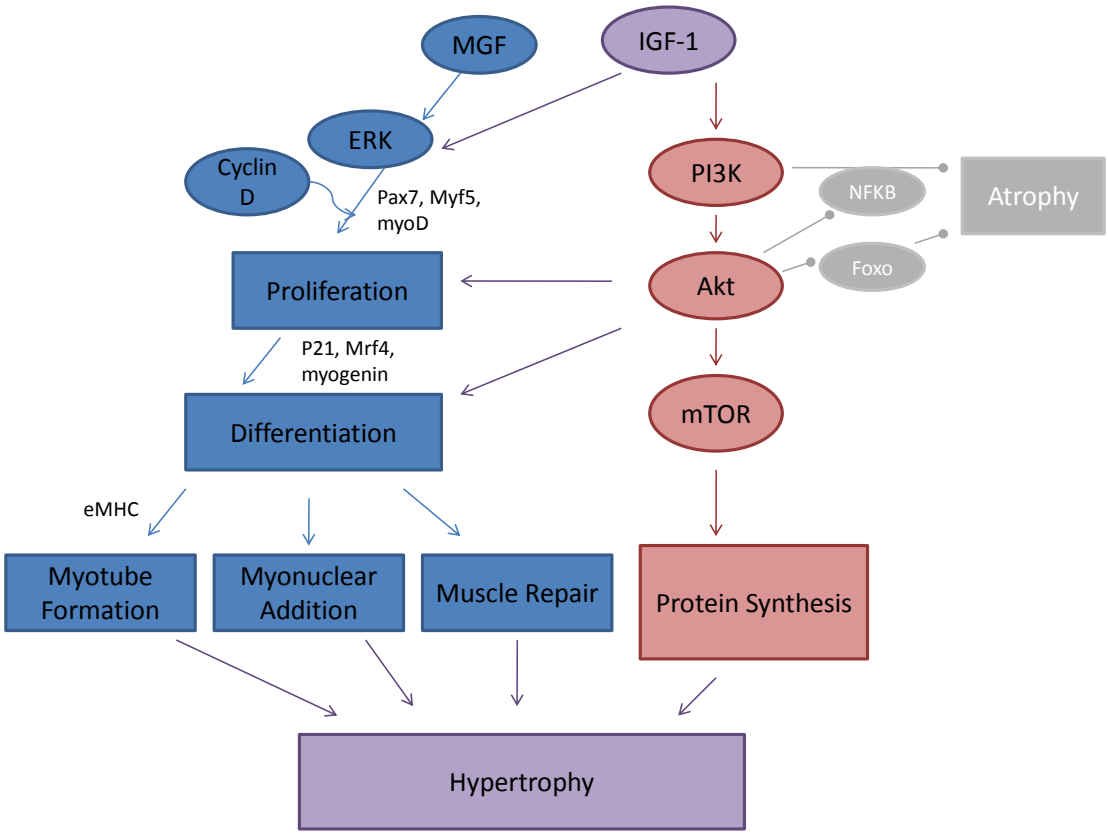

Figure 2.3. Protein synthesis and myogenic regeneration each contribute to training-induced muscle hypertrophy. A number of molecules from the PI3K-Akt family participate in cross-talk to mediate atrophy and regeneration processes and thereby manage protein homeostasis.

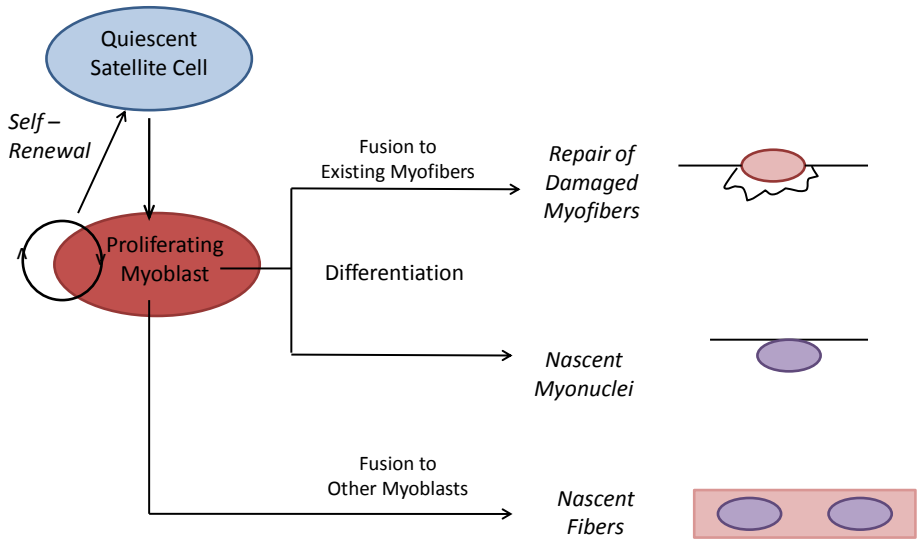

Figure 2-4. Myogenic regeneration after skeletal muscle overload. Quiescent satellite cells are activated by mechanical loading or injury, and myoblasts begin to proliferate. Some replicating myoblasts will not differentiate and will replenish the satellite cell pool. Other myoblasts differentiate and fuse to existing myofibers to repair damage or add myonuclei. Yet others fuse together, yielding new, immature myofibers.

CHAPTER 3
MATERIALS AND METHODS

Research Design and Data Analysis

The primary objective of this investigation was to identify selected histological adaptations to overload training in respiratory muscle, using an animal model of tracheal occlusion. Phase one of the investigation examined fiber hypertrophy and myosin heavy chain (MHC) phenotype adaptations of the respiratory pump (*Experiment 1*). Next, the muscles were compared for histological differences in damage and regeneration (*Experiment 2*).

Justification for an Animal Model

Invasive procedures such as surgery are needed to obtain human diaphragm specimens. Due to medically tenuous status of mechanical ventilation (MV)-dependent patients, diaphragm biopsies would involve excessive risk when an alternative animal model of training can be applied. Animal models of MV have advanced the scientific understanding of ventilator-induced diaphragm dysfunction (VIDD) (10, 64, 66, 67, 76-79, 170, 191), and the timeframe for atrophy appears to be translatable to ventilated humans (12). The Sprague-Dawley rat was chosen due to physiological similarities to humans in training and disuse atrophy muscle remodeling (192). Sixteen juvenile male rats (12-16 weeks) were selected for the study.

Animals were housed at the University of Florida Animal Care Services Center, in accordance with the criteria established by the Institutional Animal Care and Use Committee (IACUC). Tracheal occlusion experiments were approved by the University of Florida IACUC and met the stipulations of the Helsinki Declaration. A 12:12 hour

reverse light: dark cycle and *ad libitum* diet of animal chow and water were provided to the animals throughout the experimental period.

Experimental Design

The study design is outlined in Figure 3-1. Animals were randomly assigned to one of two groups, and then underwent surgical placement of a tracheal cuff. Cuff placement was followed by a post-surgical recovery period. Upon recovery, the animals began ten sessions of the assigned experimental intervention. Every day, each animal in the sham-treated group (SHAM, n=8) was placed in a plethysmograph and the tracheal cuff was connected to a pressure line. The cuff was never occluded for SHAM-trained animals. Animals assigned to the occlusion group (OCCL, n=8) were also placed in a plethysmograph daily, and the tracheal cuff was connected to a pressure line. OCCL animals received intermittent tracheal occlusions for a 10-minute daily session. After a two-week intervention, animals were euthanized. The muscle tissue was preserved, and then analyzed by a masked investigator for hypertrophy, damage, and regeneration.

Rationale

The costal diaphragm, third parasternal intercostal and soleus muscles were selected for analysis. We focused upon the medial costal diaphragm because its large appositional area results in a large degree of active shortening during inspiration and therefore may be amenable to remodeling. In addition, the majority of the published injury, training and atrophy studies published findings from medial diaphragm segments, and this data can be compared to our training regime. We also contrasted the data from the medial costal diaphragm to ventral and dorsal regions to determine whether regional training differences existed. The third intercostal muscle was analyzed because the

parasternal region has a strong inspiratory function that is activated early in a tidal breath (55). Although the fiber composition of the soleus is predominantly slow and oxidative, this muscle was selected because its duty cycle is among the greatest in the limb muscles of small quadrupeds (58, 193).

Power Analysis

A power analysis was conducted to determine the sample size for the projected hypertrophy effect. Because the experimental model was novel, we applied existing data from Rollier's study of intermittent resistive respiratory training in Wistar rats (139). In this work, rats underwent 60 minutes of alinear resistive breathing through a snout mask, three times weekly for eight weeks. Two important components of the resistive training model differed from the experimental design employed by the current study: training occurred for eight weeks rather than two, and the protocol consisted of low-level training (average tension-time index: .02) rather than brief, intense occlusion loads. The power analysis for this work indicated that a group size of 5 animals was sufficient to yield statistical significance for hypertrophy of fast, glycolytic fibers, and 3 animals for significant differences in oxidative fiber hypertrophy (139).

Despite the differences in the experimental models, we anticipated that the effect sizes for this project would equal or exceed that of Rollier's work. Tracheal occlusion elicits high ventilatory drive yielding strong to maximal respiratory efforts (194). In addition, the rodent facemasks resulted in airway leaks, while occlusions were inescapable and confirmed by cuff pressures and plethysmography in the current study. Therefore we hypothesized that tracheal occlusion should provide a greater strength and hypertrophy stimulus, despite the shorter training duration. In a sample of four animals from earlier pilot work, we identified a strong effect size (Cohen's D = 1.01) and

determined groups of 13 animals were needed. However, the analysis pooled the values of type I, IIa, and IIx/b fibers, resulting in large cross-sectional area (CSA) variability. After correcting for fiber type variability based upon Rollier's work, a Cohen's D = 1.58 confirmed that a sample size of six animals per group was sufficiently powered (1-β =.80).

Methods

Surgical Procedures

For the placement of the tracheal cuff, the animals were anesthetized using isofluorane gas (2-5% in O_2). During the procedure, the body temperature was maintained at 37 ° C with a heating blanket. Anesthetic plane of sedation was confirmed by an absent withdrawal reflex to a noxious paw pinch. Animals breathed room air without MV support. With a ventral incision, the trachea was exposed. An inflatable vascular occluder was sutured around the trachea, and the actuating line was routed and externalized dorsally, between the scapulae (Figure 5-2A). The externalized line could be connected to an air-filled syringe, in order to inflate or deflate the cuff bladder. Inflation of the cuff elicited total tracheal occlusion, while deflation restored airway patency and permitted unobstructed breathing. The external pressure line was securely stitched in place, and the tracheal incision sutured. Animals received doses of buprenorphine (.01-.05 mg/kg body weight (BW)) and carprofen (5mg/kg BW) for pain control and rehydrated with .01-.02 mL/g BW of normal saline, prior to withdrawal of anesthesia. During a 4-day recovery period and for the subsequent experimental duration, animals were provided with routine pain medication (buprenorphine .01-.05 mg/kg BW every 12-24 hours and carprofen 5mg/kg BW every 24 hours) and were

maintained in standard housing in the University animal care facility. Animals were closely monitored for signs of respiratory distress, infection, or pain.

Occlusion Protocol

After the surgical recovery period, animals underwent their assigned training intervention for ten consecutive days. All sessions occurred in the morning, and lasted 15 minutes. Prior to the first session, all animals were acclimatized to the study plethysmograph for 15 minutes (Figure 5-2B). During this session, animals were observed and no experimental interventions occurred. For the experimental sessions, the SHAM group returned to the study plethysmograph for 15 minutes daily for observation. The SHAM animals received no interventions during monitored plethysmograph sessions.

The OCCL group received intermittent, total tracheal occlusions during experimental sessions. The cuff pressure to produce reliable, complete tracheal occlusion was determined from previous work. The tracheal cuff was inflated for approximately 5-10 seconds in order to elicit 5-8 strong respiratory attempts, and then deflated for approximately 30 seconds. The occlusion cycle was repeated for a total of 10 minutes. Oscilloscope tracings of the cuff pressure and the plethysmograph were monitored during each session to confirm the onset and removal of occlusions.

Tissue Analysis

One day after the last session, animals were anesthetized with isofluorane gas (2-5% in O_2). Once animals reached a surgical plane of anesthesia, evidenced by lack of corneal reflex or absent limb withdrawal to a paw pinch, they were euthanized by decapitation. The diaphragm, third intercostal and soleus muscles were isolated and extracted. The left side of each muscle was flash-frozen in liquid nitrogen for molecular

analysis. The right-sided muscles equilibrated at 4° C for 3-5 minutes at resting length (195), and then were frozen in isopentane cooled in liquid nitrogen. Specimens were stored in a -70° C freezer until histological analysis.

Fiber phenotype and CSA

To determine the phenotype properties of the muscle tissue, 10-µm transverse serial sections were acquired using a cryostat microtome (Microm HM505, Walldorf, Germany). In order to obtain minimal fiber diameters, the orientation of the sample was adjusted in 5-degree increments, as needed. Cross-sections were confirmed with a low-power dissecting microscope (Omano OM2344, Wirtz, VA). The sections were air-dried at 25° C for 30 minutes. Slides were rinsed in 1X phosphate-buffered saline (PBS) solution and then permeabilized with 0.5% Triton-X100 in 1X PBS. The samples were incubated with primary antibodies for laminin 1:200 (anti-rabbit, IgG, Lab Vision), type I myosin heavy chain 1:15 (anti-mouse A4.840, IgM, Developmental Studies), and type IIa myosin heavy chain 1:50 (anti-mouse SC-71, IgG, Developmental Studies) for 60 minutes, and then rinsed three times for five minutes in 1X PBS. Sections were incubated with secondary antibodies for rhodamine 1:40 (goat-anti-rabbit, Invitrogen), Alexa Fluor 350 1:333 (goat-anti-mouse, IgM, Invitrogen) and Alexa Fluor 488 1:133 (goat-anti-mouse, IgG, Invitrogen) in Pierce's Superblock 1:20 (Pierce Biotechnology, Rockford, IL) and 1X PBS, for 60 minutes in a darkened, humidified tray. Three final rinses for 5 minutes in 1X PBS were then performed. Cover slips were mounted with Vectashield fluorescent mounting medium (Vector Labs, Burlingame, CA) and secured with nitrocellulose lacquer. The A4.840 and SC-71 antibodies generated by Helen M. Blau were obtained from the Developmental Studies Hybridoma Bank developed under

the auspices of the NICHD and maintained by The University of Iowa, Department of Biology, Iowa City, IA 52242.

Samples were visualized using fluorescence microscopy at 100x magnification and N21, GFP, and A4 cube filters. Type I fibers illuminated blue under the A4 filter, type IIa filters fluoresced green using a GFP filter, and type IIb/x fibers remained free of fluorescence. Cell borders were visualized with red fluorescence under the N21 filter. At least five randomly selected images were captured under each filter (Leica DM LB, Solms Germany). The images were encoded and black and white threshold images calculated for fiber CSA using Scion Image (NIH) software. The CSA of each muscle sample was calculated from at least 300 fibers per muscle specimen.

A masked investigator quantified fiber CSA and phenotype proportions. MHC isoform proportions were determined using the encoded images and recorded in a spreadsheet. The area fraction (A_A) for each fiber phenotype was also calculated, to account for the proportion of the CSA consumed by a given MHC isoform. The phenotype A_A accounted for the number of fibers with a given phenotype as well as the CSA of the fibers.

$$\textit{Phenotype } A_A = (\Sigma \textit{ CSA of phenotype})/(\textit{total CSA of all phenotypes}) * 100\%$$

Muscle fiber remodeling

To analyze the extent of inspiratory muscle fiber remodeling associated with each group, 10-µm transverse serial sections were obtained from a cryostat cooled to -20° C (Microm HM505, Walldorf, Germany). Sections were stained with hematoxylin and eosin, and then the specimens were mounted with Permount medium (Fisher Scientific), cover slips applied and secured with a nitrocellulose lacquer. Specimens were visualized with brightfield microscopy (Leica DM LB, Solms Germany) at 400x

magnification. For each animal, twenty images were acquired in all of the study muscles. Digital images of the tissue were encoded, and then analyzed for qualitative evidence of remodeling.

An analysis of morphological remodeling was undertaken using a systematic point-counting technique (162, 196) (Table 3-1). Point-counting was conducted using Adobe Photoshop CS3 software (Adobe Corporation, San Jose CA). Next, a 9x7 point grid was generated by Photoshop and superimposed onto each digital image. Partial fibers within the images were excluded from analysis. At each point-intercept of the grid, underlying tissue at the top-right quadrant was classified into one of nine morphological categories and recorded onto a spreadsheet. An (A_A) was calculated for normal and remodeled muscle fibers, inflammatory cells, and connective tissue.

$$\text{Area fraction } (A_A) = (\Sigma \text{ counts in category})/(\text{total count}) * 100\%$$

A masked investigator completed the morphological analysis. The investigator was trained by an externally-trained scientist (Sunita Mathur, PhD, PT), and then inter-rater reliability of fiber classification was examined using the standardized classification categories and definitions, over identical images. The correlation between the investigator and Dr. Mathur was 0.95.

Myofiber regeneration- embryonic myosin

Slides were air-dried at 25 degrees Celsius for 30 minutes. Slides were quick-rinsed in 1X phosphate-buffered saline (PBS), fixed in 1:1 acetone-methanol solution for five minutes at room temperature, then rinsed three times for five minutes in 1X PBS. Subsequently, slides were blocked with Pierce's Superblock (Pierce Biotechnology, Rockford, IL) for 60 minutes at 25° C, and then rinsed three times for five minutes in 1X PBS. Sections were incubated in primary antibodies for laminin 1:200 (anti-rabbit, IgG,

LabVision) and embryonic myosin heavy chain (eMHC) 1:20 (anti-mouse F1.652, IgG, Developmental Studies) in 10% normal goat serum, and 1X PBS overnight at 4° C. The F1.652 antibody developed by Helen M. Blau was obtained from the Developmental Studies Hybridoma Bank developed under the auspices of the NICHD and maintained by The University of Iowa, Department of Biology, Iowa City, IA 52242.

The next day, each section was rinsed five times using 30 mL of 1X PBS syringe-flushed onto the sample. Secondary antibody incubation occurred with rhodamine 1:500 (goat anti-rabbit, Invitrogen) and Alexa Fluor 488 1:300 (goat anti-mouse, Invitrogen) in 10% normal goat serum and 1X PBS, for two hours at 25° C in the dark. Sections were flush-rinsed five times with a 30 mL syringe of 1X PBS in the dark. Specimens were mounted in Vectashield fluorescent mounting medium with DAPI (Vector Labs, Burlingame, CA) and cover slips secured with nitrocellulose lacquer.

Samples were visualized using fluorescence microscopy at 200x magnification and using N21, GFP and A4 filter cubes. At least five randomly selected images were captured under each filter (Leica DM LB, Solms Germany). The images were encoded and the proportion of eMHC-positive fibers was calculated from at least 150 fibers per muscle specimen. Positive fibers were interpreted to be intensely-fluorescing areas within the exact borders of the sarcolemma. Faintly-fluoresced fibers or areas that fluoresced only a portion of a cell were not counted. For each animal, proportions of eMHC-positive cells were calculated automatically using a spreadsheet.

Protein immunoblotting

We confirmed presence of eMHC in the animals, using a subset of eight animals. The following methods were used to extract protein. Frozen intercostal muscle was minced (~30 mg), placed in a radio-immunoprecipitation assay (RIPA) buffer and

protease inhibitor (1:1000) cocktail, and then triturated using a DAKO mortar and pestle. Then, samples were vortexed and centrifuged at 16,000 G for 20 minutes at 4° C. The supernatant was carefully removed and the remaining pellet discarded. We calculated the concentration of protein in each muscle supernatant against a known standard, using BioRad DC protein assay reagents (BioRad, Hercules, CA). Samples were tested in triplicate and concentration read with a Bio-Rad Microplate Manager plate reader, at a wavelength of 580 nm.

Aliquots of the isolated protein were diluted to equal concentration, combined with LDS buffer and reducing agent, and then incubated at 70 degrees Celsius for 10 minutes. One-dimensional SDS-PAGE was conducted with the Nu-Page mini-gel system and bis-tris 4-12% mini-gel (Invitrogen, Carlsbas, CA), for 40 minutes at 200V. Gels were transferred to a nitrocellulose membrane (35V for one hour), and the membranes were stained with Ponceau S to identify molecular mass markers. Membranes were blocked with 5% milk in TBS-T for one hour, then incubated with primary antibody in a 4° C room overnight (F1.652, 1:50 in milk blocking buffer). After six rinses in TBS-T, a peroxidase-conjugated secondary antibody was added (goat anti-mouse, IgG, 1:2000 dilution, Rockland laboratories, Gilbertsville, PA) and incubated for one hour at room temperature. Six final 5-minute TBS-T rinses were completed. We applied enhanced chemiluminescence (ECL) reagents (luminal substrate and hydrogen peroxide) from Bio-Rad, and then exposed the protein bands with x-ray film. The intensity of the bands was quantified using Image J software (NIH).

Statistical Analysis

The animal demographic characteristics were assessed using an independent t-test. All data were examined to determine whether they met assumptions for normality

and homogeneity of variance. To account for the vastly different baseline fiber compositions between the diaphragm, intercostal, and soleus muscles, immumohistochemical tests were analyzed with separate, repeated-measures analysis of variance (ANOVA) with one within-group factor (MHC isoform: type I, IIa, and IIx/b fibers), and one between-group factor (training: OCCL or SHAM). Diaphragm regional analyses were compared using a 3-way ANOVA, with two within-group factors (region: ventral, medial, dorsal diaphragm and MHC isoform: type I, IIa, and IIx/b fibers), and one between-group factor (training: OCCL or SHAM). A 3-way mixed ANOVA (one within-subjects factor: remodeling category, two between-subjects factors: training group, muscle) compared the training effect on A_A of muscle fiber remodeling. When needed, interactions were assessed using pair-wise comparisons with a Bonferroni correction. Statistical testing for embryonic myosin was completed using the Mann-Whitney U test. For all analyses, the level of significance was established at $p<0.05$.

Table 3-1. Categories for classification of myofiber features determined by point counting.

#	Category	Definition	
0	no count	space, artifact, epimysial connective tissue, nerve, large blood vessels.	no count
1	normal muscle, capillary	polygonal fiber with acidophilic cytoplasm, plasma membrane and peripheral nuclei or capillary (small blood vessel with endothelium only).	normal
2	internal nuclei	fiber with $\geq$ 1 internally located nuclei (sarcoplasm between nucleus and sarcolemma), *8 pixels of sarcoplasm between nucleus and sarcolemma.*	re-modeled
3	small angulated fiber	(a) small fiber ($\leq$ 1/3 the lesser fiber diameter of the five largest fibers in the field) or (b) fibers with "spear-like" extensions or extensions that are less than 45 degrees or (c) fiber with $\geq$ 2 acute angles (< 90^{o})	re-modeled
4	Inflamed, necrotic fiber	fiber with $\geq$ 1 inflammatory cell or necrotic mass of inflammatory cells and muscle debris without plasma membrane.	re-modeled
5	abnormal cytoplasm, lipofuscin	includes: (a) fiber with pale acidophilic peripheral cytoplasm and enlarged peripheral nuclei with or without visible nucleoli, or (b) fiber with pale acidophilic peripheral cytoplasm and deep acidophilic "fuzzy" cytoplasm in the central region, or (c) split or whorled fibers, or (d) vacuoles or (e) uneven cytoplasm staining unrelated to processing or (f) fiber with dull or light gray staining, or (g) cytoplasmic fragmentation or (h) lipofuscin (brown-yellow pigmentation $\geq$ area of a muscle nucleus).	re-modeled
6	inflammatory cell	cell in the interstitium that has a round-shaped nucleus consistent with a monocyte, macrophage, or lymphocyte.	re-modeled
7	collagen or fibroblast	protein fibrils of endomysial or perimysial connective tissue or a cell located in the interstitium with spindle shaped nucleus that is consistent with a fibroblast.	collagen
8	adipocyte	empty space surrounded by cell membrane consistent with size and shape of adipocyte.	adipose

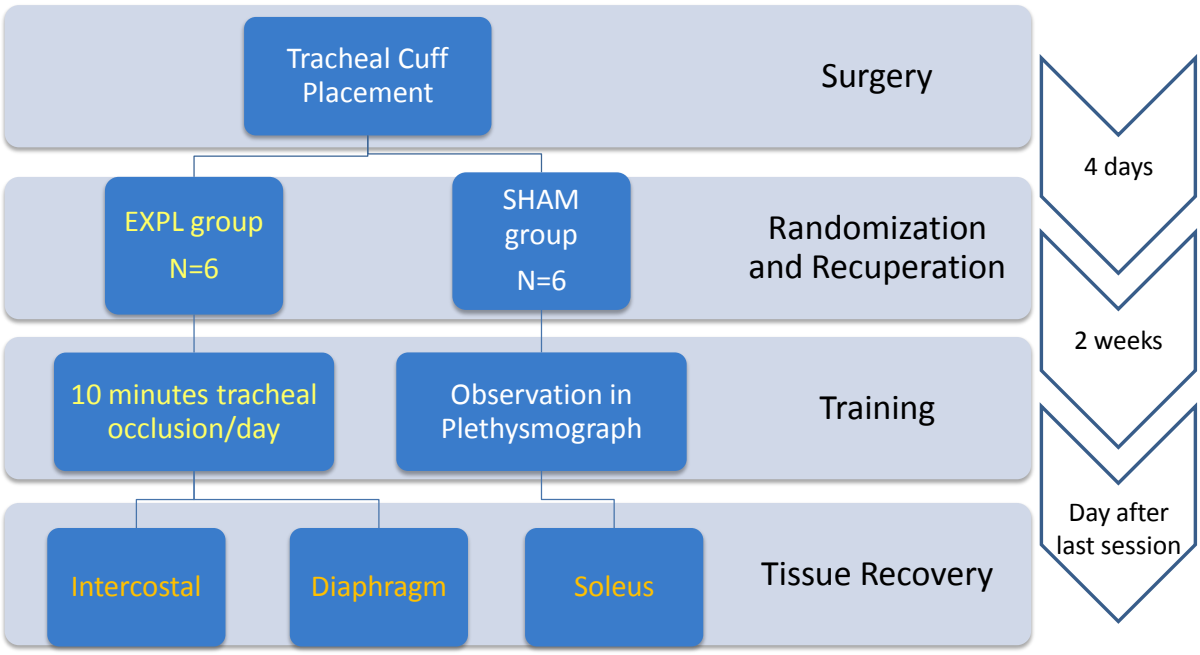

Figure 3-1. Schematic representation of the experimental design.

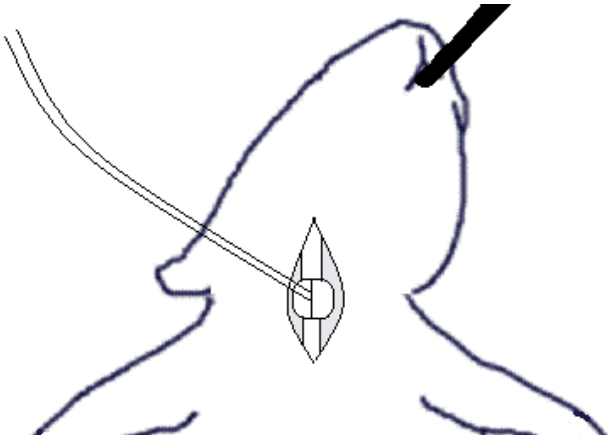

A

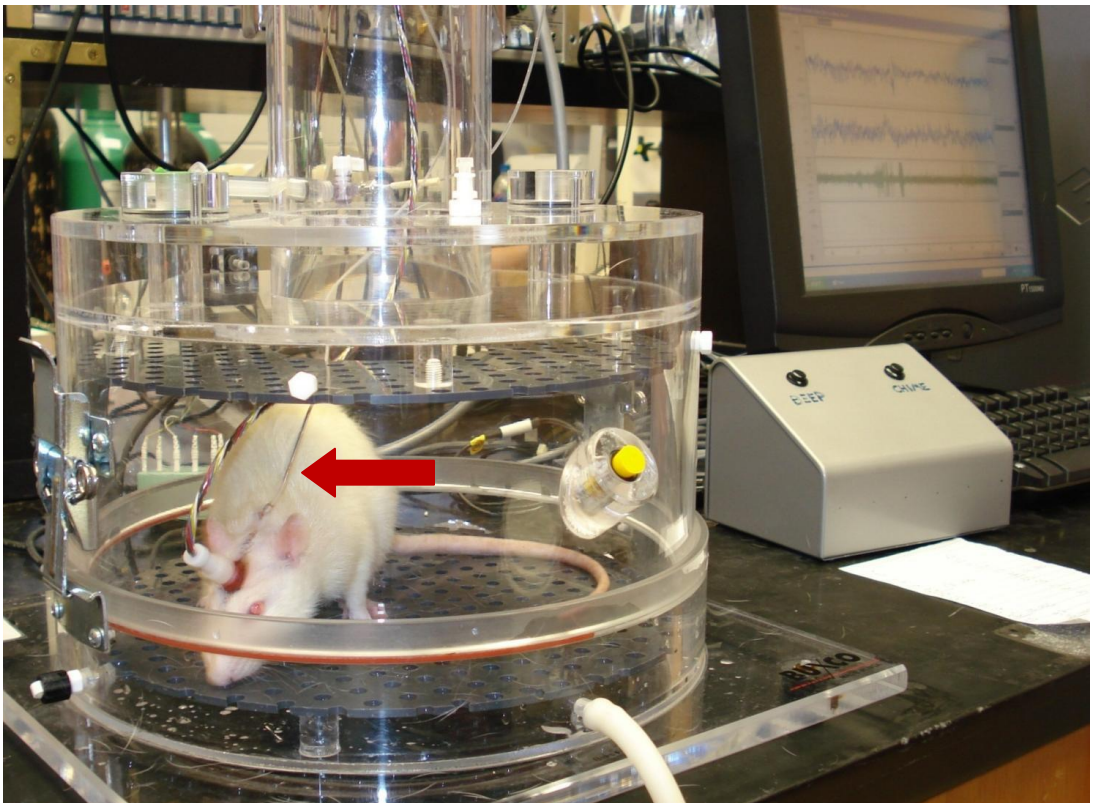

B

Figure 3-2. Experimental apparatus. A. Illustration of the tracheal occluder. B. Experimental sessions were conducted in a plethysmograph, and oscilloscope tracings recorded pressure and volume fluctuations during occlusion. The arrow distinguishes the pressure line to the tracheal cuff.

CHAPTER 4
RESULTS

Of the sixteen animals that underwent occluder placements, complete datasets were obtained from twelve. Two animals did not complete the experimental sessions due to clinical signs of infection in a sham-trained animal (n=1, SHAM) or occluder in an occlusion-trained animal failure (n=1, OCCL), and diaphragm tissue was unavailable in two others (one animal from each group). Therefore, analyses were conducted with n=12 diaphragms, and n=14 intercostal and soleus muscles. Animals in the SHAM group weighed 252 (±48) grams at the study onset and 299 (±35) grams upon conclusion. Animals in the OCCL group weighed 253 (±45) grams at the start of the study and 303 (±16) grams on completion. The animals were 14-week-old littermates, and there were no group differences in the weight or complication rate.

AIM 1- Respiratory Muscle Fiber Hypertrophy

Effect of Tracheal Occlusion on Fiber Cross-Sectional Area

Cross-sectional area of the diaphragm

Tables 4-1 and 4-2 report the cross-sectional area (CSA) of the medial costal diaphragm. Two-way, repeated-measures analysis of variance (ANOVA) was used to examine the effect of training on CSA in the medial costal diaphragm. The data did not meet the assumption of sphericity, (Mauchley's W= .320, p=.005) and data were analyzed using the Greenfield-Geisser and more conservative Lower-Bound sphericity corrections. Using the more conservative Lower-Bound correction, the interaction between fiber type and training group was significant for CSA ($F(2, 20) = 9.066$, $p<.01$). There were no significant main effects for training group. Post-hoc tests indicated that

the CSA of type IIx/b fibers was significantly larger in the OCCL animals than in the SHAM group ($p<.05$). The significant interaction is depicted in Figure 4-1.

Cross-sectional area of the third intercostal

The CSA data for the intercostals are available on Tables 4-1 and 4-3. In the IC muscle, the sphericity assumption was met for repeated measures ANOVA. There was a significant interaction between training group and fiber type ($F(2, 24) = 6.310$, $p<.01$). Post-hoc pair-wise contrast indicated that for the type IIx/b fibers, the CSA was significantly larger in the OCCL group (Figure 4-2). In the OCCL group, the CSA of type I fibers was 11.7% greater, type IIa was 17.9% larger, and type IIx/b was 18.6% greater than the CSA in the SHAM group. CSA measurements in type I and type IIa fibers did not differ between the training groups. Type IIa fibers were larger than type I ($p<.05$), and type IIx/b fibers were significantly larger than both type IIa and type I fibers, ($p<.001$). There was no group main effect.

Cross-sectional area of the soleus

Tables 4-1 and 4-4 report the results of the repeated measures ANOVA for CSA in the soleus muscle. While the interaction between fiber type and training group was not significant ($F(1, 12) = .405$, $p>.05$), there was a significant main effect for fiber type on CSA ($F(1, 12) = 27.176$, $p<.001$). The CSA of type I fibers was larger than type IIa fibers. Group assignment did not influence CSA ($F(1,12) = .002$, $p>.05$).

Regional diaphragm cross-sectional area

The three-way ANOVA with repeated measures was employed to examine regional CSA in the animals, and results are reported in Table 4-5. A Greenhouse-Geiser corrections was utilized to correct violations of the sphericity assumption. A region-phenotype interaction occurred for CSA ($F(1.922, 19.225) = 4.209$, $p<.05$). Post-

hoc tests revealed CSA was larger in the type IIx/b fibers of the medial diaphragm ($F(2,33) = 3.422$, $p<.05$). Overall, there was a significant main effect of MHC isoform on CSA. Fibers identified as type 2x/b were significantly larger than type 1 and type 2a ($p<.001$), regardless of group assignment. The main effect for group was not significant.

Effect of Tracheal Occlusion on Fiber Phenotype

Fiber phenotype of the medial diaphragm

Representative immunohistochemistry images of the diaphragm (Figure 4-3, A and B) illustrate the MHC isoform distributions in the OCCL and SHAM groups. The mixed phenotype composition of the rat medial diaphragm was consistent with other reports (29). The sphericity assumption was met for the repeated-measures ANOVA procedure. The interaction between group assignment and fiber phenotype composition was not significant in the medial costal diaphragm ($F(2, 20) = 1.428$, $p>.05$). In addition, the MHC isoform proportions did not differ between the training groups. The proportion of type IIx/b fibers in the diaphragm was lower than proportions of type I ($p<.005$) or IIa ($p<.05$) fibers. Tables 4-2 and 4-6 detail the medial diaphragm MHC isoform proportions.

The phenotype A_A represents the sampling area occupied by a given myosin heavy chain (MHC) isoform. Phenotype A_A depends upon the number of cells expressing an isoform as well as the fiber CSA. Tables 4-2 and 4-7 provide the A_A of MHC isoforms in the medial costal diaphragm. The diaphragm phenotype A_A data did not meet the assumption of sphericity (Mauchley's $W= .44$, $p=.025$), and within-subjects effects were contrasted using a Greenhouse-Geisser correction. There was no significant interaction between fiber type and training group for phenotype area fraction ($F(1.282) = 2.907$, $p>.05$), although a trend was identified, $p=.10$. Although the main

effect for training was not significant, a strong main effect for fiber type identified that type IIx/b fibers occupied a greater A_A in the diaphragms of all animals, compared to type I or IIa fibers ($p<.001$).

Fiber phenotype of the third intercostal

The third intercostal contains a majority of fast-intermediate or fast-glycolytic fibers, with the balance of the fibers equally divided between slow- and fast-oxidative fibers (Figure 4-3, images C-D). In the intercostals, a Greenhouse-Geiser sphericity correction was used (Mauchley's W= .569, p=.045). The interaction between MHC isoform and training group did not reach significance ($F(1.397, 16.769) = 1.470$, $p>.05$). There was a significant main effect for fiber type on proportion, indicating that type IIx/b fibers were more prevalent in the intercostal muscle samples than either type IIa or type I fibers ($F(1.397, 16.769) = 246.681$, $p<.001$). The proportions of type IIa and type I fibers did not differ from one another. The main effect for training group was not significant. Intercostal phenotype proportions are listed on Tables 4-3 and 4-6.

For fiber phenotype A_A, there was no significant interaction between training group and A_A of the respective MHC isoforms ($F(2, 24) = 1.952$, $p>.05$), and the training groups did not differ. Due to the larger CSA and high prevalence of type IIx/b fibers in the third intercostal muscle, the fiber type main effect for was strongly significant for A_A. Type IIx/b fibers occupied a greater A_A than type I and IIa fibers ($F(2,24) = 1954.258$, $p<.001$). Summaries of A_A in the intercostal tissue are available in Tables 4-3 and 4-7.

Fiber phenotype of the soleus

Immunohistochemistry illustrations of the soleus can be found on Figure 4-3 (images E-F). As a postural hindlimb muscle with a relatively high duty cycle, the soleus was included as an activity-control muscle. In the study sample, the soleus contained an

extremely high proportion of slow, oxidative fibers, consistent with the postural function of the muscle. The interaction between MHC isoform expression and training group was not significant ($F(1,12) = 0.335$, $p>.05$). However, there was a significantly higher proportion of type I slow fibers than type IIa fibers in soleus specimens ($F(1,12) = 969.979$, $p<.001$). No type IIx/b fibers were identified in any of the muscle specimens. The soleus phenotype proportions did not differ between the OCCL and SHAM groups ($F(1,12) = 1.0$, $p>0.05$). Fiber phenotype proportions in the soleus can be found on Table 4-4 and 4-6.

The phenotype A_A for MHC expression is summarized in Tables 4-4 and 4-7. In the SOL, no significant interaction between training group and fiber phenotype occurred ($F(1, 12) = 0.557$, $p>.05$), and there were no A_A differences between the training groups. The A_A occupied by type I fibers was significantly larger than the A_A of type IIa fibers ($F(1, 12) = 1958.441$, $p<.001$).

Regional costal diaphragm expression of fiber phenotype

Table 4-8 depicts regional phenotype proportions in the costal diaphragm. The assumption of sphericity was met for every factor. There was an interaction between the training group, region of the diaphragm, and MHC isoform on phenotype proportion ($F(4,40) = 3.535$, $p<.05$). Analysis of the interaction revealed that the proportion of type IIx/b fibers in the ventral diaphragm was significantly reduced in the SHAM training group ($F(2,20) = 5.333$, $p<0.05$). In all regions of the costal diaphragm, there were fewer type IIx/b fibers, compared to type IIa or type I fibers ($F(2,20) = 13.668$, $p<.001$). A mixed MHC isoform composition was consistent throughout the costal diaphragm.

Table 4-9 illustrates the A_A of regional diaphragm MHC isoforms in the OCCL- and SHAM-trained animals. The sphericity assumption for repeated measures was met. A

significant 3-way interaction was detected between the diaphragm region, fiber phenotype and training group for area fraction (A_A), ($F(4, 40) = 4.683$, $p<.01$). Post-hoc analyses revealed that the A_A of type IIx/b fibers was lower in the ventral diaphragm only in the SHAM-trained animals, compared to the medial region ($F(4,20) = 4.173$, $p<.05$). Although a greater proportion of fibers in the diaphragm expressed oxidative MHC isoforms, the CSA of type IIx/b fibers was larger than the oxidative fibers. As a result, the A_A of type IIx/b fibers was greater than that of type IIa or type I fibers, regardless of the region ($F(2,20) = 53.335$, $p<.001$).

In summary, the results showed type IIx/b fiber hypertrophy of the medial costal diaphragm and intercostal muscles, without training interactions in the soleus. Regional analysis indicated a CSA difference between the medial costal diaphragm and other regions. Additionally, we identified an unanticipated reduction in the expression of type IIx/b fibers of the SHAM-trained ventral costal diaphragm.

AIM 2: Respiratory Muscle Damage and Regeneration

Effect of Tracheal Occlusion on Respiratory Muscle Morphology

The categorical assessment of normal and remodeled muscle in the medial diaphragm, intercostal, and soleus is detailed in Table 4-10, and representative hematoxylin and eosin (H&E) images of each muscle can be found at Figure 4-4. In every muscle group, the majority of fibers were classified as normal. Normal fibers were characterized by polygonal-shaped cells with multiple peripherally-located myonuclei, tightly-arranged fascicles, and limited quantities of endomysial connective tissue or inflammatory cells. Connective tissue consisted of endomysium and perimysium tissue that stained pale pink, or fibroblasts contained within collagen.

There were no significant group differences in the A_A of normal and remodeled muscle tissue and connective tissue. The diaphragms of all animals contained a lower A_A of normal tissue and greater A_A of connective tissue, compared to the intercostals and soleus muscles ($p<.001$). A significantly smaller A_A of abnormal fibers was identified in the soleus ($p<.001$). Many diaphragm images contained one or more abnormal features, suggestive of remodeling tissue.

Tissue remodeling consisted of connective tissue, internally-nucleated fibers, small or angular fibers, inflamed fibers, or inflammatory cells. Inflammatory cells were identified as round basophilic cells with dark round or multi-lobar nuclei (Figure 4-5, black arrows). Inflammatory cells could be found in the interstitium and were occasionally identified in association with infiltration of connective tissue (Figure 4-5, white arrows) or an inflamed or necrotic myofiber. Inflamed cells were distinguished by the presence of one or more inflammatory cells, a disrupted plasma membrane and muscle fiber fragments (Figure 4-5, yellow arrows). Internally-nucleated fibers contained one or more myonuclei located at least eight pixels inside the plasma membrane (Figure 4-5, green arrows). Small or angulated fibers were characterized by spindle-shaped or spear-like projections or a diameter less than 1/3 the diameter of the five largest fibers in a field (Figure 4-5, blue arrows).

For each muscle tested, the A_A for internally-nucleated fibers and inflammatory cells exceeded those of small, angular fibers and inflamed or necrotic fibers ($p<.01$, all contrasts). The most common diaphragm remodeling attribute was inflammatory cell infiltration ($A_A = 1.4\pm0.2\%$), while internally-nucleated fibers occurred most frequently in

the intercostal muscles (A_A = 1.5±0.4%). The diaphragms contained larger proportions of inflamed or necrotic tissue than the intercostal or soleus muscles.

Morphological assessment of the medial costal diaphragm

The majority of diaphragm tissue consisted of normal muscle fibers. There was significantly less connective tissue than normal muscle (.105 ± .013 versus .866 ± .012, p<.001), and the A_A of remodeled tissue was significantly smaller than the A_A of connective tissue (.029 ± .005 versus .105 ± .013, p<.005). Of the remodeling attributes in the diaphragm, inflammatory cells occupied the largest A_A (.014 ± .002), followed closely by internally-nucleated fibers (.012 ± .002). Small, angular fibers and inflamed necrotic fibers were identified relatively less often (p<.05). Group assignment did not significantly affect diaphragm A_A composition. Tables 4-10 and 4-11 detail the A_A of remodeled cells in the medial diaphragm.

Morphological assessment of the third parasternal intercostal

The third parasternal intercostal muscle is an accessory inspiratory muscle that is recruited during quiet breathing. Morphology classification indicated that the majority of the intercostal muscle was comprised of normal muscle fibers (91.6±0.8%, pooled, F(2, 20) = 209.719, p<.001). Normal muscle occupied a significantly larger A_A than connective tissue or remodeled fibers (p<.001), while the A_A of connective tissue exceeded the A_A of remodeled muscle fibers (p<.001). Only minute quantities of remodeled tissue were identified. Internally-nucleated cells occupied the largest A_A of remodeled fibers (pooled proportion: .01 ± .001). By contrast, inflamed necrotic fibers occupied a significantly lower proportion of the examined tissue (p<.001). Tables 4-10 and 4-11 list the remodeling features of the intercostal.

Morphological assessment of the soleus

In the soleus muscle, the A_A majority consisted of normal muscle fibers. A significant main effect for category revealed that the A_A for normal muscle exceeded that of connective tissue, and the A_A of connective tissue was larger than the A_A of abnormal tissue (.916 ± .006 versus .071 ± .005 versus .013 ± .002, p<.001). There were no significant group differences. A closer examination of soleus tissue adaptation illustrated that the most common remodeling feature was inflammatory cells (.01 ± .001). Inflammatory cells occupied a significantly greater A_A in the soleus than inflamed fibers, the most infrequent remodeling category (p<.001). Tables 4-10 and 4-11 report the remodeling attributes of the soleus.

Morphological assessment of the regional diaphragm

Table 4-12 summarizes the A_A of normal, remodeled, and connective tissue in the costal diaphragm regions. Mauchley's test of sphericity indicated that the category descriptors failed to meet the assumption of sphericity (Mauchley's D(2) = .308, p=.009), and a Greenhouse-Geiser correction was employed (corrected ε = .591). The interactions between group assignment, tissue classification, and diaphragm region were not significant. There was a significant main effect of fiber classification for tissue A_A (F(1.182, 17.546) = 1619.122, p<.001): normal tissue exceeded the prevalence of connective tissue or remodeled cells. Group assignment had no effect on remodeling.

In each region of the costal diaphragm, the majority of cells were classified as normal muscle fibers. Most diaphragm images contained at least one abnormal feature. Table 4-13 summarizes the A_A of each remodeling characteristic in the costal diaphragm regions. The most common remodeling category in any region was presence of inflammatory cells. Inflammatory cells occupied a significantly greater A_A, compared

to other remodeling categories ($p<.005$). However, no remodeling characteristic occupied an A_A that exceeded 3%.

Effect of Tracheal Occlusion on Muscle Fiber Regeneration

Embryonic myosin expression in the diaphragm

The Kolmogorov-Smirnov test (D) was used with a Lillefors significance correction, in order to determine whether the data were normally distributed. The embryonic myosin (eMHC) proportions for the SHAM-trained diaphragm ($D(6) = .299$, ns) did not significantly deviate from normality. On the other hand, the distribution in the OCCL group was significantly non-normal ($D(6) = .326$, $p < .05$). Moreover, Shapiro-Wilk tests confirmed the sample distributions were significantly non-normal. Therefore, non-parametric data analyses were conducted, and the results reported as median/inter-quartile range.

A representative image of eMHC-positive fibers in the diaphragm is depicted in Figure 4-6, image A. The Mann-Whitney test indicated that proportions of eMHC-positive fibers were consistent with control levels reported in the literature (197) and did not significantly differ between the groups ($Z=.321$, $p>.05$). Table 4-14 and Figure 4-7 list the proportions of eMHC-positive fibers in the medial diaphragm.

Embryonic myosin expression in the third intercostal

Embryonic myosin expression in the third parasternal intercostal is depicted in Figure 4-6B and summarized in Table 4-14 and Figure 4-7. The CSA of eMHC-positive fibers in the intercostal muscles was small ($465\pm78\ \mu m^2$). According to the Kolmogorov-Smirnov and Shapiro-Wilk tests, the assumption of normality was not met in the dataset. In the 3rd intercostal muscle, a Mann-Whitney U test indicated that eMHC-positive fibers were more prevalent in the OCCL animals ($Z = -2.128$, $p<0.05$).

We examined the presence of eMHC protein in the intercostal tissue with Western Blot (Figure 4-8). Analysis revealed small, distinct bands at 200kDa that coincided with the limited expression of eMHC seen on immunohistological exam. The signal intensity tended to be larger in the OCCL animals, but this difference was not significant (p=.23).

Embryonic myosin expression in the soleus

Figure 4-6C depicts an example of an eMHC-positive fiber located in the soleus. Significant Kolmogorov-Smirnov and Shapiro-Wilk tests indicated that the dataset was non-normally distributed. Mann-Whitney U test showed no differences in the proportion of eMHC-positive fibers in the soleus ($z = -.571$, $p > .05$). Soleus expression of embryonic myosin approximated zero in this sample (Table 4-14 and Figure 4-7).

Table 4-1. Histological cross-sectional area assessment of the medial costal diaphragm, third parasternal intercostals, and soleus in sham-occluded animals and animals treated with intermittent tracheal occlusion. The type IIx/b fibers in the medial costal diaphragm and intercostals were larger in occluded animals.

	Type I fibers	Type IIa fibers	Type IIx/b fibers
Medial diaphragm*			
SHAM	1358 ± 45	1456 ± 83	3278 ± 233
OCCL	1480 ± 97	1599 ± 119	4141 ± 159*
3rd parasternal intercostal #			
SHAM	1350 ± 136	1513 ± 127	3738 ± 183
OCCL	1464 ± 79	1757 ± 122	4397 ± 153#
Soleus			
SHAM	2406 ± 116	1970 ± 55	-
OCCL	2505 ± 165	1864 ± 228	-

Values are mean ±SE.

* Significant interaction in diaphragm: increased type IIx/b CSA in OCCL animals, $p<.01$

#Significant interaction in intercostals: increased type IIx/b CSA in OCCL animals, $p<.01$

Table 4-2. Histological remodeling of the medial costal diaphragm. Phenotype proportion, cross-sectional area and area fraction of the medial costal diaphragm in sham-occluded animals and animals treated with intermittent tracheal occlusion.

	Type I fibers	Type IIa fibers	Type IIx/b fibers
		Fiber count proportion∞	
SHAM	0.34 ± 0.03	0.37 ± 0.01	0.29 ± 0.03
OCCL	0.40 ± 0.03	0.36 ± 0.03	0.24 ± 0.01
		Cross-sectional area, μm^2 *	
SHAM	1358 ± 45	1456 ± 83	3278 ± 233
OCCL	1480 ± 97	1599 ± 119	4141 ± 159
		Phenotype area fraction †	
SHAM	0.22 ± 0.02	0.27 ± 0.01	0.51 ± 0.03
OCCL	0.29 ± 0.02	0.29 ± 0.03	0.42 ± 0.04

Values are mean ±SE.

∞Significant phenotype main effect for proportion: decreased proportion of type IIx/b fibers, $p<.005$

* Significant interaction for CSA: increased type IIx/b CSA in OCCL animals, $p<.01$

†Significant phenotype main effect for A_A: increased A_A of type IIx/b fibers, $p<.001$

Table 4-3. Histological assessment of the third parasternal intercostals. Phenotype proportion, cross-sectional area and area fraction of the third parasternal intercostals in sham-occluded animals and animals treated with intermittent tracheal occlusion.

	Type I Fibers	Type IIa Fibers	Type IIx/b Fibers
		Fiber count proportion †	
SHAM	0.12 ± 0.02	0.21 ± 0.01	0.67 ± 0.02
OCCL	0.19 ± 0.03	0.17 ± 0.02	0.64 ± 0.03
		Cross-sectional area, μm^2 #	
SHAM	1350 ± 136	1513 ± 127	3738 ± 183
OCCL	1464 ± 79	1757 ± 122	4397 ± 153
		Phenotype area fraction *	
SHAM	0.05 ± 0.01	0.11 ± 0.01	0.84 ± 0.02
OCCL	0.08 ± 0.01	0.08 ± 0.01	0.84 ± 0.02

Values are mean ±SE.

†Significant phenotype main effect for fiber proportion: increased proportion of type IIx/b fibers, $p<.001$

#Significant interaction for CSA: increased type IIx/b CSA in OCCL animals, $p<.01$

*Significant phenotype main effect for A_A: increased A_A of type IIx/b fibers, $p<.001$

Table 4-4. Histological assessment of the soleus muscles. Phenotype proportion, cross-sectional area and area fraction of the soleus muscle in sham-occluded animals and animals treated with intermittent tracheal occlusion.

	Type I fibers	Type IIa fibers	Type IIx/b fibers
		Fiber count proportion ∞	
SHAM	0.92 ± 0.02	0.08 ± 0.02	-
OCCL	0.94 ± 0.02	0.06 ± 0.01	-
		Cross-sectional area, μm^2	
SHAM	2406 ± 116	1970 ± 55	-
OCCL	2505 ± 165	1864 ± 228	-
		Phenotype area fraction †	
SHAM	0.93 ± 0.02	0.07 ± 0.02	-
OCCL	0.95 ± 0.01	0.05 ± 0.01	-

Values are mean ±SE.

∞Significant phenotype main effect for fiber proportion: increased proportion of type I fibers, $p<.001$

†Significant phenotype main effect for A_A: increased A_A of type I fibers, $p<.001$

Table 4-5. Cross-sectional area assessment of the dorsal, medial and ventral costal diaphragm in sham-occluded animals and animals treated with intermittent tracheal occlusion.

	Type I fibers	Type IIa fibers	Type IIx/b fibers
Dorsal diaphragm (μm^2)			
SHAM	1347 ± 109	1429 ± 130	3296 ± 245
OCCL	1233 ± 91	1349 ± 131	3103 ± 190
Medial diaphragm (μm^2)			
SHAM	1358 ± 45	1456 ± 83	3278 ± 233
OCCL	1480 ± 97	1599 ± 119	4141 ± 159 *
Ventral diaphragm (μm^2)			
SHAM	1344 ± 124	1379 ± 128	2848 ± 305
OCCL	1398 ± 138	1391 ± 101	3249 ± 294

Values are mean ±SE.

* Significant region-phenotype interaction: $p<0.05$ versus the SHAM condition.

Table 4-6. Proportion of fiber phenotype expression in the respiratory muscles.

	Type I fibers	Type IIa fibers	Type IIx/b fibers
Medial diaphragm $^{\infty}$			
SHAM	0.34 ± 0.03	0.37 ± 0.01	0.29 ± 0.03
OCCL	0.40 ± 0.03	0.36 ± 0.03	0.24 ± 0.01
3rd parasternal intercostal †			
SHAM	0.12 ± 0.03	0.21 ± 0.01	0.67 ± 0.02
OCCL	0.19 ± 0.03	0.17 ± 0.01	0.64 ± 0.02
Soleus *			
SHAM	0.92 ± 0.02	0.08 ± 0.02	-
OCCL	0.94 ± 0.02	0.06 ± 0.02	-

Values are mean ±SE.

$^{\infty}$Significant main effect in diaphragm: decreased proportion of type IIx/b fibers, $p<.005$

†Significant main effect in intercostal: increased proportion of type IIx/b fibers, $p<.001$

*Significant main effect in soleus: increased proportion of type I fibers, $p<.001$

Table 4-7. Area fraction of fiber phenotype expression in the respiratory muscles.

	Type I fibers	Type IIa fibers	Type IIx/b fibers
Medial diaphragm *			
SHAM	0.22 ± 0.02	0.27 ± 0.01	0.51 ± 0.03
OCCL	0.28 ± 0.02	0.29 ± 0.03	0.42 ± 0.04
3rd parasternal intercostal #			
SHAM	0.05 ± 0.01	0.11 ± 0.01	0.84 ± 0.02
OCCL	0.08 ± 0.01	0.08 ± 0.01	0.84 ± 0.02
Soleus †			
SHAM	0.93 ± 0.02	0.07 ± 0.02	-
OCCL	0.95 ± 0.02	0.05 ± 0.02	-

Values are mean ±SE.
*Significant main effect for diaphragm: increased A_A of type IIx/b fibers, p<.001
#Significant interaction for intercostal: increased A_A of type IIx/b fibers, p<.001
†Significant main effect for soleus: increased A_A of type I fibers, p<.001

Table 4-8. Regional diaphragm phenotype proportions. The proportion of type IIx/b fibers was greater in the sham-occluded ventral diaphragm, compared to the other groups.

	Type I fibers	Type IIa fibers	Type IIx/b fibers
Dorsal diaphragm			
SHAM	0.37 ± 0.02	0.35 ± 0.01	0.26 ± 0.01
OCCL	0.37 ± 0.03	0.37 ± 0.03	0.29 ± 0.02
Medial diaphragm			
SHAM	0.34 ± 0.03	0.37 ± 0.01	0.29 ± 0.03
OCCL	0.40 ± 0.03	0.36 ± 0.03	0.24 ± 0.01
Ventral diaphragm			
SHAM	0.40 ± 0.03	0.37 ± 0.03	0.23 ± 0.01*
OCCL	0.35 ± 0.02	0.35 ± 0.03	0.30 ± 0.03

Values are mean ±SE.
* Significant 3-way interaction: p<0.05 versus the OCCL condition.

Table 4-9. Regional diaphragm phenotype area fractions. Histological assessment of phenotype proportion of the dorsal, medial, and ventral costal diaphragm in sham-occluded animals and animals treated with intermittent tracheal occlusion.

	Type I fibers	Type IIa fibers	Type IIx/b fibers
Dorsal Diaphragm			
SHAM	0.27 ± 0.03	0.24 ± 0.03	0.49 ± 0.04
OCCL	0.25 ± 0.03	0.28 ± 0.03	0.46 ± 0.03
Medial Diaphragm			
SHAM	0.22 ± 0.02	0.27 ± 0.02	0.51 ± 0.04
OCCL	0.28 ± 0.02	0.29 ± 0.02	0.42 ± 0.04
Ventral Diaphragm			
SHAM	0.32 ± 0.02	0.29 ± 0.03	0.39 ± 0.04[#]
OCCL	0.25 ± 0.03	0.25 ± 0.02	0.50 ± 0.03

Values are mean ±SE.
[#] Significant 3-way interaction: $p<0.01$ versus the OCCL condition

Table 4-10. Quantitative assessment of fiber remodeling in the respiratory muscles. Numbers represent area fractions of normal fibers, remodeled fibers or connective tissue in sham-occluded animals and animals treated with intermittent tracheal occlusion.

	Normal fibers[†]	Remodeled fibers[†]	Connective fissue[†]
Medial diaphragm*			
SHAM	0.867 ± 0.051	0.028 ± 0.008	0.103 ± 0.060
OCCL	0.864 ± 0.026	0.030 ± 0.003	0.108 ± 0.027
3rd parasternal intercostal			
SHAM	0.914 ± 0.004	0.018 ± 0.002	0.068 ± 0.005
OCCL	0.918 ± 0.003	0.032 ± 0.004	0.051 ± 0.003
Soleus [#]			
SHAM	0.917 ± 0.007	0.008 ± 0.007	0.075 ± 0.005
OCCL	0.914 ± 0.010	0.018 ± 0.007	0.068 ± 0.008

[†]$p<.001$Significant main effect for category: differences between A_A of normal, remodeled and connective tissue
[#]$p<.001$: Significantly lower A_A of remodeled fibers in soleus muscle
*$p<.001$: Significantly greater A_A of connective tissue in diaphragm muscle

Table 4-11. Area fraction (A_A) of abnormal cells in the diaphragm, intercostal, and soleus muscles.

	Internal nuclei	Small, angular fibers	Inflamed, necrotic fibers	Inflammatory cells
Medial diaphragm*				
SHAM	0.014 ± 0.003	0.005 ± 0.002	0.006 ± 0.002	0.013 ± 0.003
OCCL	0.010 ± 0.003	0.007 ± 0.002	0.005 ± 0.002	0.015 ± 0.003
Third intercostal†				
SHAM	0.009 ± 0.004	0.001 ± 0.000	0.000 ± 0.000	0.012 ± 0.004
OCCL	0.021 ± 0.004	0.001 ± 0.000	0.001 ± 0.000	0.009 ± 0.004
Soleus#				
SHAM	0.002 ± 0.002	0.006 ± 0.003	0.000 ± 0.000	0.009 ± 0.002
OCCL	0.004 ± 0.002	0.003 ± 0.003	0.000 ± 0.000	0.010 ± 0.002

Values are mean ±SE.
* Significant main effect for category in diaphragm: inflammatory cells versus internal nuclei, small/angular fibers, and inflamed/necrotic fibers, $p<.05$.
† A_A Internal nuclei of intercostal significantly greater than inflamed-necrotic A_A: $p<.001$
# A_A Inflammatory cells of soleus significantly greater than inflamed-necrotic A_A: $p<.001$

Table 4-12. Quantitative assessment of fiber remodeling in the regions of the costal diaphragm. Numbers represent area fractions of normal fibers, remodeled fibers or connective tissue.

	Normal fibers †	Remodeled fibers	Connective tissue
Dorsal diaphragm			
SHAM	0.833 ± 0.009	0.048 ± 0.004	0.090 ± 0.003
OCCL	0.827 ± 0.019	0.050 ± 0.008	0.095 ± 0.007
Medial diaphragm			
SHAM	0.853 ± 0.022	0.040 ± 0.009	0.107 ± 0.030
OCCL	0.855 ± 0.010	0.037 ± 0.007	0.108 ± 0.011
Ventral diaphragm			
SHAM	0.833 ± 0.017	0.049 ± 0.008	0.092 ± 0.015
OCCL	0.803 ± 0.038	0.066 ± 0.020	0.103 ± 0.016

Values are mean ±SE.
† Significant main effect for category: normal>connective tissue>remodeled fibers ($p<0.001$ versus other categories)

Table 4-13. Area fraction of abnormal cells in the regions of the costal diaphragm. The prevalence of inflammatory cells was significantly greater than other remodeling characteristics.

	Internal nuclei	Small, angular fibers	Inflamed, necrotic fibers	Inflammatory cells *
Dorsal diaphragm				
SHAM	0.010 ± 0.004	0.002 ± 0.004	0.005 ± 0.002	0.028 ± 0.005
OCCL	0.012 ± 0.004	0.007 ± 0.003	0.006 ± 0.002	0.028 ± 0.004
Medial diaphragm				
SHAM	0.013 ± 0.004	0.005 ± 0.002	0.006 ± 0.013	0.014 ± 0.003
OCCL	0.010 ± 0.003	0.864 ± 0.026	0.005 ± 0.002	0.015 ± 0.003
Ventral diaphragm				
SHAM	0.012 ± 0.005	0.002 ± 0.002	0.008 ± 0.012	0.028 ± 0.004
OCCL	0.012 ± 0.005	0.005 ± 0.002	0.023 ± 0.011	0.029 ± 0.003

Values are mean ±SE.
* Significant main effect: $p<0.05$ versus internal nuclei, small/angular fibers, and inflamed/necrotic fibers

Table 4-14. Embryonic myosin-positive fibers in the respiratory muscles. A significantly greater percentage of positive fibers was present in the intercostal muscles of the occluded animals.

	Embryonic myosin-positive fibers
Medial Diaphragm	
SHAM	0.42 (0.36 -0.60)%
OCCL	0.94 (0.00 -1.00)%
3rd Parasternal Intercostal	
SHAM	0.00 (0.00 - 0.63)%
OCCL	1.20 (0.68 - 3.37)% *
Soleus	
SHAM	0.00 (0.00 – 1.51)%
OCCL	0.98 (0.00 – 1.31)%

Note: values are median ±interquartile range.
* $p<0.05$ versus the SHAM condition

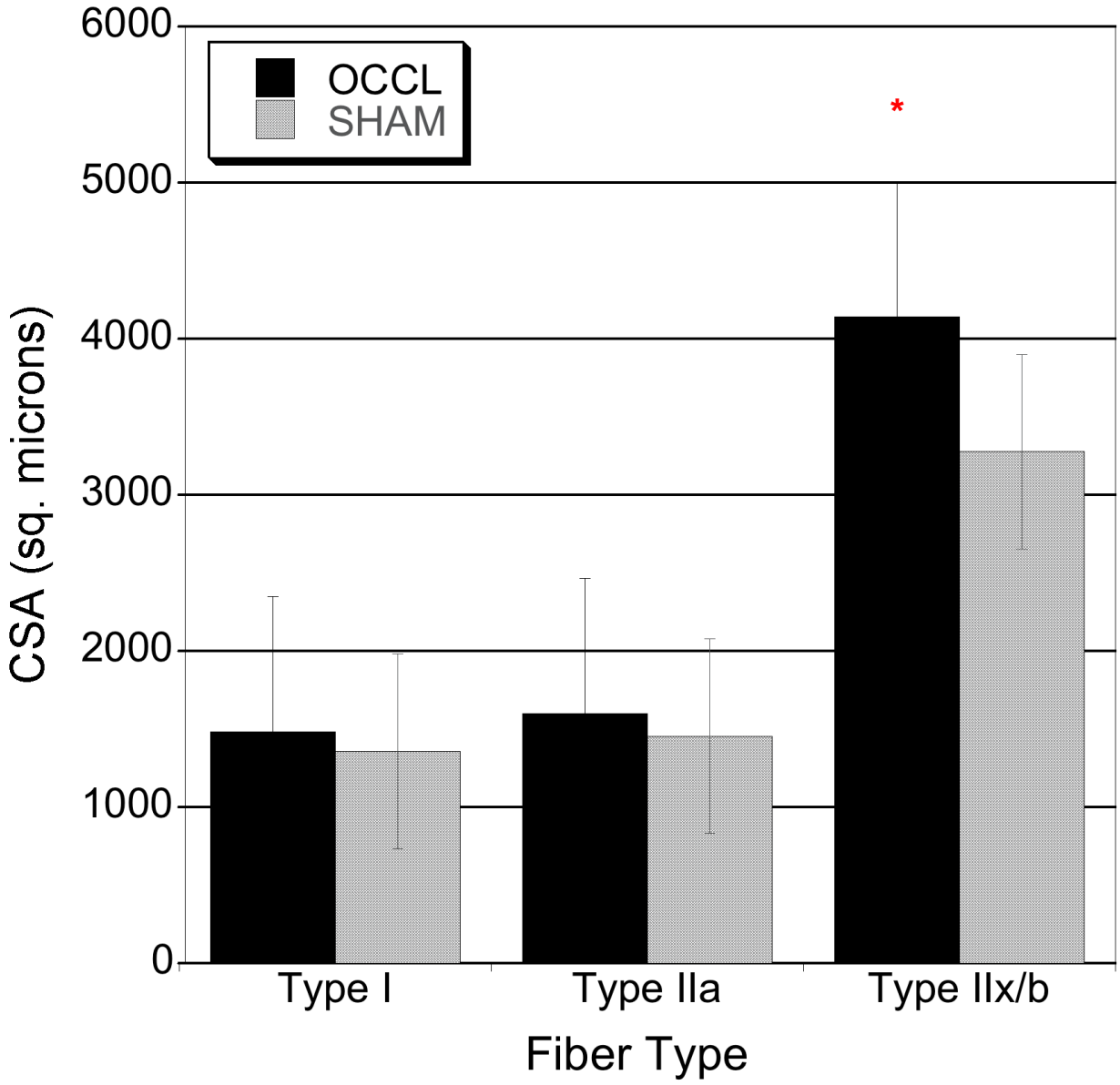

Figure 4-1. Cross-sectional area (CSA) of the medial costal diaphragm. The CSA of type IIx/b fibers was significantly greater in the occluded group (ANOVA, *p<.01).

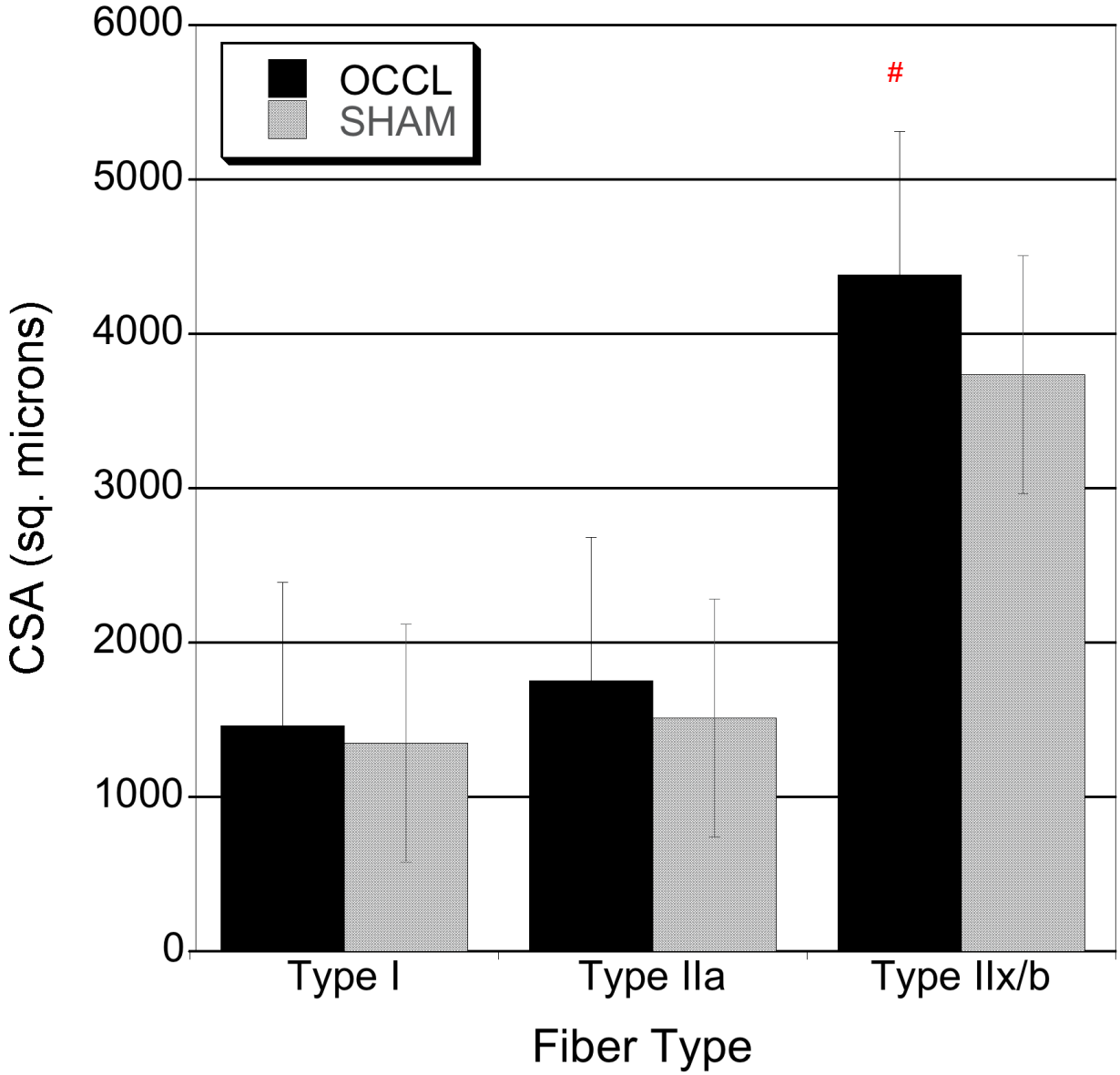

Figure 4-2. Fiber CSA in the third parasternal intercostal muscles. The CSA was significantly greater in the type IIx/b fibers of the occluded animals (ANOVA, $^{\#}p<.01$).

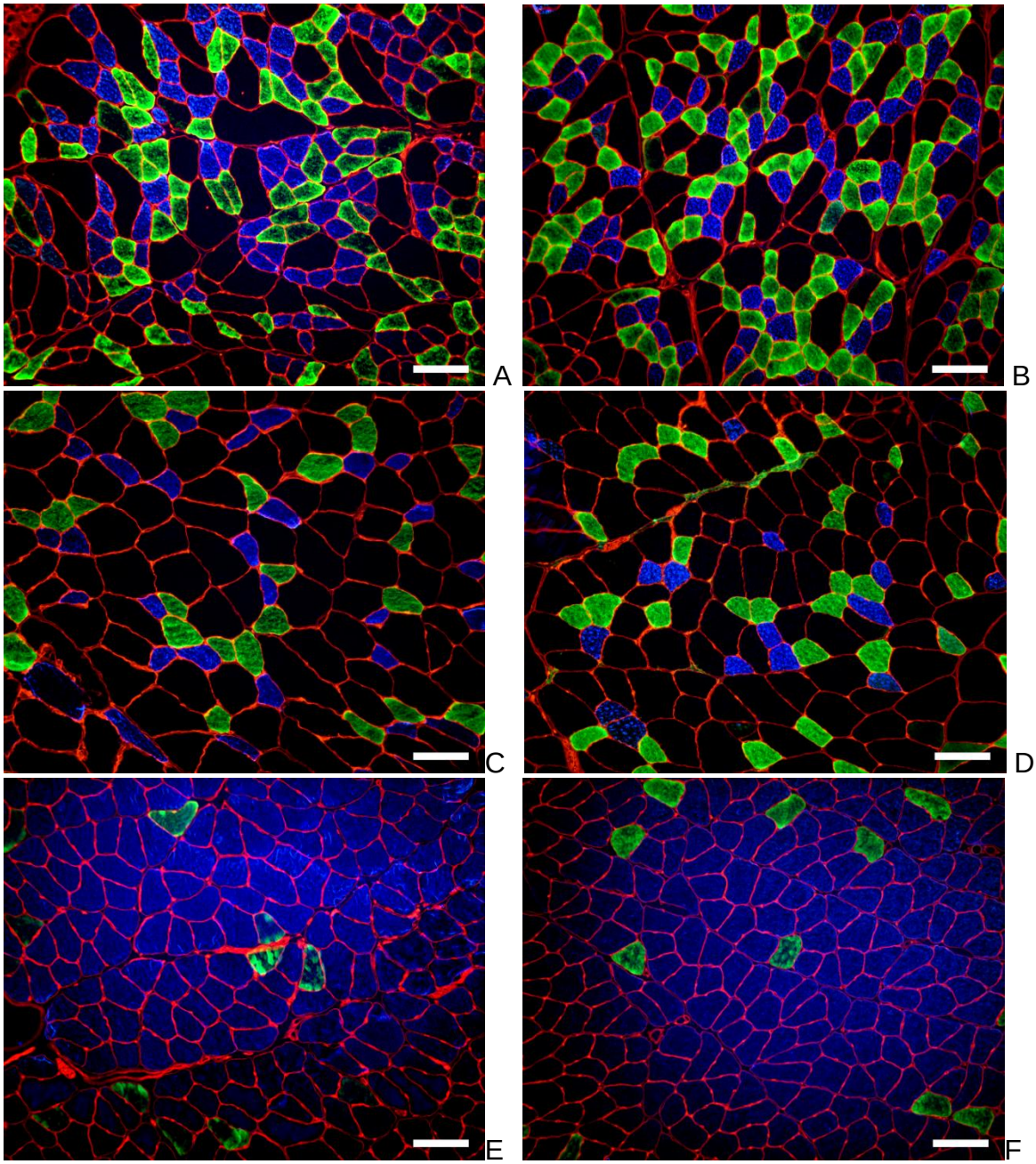

Figure 4-3. Diaphragm, intercostal, and soleus muscle immunohistochemistry for myosin heavy chain isoform. A). Diaphragm from OCCL animal. B). Diaphragm from SHAM animal. C). Third intercostal from OCCL animal. D). Third intercostal from SHAM animal. E). Soleus from OCCL animal. F). Soleus from SHAM animal. Type I fibers fluoresce blue, type IIa illuminate green, and type IIx/b fibers remain free of fluorescence. Images were captured with 40X magnification and 10X objective. Scale bar represents 100 µm.

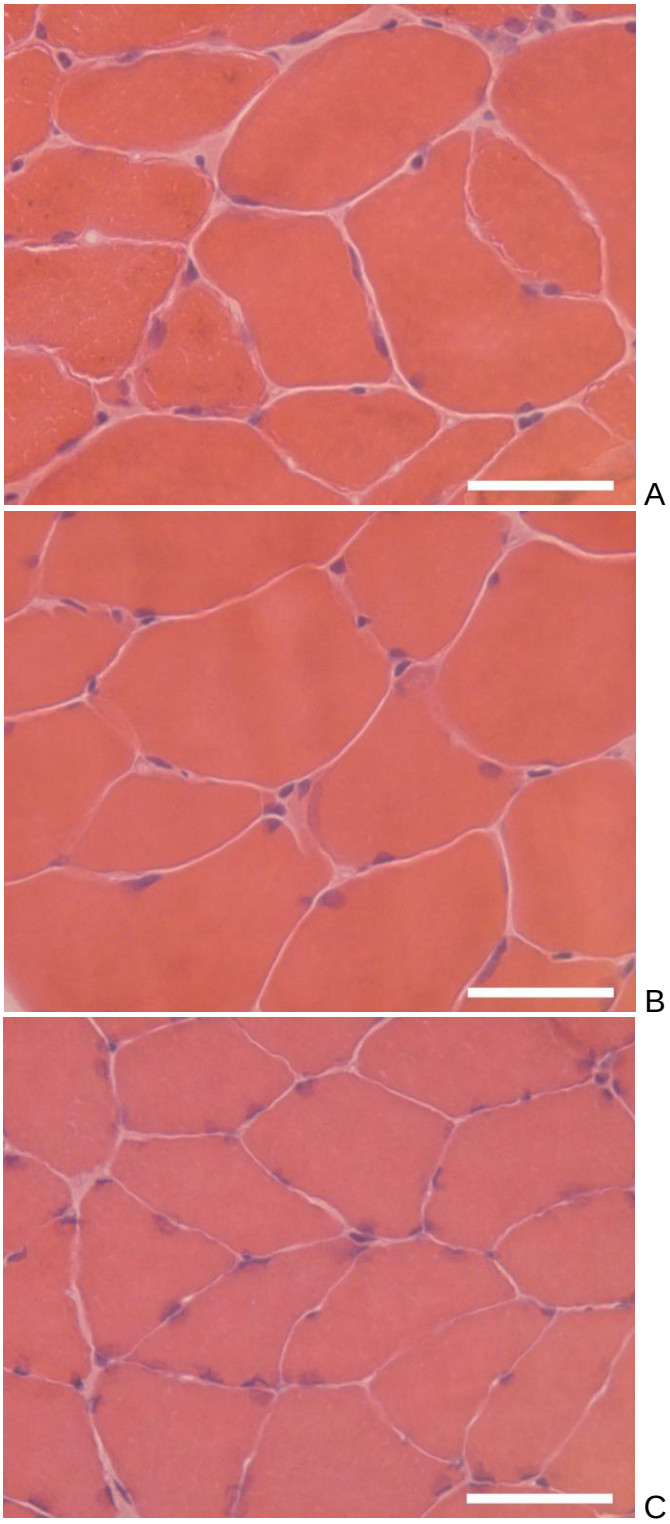

Figure 4-4. Hematoxylin and eosin-stained images. A) Diaphragm, B) 3rd Parasternal Intercostals, C) Soleus. Images were captured with 40X magnification and 10X objective, scale bar represents 50 µm.

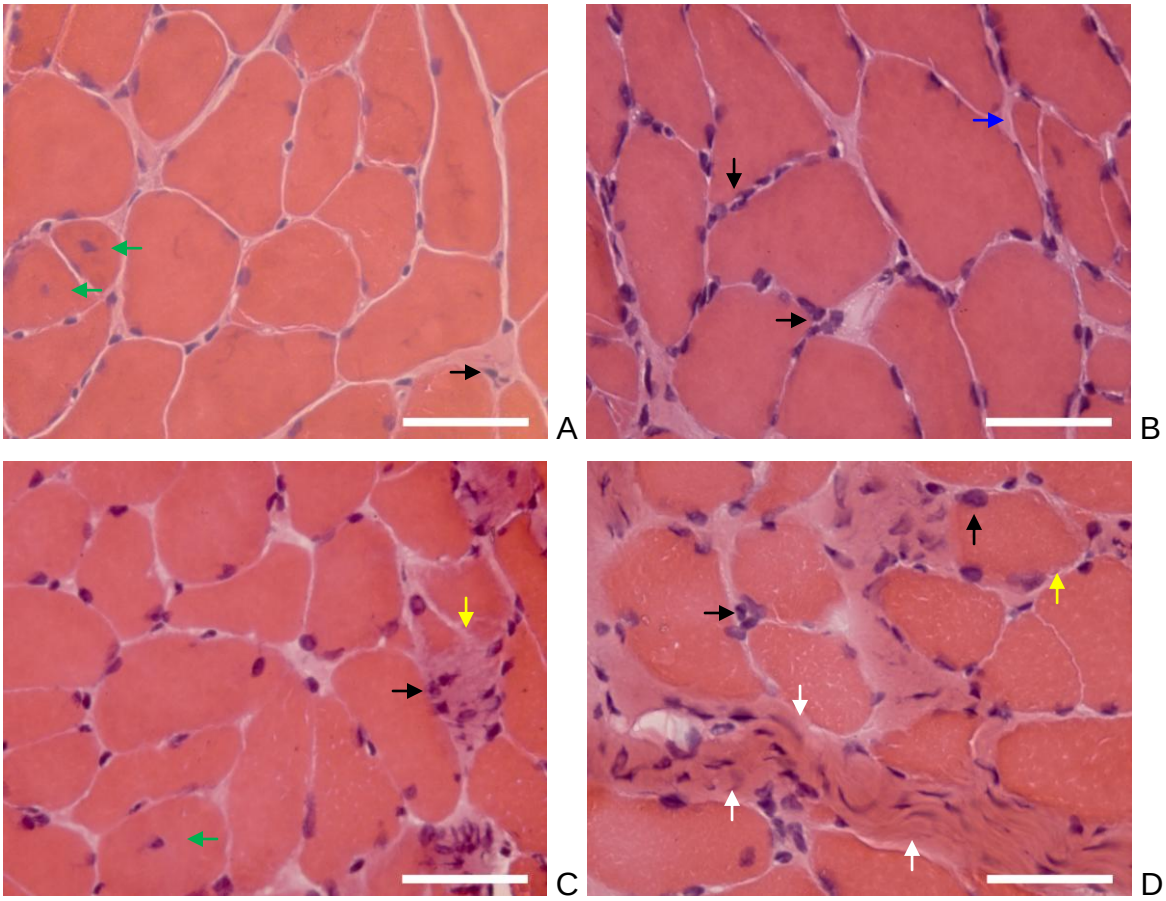

Figure 4-5. Categories of fiber remodeling in the diaphragms of the experimental sample. Color-coded arrows highlight inflammatory cells (black), collagen/fibroblasts (white), inflamed or necrotic tissue (yellow), D) internally-nucleated fibers (green) and small round or angular fibers (blue). Images were captured with 40X magnification and 10X objective, scale bar represents excursion 50 µm.

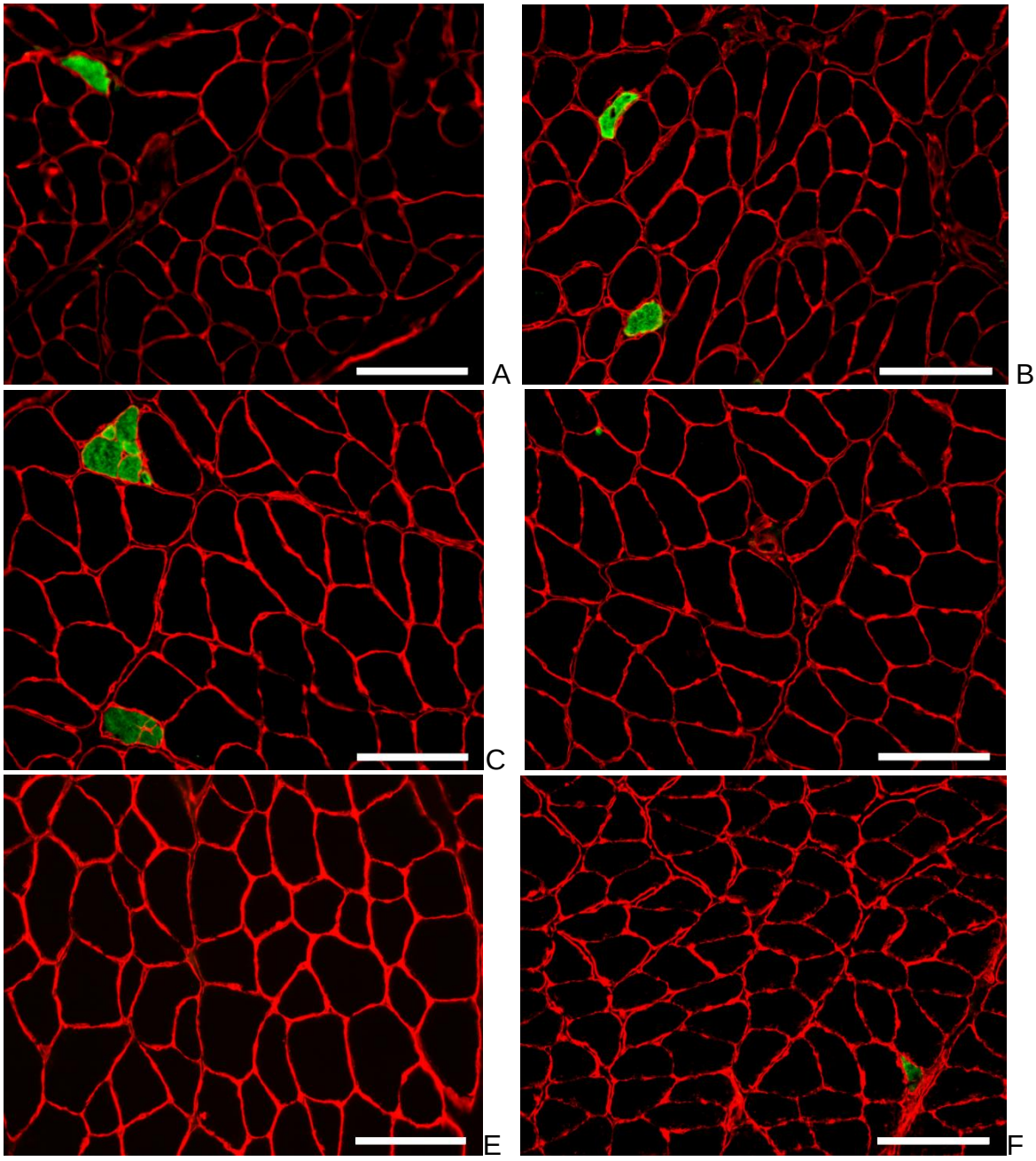

Figure 4-6. Embryonic myosin-positive cells. A). Diaphragm from OCCL animal. B). Diaphragm from SHAM animal. C). Third intercostal from OCCL animal. D). Third intercostal from SHAM animal. E). Soleus from OCCL animal. F). Soleus from SHAM animal.. Positive cells fluoresce green. Images were captured with 20X magnification and 10X objective, scale bar represents 100 µm.

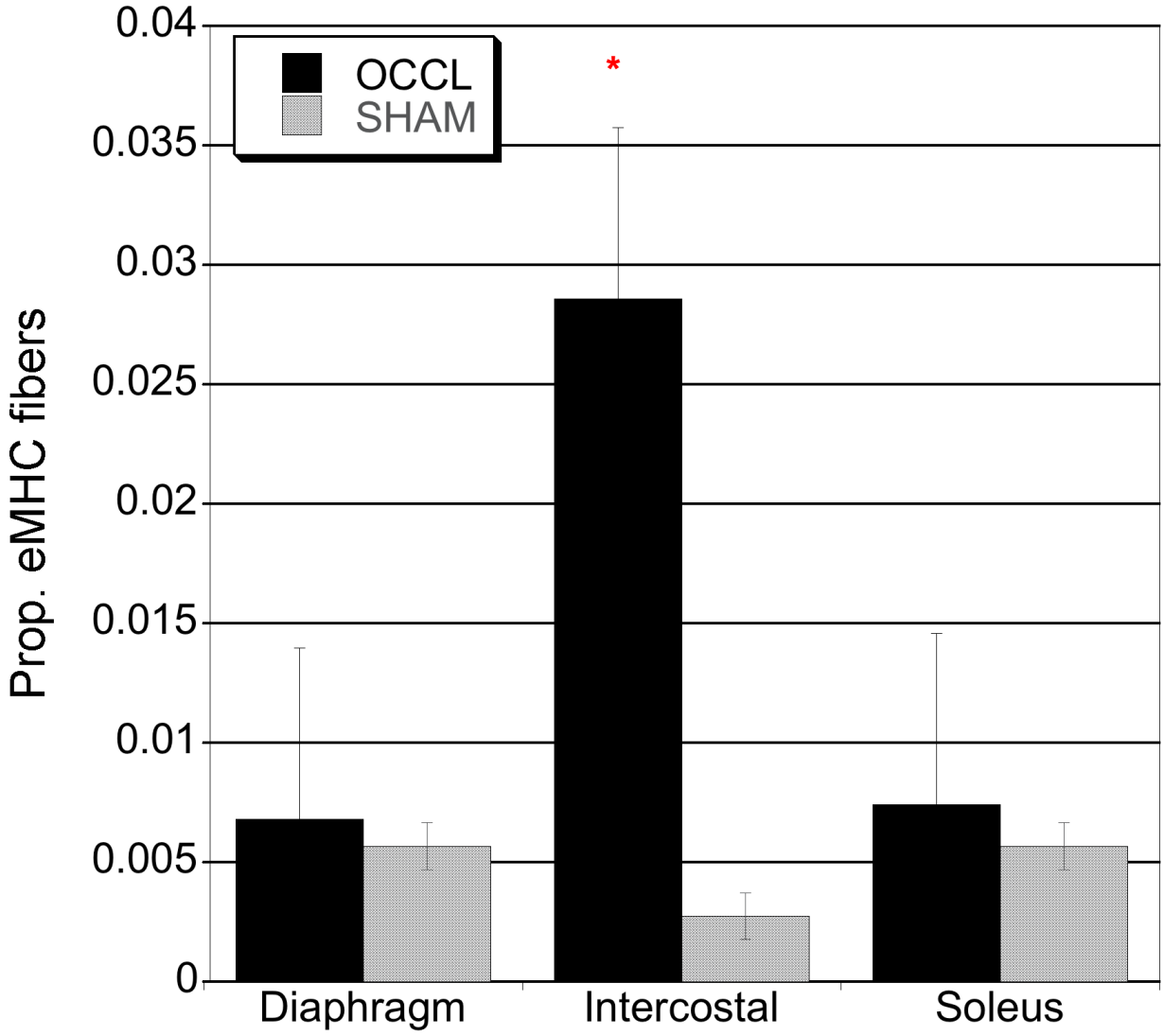

Figure 4-7. Proportions of embryonic myosin-positive fibers in the respiratory muscles. The expression of embryonic myosin was greater in the intercostals of the occluded animals (Mann-Whitney *U*, *p<.05).

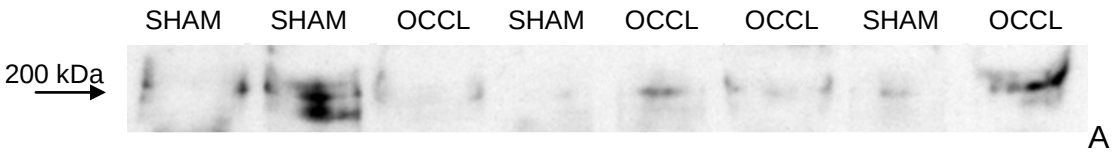

A

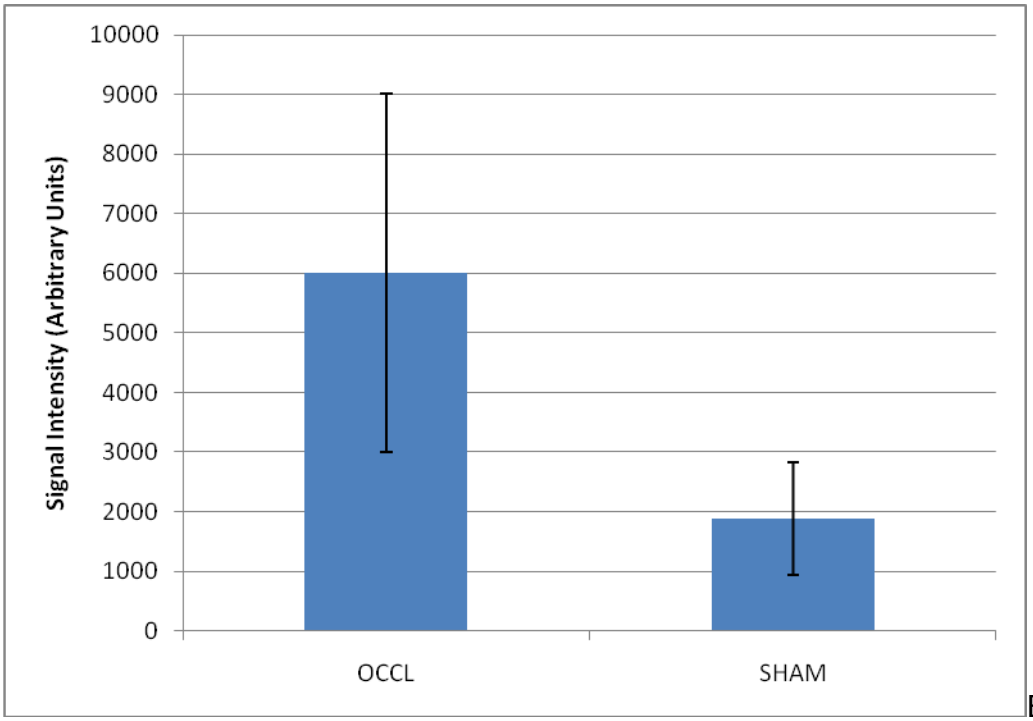

B

Figure 4-8. Verification of embryonic myosin in intercostal muscle. A). Western Blot images showed faint, distinct bands at 200 kDa, consistent with eMHC. B). The signal intensity of bands tended to be greater in the occluded animals, but the results were not statistically significant (p>.05).

CHAPTER 5
DICUSSION

Principal Findings

These experiments provide novel information regarding the effects of brief, intense overload training on respiratory muscle remodeling. In Aim 1, we hypothesized that brief occlusions would provide a sufficient stimulus to facilitate muscle hypertrophy without significantly altering the fiber phenotype. The findings from this project support the postulate that occlusion training was associated with rapid, preferential hypertrophy of IIx/b respiratory muscle fibers. In the occlusion-trained (OCCL) animals, the type IIx/b fibers was 27% larger in the medial diaphragm, and 22% greater in the 3rd intercostal. The data also indicate that the cross-sectional area (CSA) of the medial costal diaphragm was greater in type IIx/b fibers, compared to the dorsal and ventral regions. We did not identify a shift in myosin heavy chain (MHC) isoform composition after training. An additional unexpected finding revealed significant group-region- differences in the ventral diaphragm expression of type IIx/b MHC. The data suggest that the nature of remodeling could vary based upon regional structure and function.

In Aim 2, we tested the hypothesis that the intensity of tracheal occlusion would induce myogenic activity in the respiratory muscles, yet the brevity of the overload would minimize fiber damage. In agreement with our hypothesis, a limited degree of fiber remodeling was present in the respiratory muscles. However, the training program only induced modest regeneration of the third intercostal muscle. Detailed interpretations of the findings follow in subsequent sections of this chapter.

Training Elicited Fast-Fiber Hypertrophy

After ten sessions of tracheal occlusion, the CSA of type IIx/b fibers was increased in the medial diaphragm and third intercostals. Increased diaphragm fiber CSA has been reported in other models of muscle plasticity and could provide alternative justification for our findings. For example, an enlarged fiber CSA without force improvement occurs in models of passive stretching, injury or myopathy (198-200). It should be noted that we did not identify concurrent histological markers of injury and regeneration typical of these alternative models. Diaphragm fiber hypertrophy has also been reported following tetrodotoxin nerve blockade or denervation-induced inactivity (201). It is possible that placement of the occluder cuff could have injured a nearby phrenic nerve. Denervation-related hypertrophy occurs predominately in slow, oxidative fibers, with corresponding type IIx/b atrophy can be detected within two weeks of nerve injury (202). A denervation CSA remodeling pattern was not present the current study, and we did not visualize morphological evidence of denervated or regenerating fibers. Therefore, it is unlikely that these other factors influenced fiber CSA.

Notably, significant CSA differences were detected after only 10 training sessions, a timeframe that is considerably shorter than typical hypertrophy responses expected clinically. In adults with chronic obstructive pulmonary disease (COPD), significant intercostal fiber hypertrophy has been found within five weeks (14). In young adults, four weeks of intense strength training resulted in fast fiber hypertrophy of the limb muscles (203). We are not aware of clinical reports of diaphragm fiber hypertrophy after training. In contrast, rodent tissue remodeling is thought to occur more rapidly than in humans. Significant increases in limb muscle CSA have been reported after as few as 14 days of functional overload training (204, 205). Group variation in fast fiber CSA after high-

intensity limb strengthening was comparable to the respiratory CSA differences attained with ten days of tracheal occlusion.

The rapidity of respiratory remodeling could be influenced by the high baseline activity of respiratory motor units. Muscles with a high duty cycle respond rapidly to changes in activity (206). Furthermore, much more is known about respiratory responses to inactivity than with increased activity. With quiescence, diaphragm gene expression downregulates eight times more rapidly than limb muscle (5). Initially, slow and fast fiber atrophy equally, but prolonged inactivity preferentially atrophies fast fibers (61, 68). Altered diaphragm activity also affects neural coupling and signal transduction by trophic factors within days. These mechanisms significantly alter diaphragm protein synthesis within hours and may act as a representative “activity rheostat” (206, 207).

The OCCL animals exhibited hypertrophy only in type IIx/b fibers. There is other evidence of preferential fast-fiber hypertrophy in intense strength training of respiratory and limb muscles, in agreement with our findings (21, 205). In the respiratory muscles, a less intense, flow-resistance training protocol elicits modest CSA enlargement in all phenotypes (14, 139). These disparate results likely arise from differences in training intensity and duration.

The extent of hypertrophy can vary based upon motor unit recruitment, which in turn depends upon the intensity of the training load. At resting tidal volume, the diaphragm generates ~10% of its peak pressure, by predominately activating slow, oxidative fibers (33). Fast, fatigable fibers are not thought to be recruited during eupnea. Oxidative fibers generate lower specific tension but remain fatigue-resistant. With increasing levels of inspiratory drive, diaphragm motor units contract at a higher

frequency, although individual motor unit recruitment appears programmed according to the inspiratory volume (208). Nevertheless, significant type IIx/b fiber recruitment requires intense loads. In order to promote fast fiber hypertrophy of the respiratory pump, the training intensity must be sufficient to recruit these fibers. Additionally, training intensity should exceed 60% of peak force in order to significantly increase skeletal muscle protein synthesis (209).

Occlusion maneuvers generate strong recruitment of the ventilatory pump. Sieck (33) estimated occluded inspiratory attempts recruited only 50% of feline diaphragm motor units. The most recent neurophysiological models identify that 40-50% of type IIx/b fibers are recruited during tracheal occlusion (210). Additionally, up to 10 ventilatory attempts may be necessary to achieve maximal transdiaphragmatic pressures during occlusion (211). Our studies imposed 5-8 seconds of tracheal occlusion and yielded 5-10 ventilatory attempts per occlusion. It is likely that strong to maximal efforts in the animals produced robust activation of the respiratory pump and provided an atypical loading stimulus to preferentially remodel fast fibers. It is known that the greatest transdiaphragmatic pressures can be achieved with expulsive reflexes (33).

Our ability to detect oxidative fiber hypertrophy could have been limited by statistical power. A power analysis was based upon published evidence of training-induced diaphragm hypertrophy in rodents (139). In the referenced study, moderate respiratory endurance exercise promoted a small degree of hypertrophy in type IIx/b fibers, and five animals per group were needed to show training differences in type IIx/b fibers. However, only three animals per group were needed to achieve significance with

type IIa fibers and only one animal per group was needed to show differences in type I fibers. In contrast, a post-hoc power analysis of our animals confirmed that 54 (effect size: .544) animals per group would be needed to detect type I hypertrophy, and 55 (effect size .540) animals per group needed for type IIa hypertrophy. Therefore, the preferential changes in fast-fiber CSA were attributed to the training protocol, and this project appears adequately powered.

Regional Heterogeneity in the Costal Diaphragm

Regional Heterogeneity in CSA

Our findings showed that type IIx-b fibers in the medial costal diaphragm were larger than in the other regions. Additionally, training facilitated type IIx/b hypertrophy in the medial costal diaphragm, beyond baseline regional differences. A number of factors could have influenced regional fiber remodeling. Diaphragm contractions yield inspiratory pressures that can be affected by the neural drive to the muscle, its strength, and force-length and force-velocity properties of the muscle. Some of these features could differ regionally. Regional costal motor unit recruitment has been studied little but is not thought to vary substantially (212). It is known that the number of sarcomeres in parallel dictates specific force, and varies due to fiber size as well as muscle size. Medial costal muscle size is thicker than other regions and thus may generate more force. In conjunction, the regional architecture may influence force-length and force-velocity properties of the costal diaphragm.

Muscle length and lung volume each influence the mechanical efficiency of the inspiratory pump. As a result, diaphragmatic pressure varies based upon the operating muscle length and regional shortening. The degree of diaphragm muscle shortening correlates well with zone of apposition (ZAP) shortening (213), and relative ZAP

shortening correlates to the work of breathing (22). The ZAP is larger and the degree of appositional shortening is greater in the medial costal diaphragm, compared to adjacent regions braced by vertebral and sternal attachments. Functionally, ZAP excursion is facilitated by the ribcage muscles during inspiration. Accordingly, contraction of the accessory chest wall muscles optimizes length-tension properties in the medial diaphragm (214, 215). This project did not measure or manipulate muscle length, yet regional shortening may favor a high work output in the medial region.

Regional architecture may have also influenced force-velocity attributes during occlusion. Caiozzo noted “the ultimate design constraint of skeletal muscle is the force-velocity relationship,” (216) and force-velocity properties determine the work performed by a contracting muscle and describe its mechanical efficiency. The velocity of muscle shortening decreases as tension progressively increases. While tracheal occlusion generated strong diaphragm efforts that may have approximated optimal isometric force, even greater muscle tension can be generated by lengthening contractions.

The mid-costal diaphragm is reported to lengthen during occluded inspiratory efforts, while other regions shorten (48). The force-velocity properties of the lengthening ventilatory pump can be quantified functionally by trans-diaphragmatic pressure. Peak trans-diaphragmatic pressures occur during expulsive reflexes (33, 217). We note that tracheal occlusions induced both inspiratory and expiratory efforts by animals. Furthermore, strong expiratory efforts produce diaphragmatic lengthening (47, 48). Because mid-costal fibers can lengthen with occluded inspiration or expiration, they may be more susceptible to remodeling. Our studies were not designed to measure force adaptations with training, but this is suggested for future studies.

Regional Differences in Fiber Phenotype

In addition to significant CSA differences in the medial diaphragm, we found a reduced presence of type IIx/b fibers in the sham-trained (SHAM) ventral diaphragm, compared to other regions and MHC isoforms. MHC isoform expression can be affected by activity and loading properties. Muscles recruited more frequently at lower forces typically display a greater prevalence of oxidative fibers. Attributes of oxidative fibers include greater capillarization, higher contents of oxidative enzymes, and greater glycogen depletion with exercise. Our results suggested a greater oxidative phenotype in the untrained ventral diaphragm region, and showed relatively increased expression of fast-fatigable fibers in the ventral region of occluded animals.

Occasional reports in the literature suggest the ventral diaphragm may be more oxidative than other regions (218). Yet more evidence indicates the ventral diaphragm's oxidative activity and MHC composition are similar or lower to other regions (28, 201, 219, 220). Reid noted an exceptionally low oxidative capacity in type IIb fibers of the ventral-sternal hamster diaphragm (39), and glycogen utilization is lowest in the ventral diaphragm, both at rest and with aerobic exercise (42). Additionally, the diaphragm oxygen consumption and blood flow are correlated (26). Sexton and Poole (221) noted that blood flow of the rodent diaphragm is lowest in the ventral costal region.

In the dorsal, medial, and OCCL-ventral regions of our sample, fiber type proportions and phenotype area fraction (A_A) closely resemble reference values reported in the literature, but the SHAM-ventral proportions are lower than most other reports. In addition, low-intensity endurance inspiratory exercise does not significantly alter MHC proportions in the diaphragm (21, 139, 222). Thus, the altered ventral MHC composition in the SHAM-trained animals could be an incidental statistical artifact.

Greater metabolic differences appear to occur between the costal and crural diaphragm (39, 219, 223) than between costal diaphragm regions.

Sustained Damage was not Present in Overloaded Muscle

In the diaphragm third intercostal and soleus, normal fibers were by far more prevalent than connective tissue or remodeling fibers. The A_A of connective tissue and abnormal cells found in the diaphragm and intercostal muscles was comparable to those found in untrained or sham-trained respiratory muscles (163). Additionally, there were no significant group differences in the prevalence of abnormal or connective tissue for any of the muscles. The results indicate that either the occlusion training did not elicit significant fiber disruption or that tissue repair had already occurred.

We specifically examined differences in fiber shape and structure, degeneration and regeneration, fibrosis, and cellular reactions. We found a higher A_A of connective tissue in the diaphragm compared to the other muscles studied. However, we did not find the excessive quantities of collagen and fibroblasts associated clinically with respiratory diseases in adults (224) or infants (225). Connective tissue deposition may occur in proportion to the severity of an injury, and can indicate incomplete or impaired regeneration (185). While adipose deposition can arise in conjunction with excessive tissue fibrosis, none were observed in any images.

The most commonly observed abnormal cell type identified was inflammatory cells. While neutrophils have a polymorphic nucleus and migrate to the site of injury almost immediately after severe respiratory loading (163), their presence may delay upregulation of muscle regenerative transcriptional factors (181). On the other hand, macrophages can promote activation and proliferation of satellite cells (168). It should be noted that we did not conduct immunohistochemical analysis to differentiate between

inflammatory cells. Necrotic and inflamed cells were seen infrequently, suggesting that mechanical loads were insufficient to result in extensive injury. Additionally, angular fibers have been reported in instances of denervation, and these cells may occur in small groups (185). Although surgical placement of an occluder cuff could potentially elicit a phrenic nerve injury, low proportions of angular fibers in our diaphragm images suggest that the phrenic nerves did not sustain damage. Additionally, the occluder placement was proximal to the superficial location of the phrenic nerve.

Centrally nucleated fibers are a histological indicator of muscle regeneration. Elevated proportions in the diaphragms of COPD or Duchenne muscular dystrophy models suggest ongoing damage and regeneration (20, 226). In this study, the A_A of internally-nucleated fibers fell within the 3% proportions contained in normal adult skeletal muscle (185). After eccentric contraction-induced muscle injury, increased centrally nucleated fibers appear within 48-72 hours and peak by 7days (184). We did not observe other traits of regenerating fibers, such as granular, basophilic, or split features (185). Additional cytoplasmic changes can be described as hyaline, lipofuscin or “fuzzy” appearing and most frequently indicate impaired metabolic states or chronic loads (185). We found very few cytoplasmic changes in the respiratory muscles.

The low presence of damage could be due to the assessment timeframe. Single injurious loads have been reported to increase calpain activity and promote early accumulation of macrophages and neutrophils (227). While injury can increase the prevalence of abnormal cells in the diaphragm, and to a lesser extent the parasternal intercostals (163), evidence of damage may be delayed (165). Significant morphological changes occur within one day of injury, and peak at three days. In the absence of

additional mechanical overloads, proportions of connective tissue and abnormal cells begin to decrease toward baseline after 4 days (165, 166). Models of widespread chemical or thermal injury reveal inflammation, necrotic cells and histological signs of regeneration up to 14 days after injury (184).

Repeated respiratory loads can perpetuate histological signs of muscle damage. Two hours of daily resistive loading for four consecutive days damaged cell membranes and increased the prevalence of sarcomere disruption in the diaphragm (19, 140). While abnormal cell A_A peaks on the third day after constant loading, proportions of connective tissue and abnormal fibers remain elevated in subsequent days (162, 166). After 30 days of tracheal banding, the A_A of abnormal fibers was five times higher than the unbanded animals, despite a larger diaphragm mass (17). While we did not find histological signs of damage in the respiratory muscles in the sample, force measurements provide the most sensitive gauge of muscle injury. It should be noted that evidence of ultrastructural disruption and inflammation is commonly present during resistance training in human and animal muscles and may accompany large and significant force gains. Therefore, we suggest that future studies examine the effects of occlusion on evoked respiratory muscle force.

Limited Presence Embryonic Myosin after Training

We found modest yet significant increases in intercostal expression of embryonic myosin, but in contrast to our hypothesis, we did not find elevated embryonic myosin in diaphragms of occluded animals. The immunohistological findings were supported by the limited A_A of internally-nucleated fibers and minimal increases in embryonic myosin (eMHC) protein with immunoblotting. The intercostal eMHC levels were statistically different between training groups, but absolute quantities did not reach expected values

that occur with injury (181, 228). In contrast, strength training in humans elicited similar proportions of eMHC-positive fibers (mean: 3%) to the levels found in the intercostal muscles of the OCCL animals (229).

Embryonic MHC expression occurs in a similar timeframe to morphological features of damage and regeneration. Embryonic myosin is one of the earliest MHC isoforms expressed in development. During prenatal development, proliferating myoblasts exit the cell cycle and differentiate. Differentiation activates expression of eMHC. Developmental MHC forms predominate in prenatal and early postnatal periods, and then expression downregulates (230-232). After skeletal muscle fiber maturation in early infancy, adult MHC isoforms prevail throughout the life span(233). Reemergence of eMHC can be observed periodically, following mechanical overload or other injury. Specifically, myoblasts that exit the cell cycle, differentiate and fuse together express eMHC, distinguishing nascent or regenerating fibers. Myf5 appears to initiate eMHC activation, while MyoD and calcineurin facilitate its expression (234). Widespread eMHC-positive cells can also be found in DMD and SCI models of neuromuscular injury and regeneration (226, 235).

Regeneration has been tracked in rodents following a single mechanical, chemical or thermal injury. As with other quantitative markers of damage or regeneration, the prevalence of eMHC varies with the size and severity of the injurious load (184). Gene expression of eMHC trails upregulation of proliferative transcription factors by 2-3 days. Significant increases in expression occur after three days, peak by seven days and remain elevated at 14 days (180). Expression of immature MHC may be delayed or

inhibited by overabundant inflammation (181). The CSA of regenerating fibers is smaller, and many co-express a slow MHC isoform (228).

In the current study, fewer than1% of diaphragm fibers fluoresced for eMHC, regardless of group assignment. This rate approximates the expected normal values in rats (159, 160). The limited diaphragm eMHC expression could indicate that myogenesis was unnecessary because significant damage did not occur. A lack of damage could be due to an insufficient training intensity or duration. While we observed vigorous respiratory attempts by the animals, we did not measure occlusion-generated pressures. On the other hand, recruitment of accessory respiratory muscles may have spared the diaphragm from excessive strain during OCCL. Larger mammals and humans frequently recruit accessory muscles and alter their breathing pattern during heavy respiratory loading. Each of these strategies may deter fatigue in the diaphragm (109, 114). A low diaphragm eMHC expression accompanied by increased expression in the loaded intercostals may indicate that animals adopted a different ventilatory recruitment strategy during occlusions, in order to minimize diaphragm fatigue or injury.

Regeneration may have also been inhibited by stress-related transcriptional activity in muscle. Our collaborators illustrated that occlusion acutely elevated mRNA expression of stress-response transcriptional pathways in the medial thalamus (236). Two weeks of daily occlusions elevated serum corticosterone levels (unpublished pilot data) and heightened stress-related behavior in occlusion-trained animals (237). The neuroendocrine responses to stress differ based upon the nature of the stressor. Therefore, psychological stressors engender different physiological adaptations than metabolic stressors (238). Chronic stressors increase basal levels of serum

corticosterone and diminish acute responsiveness to stressors (239). The resultant increases in circulating glucocorticoids could attenuate muscle fiber regeneration.

When excess circulating glucocorticoids accompany psychological stress, they reduce muscle protein synthesis and increase gene expression of pathways leading to degeneration, atrophy and apoptosis (240). In addition, GCs elevate myostatin levels in skeletal muscle (182, 241). While myostatin may not alter satellite cell proliferation or directly induce atrophy, it inhibits myoblast differentiation by blocking signaling molecules downstream of Akt (158, 242). In rodents, four weeks of daily restraint stress resulted in increases of limb muscle myostatin, caspase-3, p53, and p38 MAPK, and facilitated significant muscle fiber atrophy. Additionally, the authors attributed the altered apoptosis and protein metabolism signaling to high levels of glucocorticoids (240).

Myostatin and glucocorticoids cooperatively oppose protein synthesis and muscle regeneration (153, 243). Chronic stress specifically decreased MyoD and phosphorylated Akt protein expression (240). Conversely, IGF-1 antagonizes myostatin and glucocorticoid-mediated catabolic activity in skeletal muscle, and supports hypertrophy through PI3K-Akt-mTOR protein synthesis pathways or myogenic regeneration. Additional control of regeneration occurs through cyclin and MAPK signaling, mediated by MRF transcription factors (156). Ultimately, net muscle growth necessitates that protein synthesis exceeds proteolysis.

Study Limitations

Application of the study findings is limited by some aspects of the design. The magnitude and timing of protein synthesis after resistance exercise varies between rodents and humans (147), and we cannot make direct translations. Also, the experiments were terminal, and therefore pre-post changes in muscle CSA, phenotype,

and myogenic activity could not be directly measured. However, inclusion of an operated, sham-trained animal group served to control for the effects of growth, surgery, and daily handling during the experiment. Therefore, the similar group demographic characteristics suggest that occlusions did not alter animal growth.

Replication of the experiment may be restricted because occlusion training loads were not quantified. The efficiency of respiratory muscle contractions varies by lung volume, and we were unable control lung volume during training. In addition, we could not determine with precision the exact pressure load generated by the animals. Plethysmograph recordings allow investigators to non-invasively track pressure and volume fluctuations, usually on sedated animals. Although animals were housed in a plethysmograph for daily training sessions, pressure fluctuations with occlusion were obscured by movement artifact of animals. In future work, the inclusion of esophageal pressure transducers may provide additional information.

In addition to the design-related limitations, the tissue analysis methods were limited in scope. Since histological analyses utilize only a small portion of a muscle specimen, they therefore can be influenced by the sampling region of the muscle. Diaphragm samples were taken midway between its costal attachment and the central tendon insertion, because in larger mammals, fiber size and connective tissue content differ at the attachments (196, 244). Additionally, samples were taken from the midbelly of the intercostal and soleus muscles (185). We suggest that histological findings be verified with quantification of protein synthesis and myogenesis biomarkers. Also, while remodeling was examined after ten days of training,acute adaptations to occlusion remain unknown.

Finally, the study did not analyze whether specific respiratory muscle force (force per unit area) or ventilatory function were altered by tracheal occlusion training. Although fiber size influences peak tension in skeletal muscle, the quasi-isometric training does not replicate the timing or biomechanical properties of tidal breathing. Therefore, we do not know whether in vivo pressure-flow properties of the ventilatory muscles, and subsequently breathing pattern, differed in the OCCL animals.

Application of the Model

The tracheal occlusion model provides important applications for the physiology of IMST. In contrast to many other animal models of loading, it demonstrates that rapid fast-fiber hypertrophy of the respiratory muscles is possible, without eliciting substantial structural injury. Compared to previous loading models, ours most closely replicated principles of brief, intense overloads to elicit hypertrophy.

Clinical inspiratory exercises have typically involved modest, sustained training regimes. Modest resistive inspiratory training in adults with COPD facilitated slow, and to a lesser extent, fast fiber hypertrophy in the intercostal muscles (14). Training also resulted in significant gains in respiratory strength and endurance. While training improved function and fiber CSA, a more vigorous training intensity may have generated preferential type IIx/b hypertrophy. On the other hand, respiratory loading to exhaustion can induce diaphragm damage in healthy adults and patients with COPD (245). In addition, maximal inspiratory pressure (MIP) of patients was lower in the patients 24 hours after the injurious bout. Our findings reinforce that intense respiratory loads may facilitate preferential type II fiber hypertrophy, but brevity of the mechanical overload is essential to avoid widespread damage and decrements in excitation-contraction coupling.

The training model also suggests that poorly cooperative patients may benefit from occlusion training. Occlusion rapidly increases neural drive, and yields maximal efforts within approximately ten inspiratory attempts. Adults achieve MIP within 20-25 seconds and children reach maximal effort in ~15 seconds (190, 211). Strong to near-maximal training intensities can be elicited by occlusion without active patient cooperation. Occlusion IMST could be applied to equine or canine veterinary training as well as clinical pediatric or neurologically-impaired patients. In the next chapter, we describe an infant recipient of occlusion-IMST and recommend that future research examine training effects in these emerging areas.

CHAPTER 6
CLINICAL APPLICATION OF OCCLUSION TRAINING: CASE REPORT OF AN INFANT WITH POST-OPERATIVE WEANING FAILURE

Case Report

Diagnostic Background

This report describes an infant female born at 34 weeks gestation and diagnosed with DiGeorge syndrome and type I truncus arteriosus (TA) at birth. DiGeorge syndrome is a chromosomal disease characterized by gene deletion at the long arm of chromosome 22 (del22q11.2). Associated signs and symptoms of del22q11.2 frequently include palate and pharyngeal defects, hypoparathyroidism, thymus insufficiency, learning disabilities, and congenital heart disease. Although DiGeorge syndrome does not alter primary lung physiology, respiratory complications are common, due to impaired immune function and bronchopharyngeal structural deficits (247).

Approximately 40% of children with del22q11.2 have a concurrent congenital heart defect (248). The child in this case presented with TA, a developmental anomaly that occurs when the pulmonary artery and aorta do not mature from a single large arterial trunk. This single vascular outlet receives blood from the right and left ventricles, and delivers blood to the systemic, coronary and pulmonary vascular systems. There are three types of TA, depending upon the anatomy of the pulmonary arteries. In type I TA, a small vessel emerges from the left side of the truncus and then rapidly divides into undersized right and left pulmonary arteries (Figure 6-1). Approximately one-third of patients born with TA carry del22q11.2 (248, 249). Other congenital heart defects associated with TA include patent ductus arteriosus, ventricular septal defect (VSD), patent foramen ovale, and interrupted aortic arch. Corrective procedures consist of repair of the VSD and establishment of communication between the left ventricle and

the aorta; construction of a valved conduit between the pulmonary arteries and right ventricle; and anastomosis of interruptions in the aorta. Early surgical repair reduces an otherwise high infant mortality from pulmonary hypertension and hypoxemia (248, 250).

Clinical Presentation

The infant underwent surgical repair of TA, VSD and interrupted aortic arch, at 11 days of age. Her post-operative course was complicated by feeding intolerance requiring gastric tube placement and Nissen fundoplication for gastro-esophageal reflux disease, as well as respiratory insufficiency and delayed extubation following each of the surgical interventions. She was originally discharged to home at 81 days of age.

Three days later, she was readmitted with increased gastric tube discharge and respiratory distress, and she was intubated upon arrival. During the hospitalization, the infant received treatment for presumed pneumonia and management of the gastric wound. However, weaning from mechanical ventilation (MV) was limited by pulmonary hypertension and left ventricular dysfunction. On hospital day #39, she underwent pulmonary valve replacement with a 9 mm allograft, VSD re-closure with a core matrix patch, right pulmonary artery patch, right ventricular tract augmentation with a core matrix patch, and atrial catheter placement, followed by delayed sternal closure. Throughout the hospitalization, the infant required continuous MV support. Despite optimization of her post-operative cardiac status, she failed three extubation trials. Each time, failure was attributed to increased work of breathing and hypercapnic respiratory failure accompanied by hypoxemia.

On hospital day #53, we were consulted to evaluate the patient for inspiratory muscle strength training (IMST). Her medical team felt that other pharmacological, surgical, and clinical therapies had been optimized, and her parent consented to

assessment and treatment. At University of Florida, Institutional Review Board approval is not required for case studies of three or fewer patients, but her parent provided consent for a case report. Table 6-1 lists common clinical indications and contra-indications for IMST. Although the patient could not actively participate and follow commands, we judged that IMST was indicated due to (1) a sustained decline from baseline respiratory function; (2) repeated hypercapnic respiratory failure, indicating ventilatory muscle dysfunction; (3) pre-existing cardiac dysfunction; and (4) medical and nutritional stabilization.

Respiratory Muscle Testing

On the day of evaluation, the infant was 3.5 months of age, and weighed 3.5 kg. We assessed minute ventilation on baseline MV settings and estimated strength of the ventilatory muscles using maximal inspiratory pressure (MIP). MIP was tested with a 15-second inspiratory occlusion maneuver, the preferred strength testing mode for infants and young children (211, 251). The patient was tested in supine with approximately 40 degrees of head and trunk elevation. The patient was briefly disconnected from the ventilator, and then occlusion was provided by way of a unidirectional valve attached to the endotracheal tube, permitting exhalation. With each subsequent exhalation, the patient exhaled toward residual volume, but a standardized testing volume could not be imposed. The most negative pressure achieved in 15 seconds was recorded as the MIP, and the best of four trials was used for day to day comparison.

Training Program

The training options were limited for the patient, because all commercially-available devices have ~30 mL of dead space and are intended for use in the adult population. Anatomic dead space varies with size and posture. Neonates and small

infants have an anatomic dead space estimated at 2.25-3.0 ml/kg of body mass (252). The combined dead space of our monitoring sensor and unidirectional valve was measured by volume displacement and was found to be approximately five mL. Insertion of a pressure transducer added another seven mL of dead space (Figure 6-2). ATS guidelines suggest that the dead space of respiratory testing equipment remain below 1.5 mL/kg body mass (251).

To account for dead space volume, the occlusion maneuvers used to measure MIP were used to deliver IMST. Training sessions were conducted six days per week and consisted of four sets of 15-second occlusions (8-12 inspiratory attempts), with three minutes of rest between sets. In addition to IMST sessions, the infant also underwent daily breathing trials at progressively reduced pressure support and intermittent mandatory ventilation (IMV) levels.

Data Analysis

We calculated ventilatory muscle performance during testing and training sessions. Ventilatory parameters were determined using a neonatal respiratory monitor (CO_2SMO Plus with Capnostat neonatal adaptor, Philips-Respironics, Murrysville, PA) connected to a laptop computer. An intrinsic pneumotachograph and pressure transducer captured airflow and pressure at a rate of 100 Hz, and airflow was integrated to obtain volume. During occluded breaths, pressure performance variables were calculated for the most negative inspiratory effort. Rate of pressure development (dP/dt) was measured as the time to reach peak MIP. Maximal rate of pressure development (maxRPD) was the largest pressure gain in a 10 msec time interval. Additionally, the most negative occlusion pressure was confirmed by a pressure transducer attached to a

side port (Sper Scientific, Scottsdale, AZ) Data were integrated with *AnalysisPlus* software (Philips-Respironics, Murrysville, PA).

Training Outcomes

The infant participated in 13 IMST sessions over 15 days. During IMST sessions, respiratory parameters and vital signs were monitored continuously (Table 6-2). The infant did not experience desaturation or hypercapnia during or after training, and transient increases in systolic blood pressure and heart rate returned to baseline levels within approximately three minutes. MIP increased 14% from -55.4 to -63.3 cm H_2O (Table 6-3). Time to reach MIP quickened by 27%. As a result of pressure and time improvements, the infant was able to generate negative pressure more rapidly. With training, inspiratory dP/dt increased 43% from 92 cm H_2O/s to 132 cm H_2O/s. We detected small fluctuations in inspiratory flow and volume on waveform tracings, because the infant's endotracheal tube was not cuffed. Small quantities (~20 mL) of air leaked around the tube during IMST bouts.

In addition to strength gains, IMST improved breathing function. During the training period, the infant's breathing pattern improved toward age-appropriate values (Figure 6-4). Baseline respiratory rate decreased by 34% (Figure 2-3), and resting spontaneous tidal volumes increased by nearly 60% (Figure 2-4). After the 13th IMST session, the patient was extubated to a high-flow nasal canula. She was discharged to home using supplemental oxygen with a nasal canula two weeks after extubation.

Discussion

We describe an infant who required 68 days of MV and experienced repeated post-operative weaning failures. MIP increased with training, accompanied by faster pressure-timing of occluded breaths. It is known that the rate of pressure generation can

be influenced by a number of muscular factors, including the myosin heavy chain (MHC) isoform composition, cross-sectional area (CSA), and tissue elasticity (253, 254). Neural drive can also affect dP/dt (255). A faster dP/dt resulted from a greater MIP as well as a faster pressure generation time. We are unable to determine the relative degrees of muscular and neural remodeling exclusively from non-invasive measures of ventilatory performance, and suggest additional respiratory testing, including occlusion pressure, electromyography, and phrenic stimulation. Improved pressure and time performance appeared to translate into gains in breathing pattern. The breathing pattern became slower and deeper, and the infant weaned from MV after 13 days of training.

A number of factors may affect the ability of infants and young children to wean from MV. Important influences include fluid status, medications, cardiopulmonary function, and strength (256). During our 15-day intervention, the patient's fluid balance fluctuated by less than 100 mL daily, and blood urea nitrogen (7-10 mg/dL) and creatinine (0.1-0.2 mg/dL) measurements remained at age-expected values. Analgesics (fentanyl, 2-4 mcg prn, daily average: 8 mcg) and inotropic (milrinone, 200mcg/mL, 0.3 mL/hr) medications were not altered during training, and she did not receive corticosteroids or neuromuscular blocking agents that could have influenced skeletal muscle contractility. Nutritional management was not modified. In addition, the chest radiograph and laboratory values remained stable. Thus, many variables that can shape ventilatory status did not appear to consistently affect the infant's ability to participate in and benefit from IMST.

The infant's congenital heart disease was accompanied by a number of co-morbid factors that can impair respiratory function. Despite her pre-existing pulmonary

hypertension, hypoxemia was controlled, as reflected by resting arterial blood gases (pH: 7.44, $PaCO_2$: 39 torr, PaO_2: 80 torr, SaO_2: 96%, HCO_3: 26 mEq/L). Moreover, baseline dynamic resistance and compliance did not differ substantially from reference values for infants (257, 258) and did not fluctuate substantially over the course of IMST (Table 6-3). After cardiac surgery in infants and children, pneumonia, delayed sternal closure and pulmonary hypertension can independently deter MV weaning (259). Although each of these risk factors transpired for the child, they were corrected or optimized prior to initiating IMST. It appeared that the patient's cardiac function did not change during IMST or influence changes in ventilation and strength. We conclude that the enhanced ventilatory performance was at least partially attributed to the IMST intervention.

Inspiratory Occlusions and Cardiac Function

Because the patient's pre-existing cardiac function was impaired, special attention was given to potential cardiovascular effects of IMST. Negative thoracic pressure can increase preload (right sided venous return) as well as afterload (left ventricular systolic pressure and myocardial workload). When ventilatory mode shifts from mechanically-assisted to unassisted breathing, intrathoracic pressure decreases, facilitating venous return to the right ventricle. However, the relative right ventricular overload during inspiratory occlusion was tempered by flow-limited venous return, even with large negative pressure fluctuations (260).

Inspiratory occlusion may also affect pulmonary vascular function or left ventricular work. Occlusion generates a large increase in pulmonary blood flow and elevates pulmonary pressure. However, hypoxemia and lung inflation elevate pulmonary vascular resistance (PVR) to a greater degree than intrathoracic pressure

swings (257). Neither hypoxemia nor overinflation applied to the infant. Clinical monitoring verified that SpO_2 was maintained. Even though small quantities of air leaked around the endotracheal tube, lung volumes decreased during the IMST sets. Together, the PVR and the diameter of the pulmonary arteries modulate pulmonary shunt in congenital heart diseases. In this case, cardiothoracic surgery mitigated a large shunt and consequential left ventricular overload.

While repeated episodes of concurrent inspiratory occlusion and hypoxemia can diminish arterial pressure, stimulate LV diastolic dysfunction and induce multifocal infarcts in an animal model (261), we do not anticipate that the findings apply to our patient. The animal model produced a cumulative overload that was 45 times more intense than the clinical training protocol, and PaO_2 of the experimental animals dropped to ~25 mm Hg every three minutes. In contrast, IMST occlusion durations were short, SpO_2 remained well above 90% during and after occlusions, and we observed no acute or chronic changes in blood pressure.

Even though large fluctuations in negative pressure can transiently increase LV afterload and amplify myocardial oxygen consumption (262), nevertheless IMST did not induce a lasting shift in cardiopulmonary function. Echocardiograms were taken weekly during the intervention, including the day prior to initiating IMST, and within 24 hours of extubation. After extubation, LV fractional shortening decreased slightly from 36.2 to 34.9% (z-score from -1.32 to -1.83), while the RV diastolic dimension was reduced slightly from 2.61 to 2.41 cm. LPA diameter increased from .49 to .51 cm (z-score: .11 to .16), RPA diameter increased from .44 to.45 cm, (z-score: -0.52 to -0.5) and the

Pulmonary Artery Index (Nakata) decreased from 155 to 146. Despite pre-existing impairments, it does not appear that IMST altered cardiac function appreciably.

Considerations for Respiratory Mechanics

We did not find a large difference in dynamic compliance during training. Absolute compliance values are low in infants (5-10 mL/cm H_2O) compared to adults (120-180 mL/cm H_2O). When compliance is referenced to body mass though, it fluctuates little across the lifespan (2-5 ml/kg/H_2O). Infants have a highly compliant chest wall due to low mineralization of the thoracic cage. Consequently, the chest wall does not exert outward recoil pressure against the relatively stiff lung tissue, and the functional residual capacity (FRC) of infants is comparatively lower than adult volumes. Pediatric FRC varies by height, weight, and age, and is not significantly influenced by presence of congenital heart disease (263).

Airway resistance of infants and toddlers (20-40 cm H_2O/L/s) may be 10-20 times greater than in adults (1-2 cm H_2O/L/s), due to a particularly low airway caliber within the respiratory zone (18^{th} generation and smaller) (257). Airway caliber varies with lung inflation. Above FRC, airway resistance decreases slightly, but small volume changes below FRC correspond to large gains in resistance. At low lung volumes, airways close in dependent regions of the lung. The interaction between the compliant thoracic cage and relatively stiff, resistive lung tissue results an airway closing volume above FRC in infants (264). However, end-expiratory volumes are greater than FRC in infants, due to the postinspiratory activity of the diaphragm and upper airway muscles (265).

Maturation of the Ventilatory Pump

As neonates grow, so does the diaphragm. Rapid diaphragm growth results in significant increases of fiber CSA and muscle thickness (15, 266). During this period of

rapid postnatal growth, adult MHC isoforms replace immature MHC. Initially the newborn and infant respiratory muscles contain a lower proportion of type I fibers than children and adults (15, 267). Fast isoforms replace developmental MHC and correlate with increases in specific force, maximum shortening, and actomyosin ATPase activity (268). Expression of immature MHC accounts for 60% of the variance in fatigue resistance postnatally (269).

The infant respiratory muscle pump is capable of generating a relatively high MIP, owing to the mechanical advantage described by LaPlace's Law. The narrow diameter of the infant ribcage translates small quantities of tension into relatively large pressures. However, the costovertebral angles approximate 90 degrees in newborns. This inefficient orientation minimizes the contributions of intercostal muscles to tidal volume changes, until costal angles become more acute with age (270). In conjunction, MIP has not been found to correlate significantly to infant size (271). Although infants are capable of generating high MIP values, this capacity is counteracted by high minute ventilation and oxygen consumption requirements. Furthermore, inspiratory load consumes a high proportion of capacity in infants, compared to adults (251). Although the patient generated a normal MIP, her ventilatory loads were multiplied due to high minute ventilation and metabolic rates, as well as the presence of pulmonary arterial stenosis and elevated myocardial work.

Mechanical Ventilation and Weaning of Infants

MV alters the timing and mechanics of ventilation in infants. Inspiratory and expiratory volume-mediated reflexes normally dominate the control of breathing in early infancy, prior to the maturation of chemoreflexes (272). In non-ventilated neonates there is greater variability in expiratory than inspiratory timing, but variability differences erase

during MV (273). With MV, large inspiratory volumes prolong exhalation without altering the timing or amplitude of diaphragm activity during inhalation. The timing of spontaneous and mandatory ventilated breaths do not differ substantially (274). Although MV generates large tidal volumes, it results in decreased diaphragm movement (275).

Ventilator weaning of pediatric patients can involve reduction of the programmed mandatory ventilation rate or gradual reduction of inspiratory pressure support. As our patient's respiratory rate slowed and spontaneous tidal volume increased, the ventilator IMV settings were reduced progressively. Reductions in ventilator settings typically accompany extubation readiness tests on minimal ventilatory support. However, weaning readiness indices such as the rapid, shallow breathing index (RSBI = f/V_T) and Compliance, Resistance, Oxygenation, Pressure Index (CROP Index = C_{dyn} * MIP * PaO_2/PAO_2 * f) have showed poor predictive value when applied to ventilated infants and children (256). Likewise, strength alone does not reliably predict weaning success (251).

On the other hand, tension-time index (TTI) is a highly significant predictor of weaning in infants and children (112). Successful pediatric MV weaning requires improvements in both respiratory strength and ventilatory timing. After IMST, our patient demonstrated improved strength and ventilatory pattern. However, few other data are available regarding the role of respiratory training to facilitate ventilator weaning in infants. A single published study of neonates demonstrated that flow-resistive inspiratory exercises increased endurance and improved resting tidal volume (276). In the previous study, peak airway pressures did not differ after training, but airway

occlusion tests lasted for only three breaths while the infants were asleep. It is unlikely the investigators obtained maximal pressures by these brief occlusion tests. A difference in the training intensity could also explain the greater MIP outcome reported in our patient. Nevertheless, the results suggest that training may improve breathing pattern and performance, in general agreement with our results.

Conclusions

Brief inspiratory occlusion offers a training alternative for infants or patients who cannot follow directions for IMST with threshold or resistive devices. Our report is clinically meaningful, because developmental delay, hospital stay, cost, and mortality are significantly greater for infants who fail MV weaning after cardiac surgery (277-279). IMST may be feasible for stable infants with clinical signs of VIDD and warrants further study. Specific suggestions for further study include acute effects of inspiratory occlusion on central arterial pressures and myocardial function; effects of occlusion training on heart rate variability and circulating glucocorticoids; cardiac functional and histological properties of occlusion-training in an animal model, and breathing pattern changes alter occlusion training.

Table 6-1. Suggested clinical indications and contraindications for inspiratory muscle strength training.

Clinical Indications for Inspiratory Muscle Strength Training	Contraindications for Inspiratory Muscle Strength Training
Inspiratory strength below age and gender-predicted normal values and/or ventilatory loads estimated to elicit fatigue (per tension-time index)	Hemodynamic instability (systolic BP <90 mm Hg, or resting HR > 110 bpm) or requirement of continuous vasopressor medications
Decline from pre-morbid level of ventilatory function – acute requirement for assisted ventilation	Evidence of uncontrolled infection (temperature >36.0 °C or > 38.5 °C, white blood cell count > 19/mm^2)
Failure to wean with routine clinical methods (i.e. reduced IMV, pressure support, lengthening spontaneous breathing trials)	Acute pulmonary instability: untreated hemothorax or pneumothorax, unstable fractures
Gas exchange maintained with minimal ventilatory support (ie. F_IO_2 < .6, IMV <8, PS <15, PEEP <8)	Presence of seizure activity, ventriculostomy, or evolving neurological injury
Current or previously prescribed medication known to impair skeletal muscle excitation-contraction coupling (such as corticosteroids, beta-blockers, neuromuscular blockade, aminoglycoside antibiotics, immunosuppressants)	Inability to follow commands

Table 6-2. Vital signs during the course of occlusion training sessions.

	Pre				Post			
Training day	Heart rate	Respiratory rate	Mean arterial pressure	SpO_2	Heart rate	Respiratory rate	Mean arterial pressure	SpO_2
1	156	70	62	96	166	77	61	98
2	167	51	73	94	182	76	80	96
3	166	51	71	100	182	57	82	96
4	176	49	83	90	180	60	80	99
5								
6	170	61	59	97	175	60	64	98
7	150	43	64	96	170	55	64	97
8	160	46	51	96	175	58	57	98
9	165	54	59	93	180	57	59	97
10	187	50	61	94	190	53	64	96
11	164	62	52	97	174	67	70	99
12								
13	165	57	56	98	169	51	65	94
14	147	47	64	98	162	49	65	96
15	148	46	55	96	162	68	72	95

Note: Vital signs were monitored continuously. Reported values were taken from the onset of daily training, and within two minutes of completing the final exercise set. The patient did not receive training on days 5 and 12.

Table 6-3. Respiratory performance variables during inspiratory occlusion. Parameters were obtained from the single inspiratory effort that yielded maximal inspiratory pressure.

Training day	Maximal inspiratory pressure (cm H_2O)	Time to maximal inspiratory pressure (s)	dP/dt (cm H_2O/s)	Max RPD (cm H_2O/s)	Max RPD/MIP (%/s)
1	55.4	0.66	91.5	410	740
2					
3	63.6	0.42	153.1	615	967
4					
5					
6	63.3	0.52	125.4	300	474
7	58.6	0.59	109.7	250	427
8	66.3	0.6	122.8	335	505
9	64.6	0.53	125.1	615	952
10	65.6	0.45	153.3	540	823
11	62.1	0.46	143.0	445	717
12					
13	62.5	0.55	125.5	305	488
14	60.3	0.5	131.0	295	489
15	63.3	0.48	132.0	575	908

Notes: MIP: maximal inspiratory pressure; dP/dt: inspiratory pressure development; Max RPD: maximal rate of pressure development; max RPD/MIP: maximal rate of pressure development normalized to strength

Table 6-4. Ventilator settings and pulmonary mechanics during the course of treatment. The baseline ventilation of the infant was assessed in an awake, restful state prior to starting inspiratory muscle strength training bouts.

Training Day	IMV rate	Total rate	Spontaneous inspired volume (ml)	Pressure Support (cm H_2O)	PEEP (cm H_2O)	C_{dyn} (mL/cm H_2O)	C_{dyn} (mL/cm H_2O/kg)	R_{awi} (cm/mL/s)	R_{awe} (cm/mL/s)
1	24	44	16	12	5				
2	24	65	29	12	5				
3	22	64	28	12	5				
4	20	60	28	12	5	10.2	2.9	13.9	14.8
5	18	64	29	12	5				
6	18	48	29	12	5				
7	16	51	26	12	5				
8	20	46	38	12	5	4.2	1.2	32.3	35.2
9	18	44	27	10	5	12.5	3.6	17.1	18.1
10	10	59	34	10	5	11.7	3.4	11.7	12.2
11	10	47	28	10	5	12.4	3.5	14.2	15.3
12	10	48	36	10	5				
13	8	52	30	10	5	12.1	3.5	16.6	17.1
14	8	40	25	10	5				
15	8	42	32	10	5	8.2	2.3	23.4	24.4

Notes: IMV: intermittent mandatory ventilation; PEEP: positive end-expiratory pressure; C_{dyn}: dynamic compliance; R_{awi}: dynamic inspiratory airway resistance; R_{awe}: dynamic expiratory airway resistance

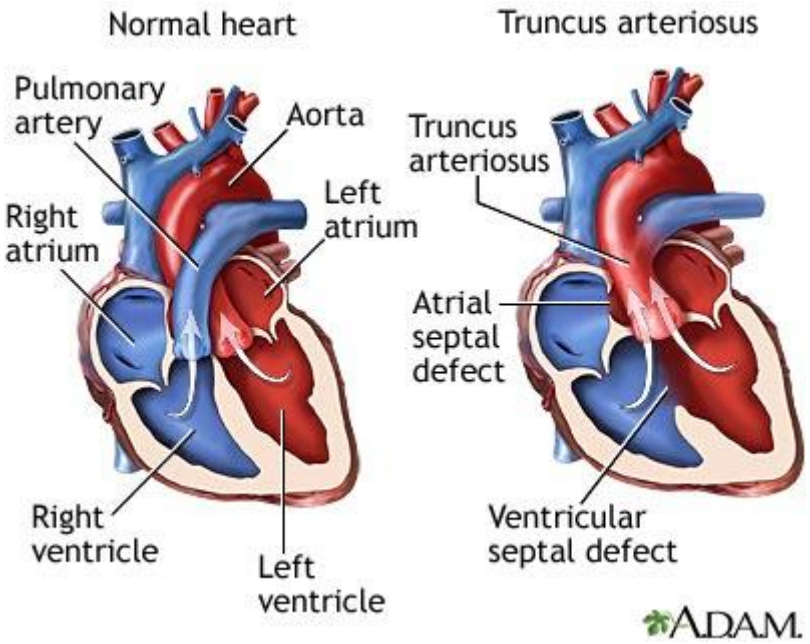

Figure 6-1. Type I Truncus Arteriosus. The right and left ventricles communicate due to a septal defect, and blood exits a common vessel to enter the pulmonary, coronary, and systemic vascular systems. In type I truncus arteriosus, the pulmonary arteries emerge from the left side of the truncus and then divide into right and left branches. Used with permission from A.D.A.M. Images.

Figure 6-2. Inspiratory muscle testing and training device. A one-way valve prevented inhalation, while exhalation was unimpeded.

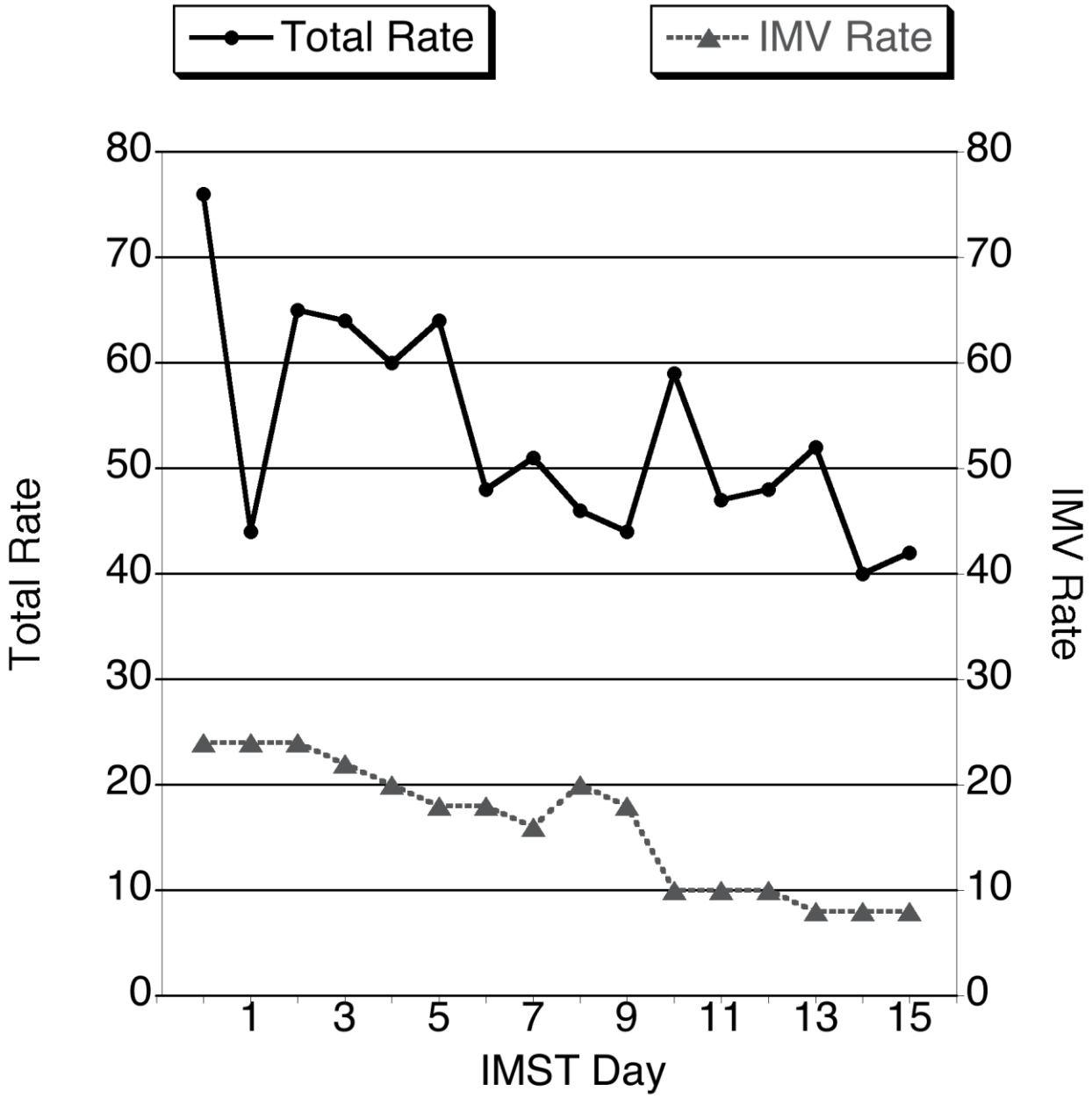

Figure 6-3. Ventilatory rate slowed during inspiratory muscle strength training. Assisted and total ventilator rate. The IMV rate was progressively decreased as spontaneous ventilatory rate slowed.

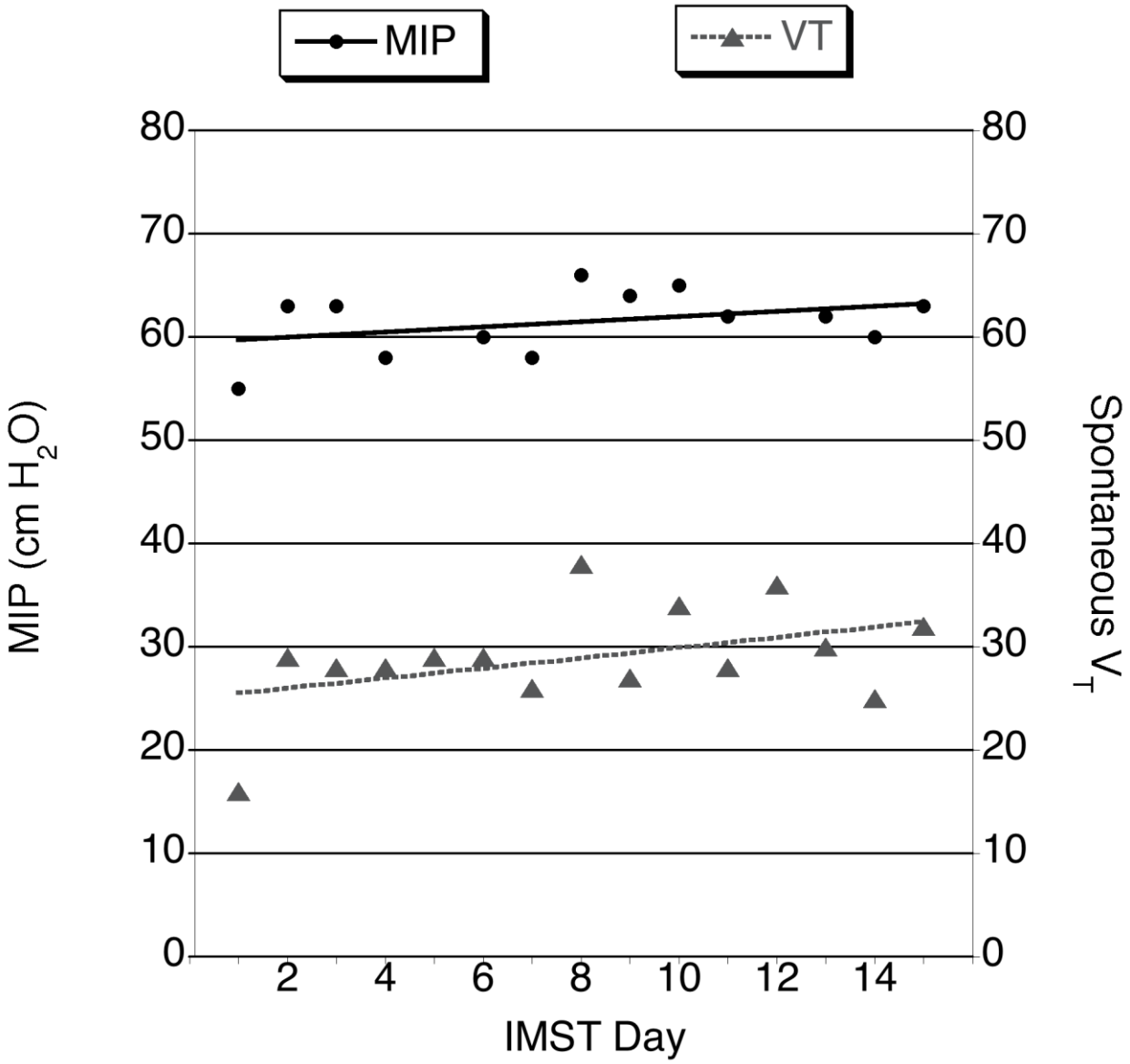

Figure 6-4. Spontaneous tidal volume and maximal inspiratory pressure. A 14% increase in MIP was accompanied by a nearly 60% improvement in tidal volume. Lines are regression lines.

CHAPTER 7
CONCLUSIONS

This study provides the first evidence that respiratory muscle strength training may elicit muscle fiber hypertrophy in the respiratory muscles. Specifically daily, intermittent tracheal occlusion was associated with increased cross-sectional area (CSA) in fast-fatigable fibers of the medial costal region of the diaphragm and the third parasternal intercostals. A shift in myosin heavy chain isoform composition did not accompany CSA differences. Significant group differences were detected after just ten days of training. Muscle fiber hypertrophy was not associated with evidence of fiber injury. While expression of embryonic myosin did not vary in the diaphragm, modest regeneration was present in the intercostal muscles of occluded animals. The results indicate that occlusion may be a feasible mode for strengthening patients without inducing muscle damage. Clinically, our case patient experienced a modest increase in maximal inspiratory pressure after two weeks of training and functional gains that included a slower, deeper breathing pattern and ventilator weaning. These results are significant because respiratory muscle contractile dysfunction is thought to be a primary contributor to ventilator dependence.

We recommend that future studies examine the effect of tracheal occlusion on the diaphragm gene expression of synthesis and myogenic transcriptional regulators. In addition, it is essential to determine the effects of occlusion upon evoked force of the diaphragm and resultant breathing pattern. Moreover, translational models should examine human diaphragm remodeling following preoperative inspiratory muscle strength training. A more complete understanding of respiratory muscle remodeling will

help scientists to develop effective rehabilitation strategies to prevent or reverse ventilator-induced diaphragm dysfunction and improve ventilator weaning.

LIST OF REFERENCES

1. MacIntyre NR, Epstein SK, Carson S, et al. Management of patients requiring prolonged mechanical ventilation: report of a NAMDRC consensus conference. Chest 2005;128(6):3937-3954.

2. Epstein SK. Size of the Problem, What Constitutes Prolonged Mechanical Ventilation, Natural History, Epidemiology. In: Ambrosino N, Goldstein RS, editors. Ventilatory Support for Chronic Respiratory Failure. New York: Informa Healthcare; 2008. p. 39-56.

3. Carson SS, Garrett J, Hanson LC, et al. A prognostic model for one-year mortality in patients requiring prolonged mechanical ventilation. Crit Care Med 2008;36(7):2061-2069.

4. Cox CE, Carson SS, Govert JA, et al. An economic evaluation of prolonged mechanical ventilation. Crit Care Med 2007;35(8):1918-1927.

5. DeRuisseau KC, Shanely RA, Akunuri N, et al. Diaphragm unloading via controlled mechanical ventilation alters the gene expression profile. American Journal of Respiratory and Critical Care Medicine 2005;172(10):1267-1275.

6. Falk DJ, DeRuisseau KC, Van Gammeren DL, et al. Mechanical ventilation promotes redox status alterations in the diaphragm. Journal of Applied Physiology 2006;101(4):1017-1024.

7. McClung JM, Whidden MA, Kavazis AN, et al. Redox regulation of diaphragm proteolysis during mechanical ventilation. American Journal of Physiology-Regulatory Integrative and Comparative Physiology 2008;294(5):R1608-R1617.

8. Powers SK, Kavazis AN, McClung JM. Oxidative stress and disuse muscle atrophy. J Appl Physiol 2007;102(6):2389-2397.

9. Zergeroglu MA, McKenzie MJ, Shanely RA, et al. Mechanical ventilation-induced oxidative stress in the diaphragm. Journal of Applied Physiology 2003;95(3):1116-1124.

10. Powers SK, Shanely RA, Coombes JS, et al. Mechanical ventilation results in progressive contractile dysfunction in the diaphragm. Journal of Applied Physiology 2002;92(5):1851-1858.

11. McClung JM, Kavazis AN, DeRuisseau KC, et al. Caspase-3 regulation of diaphragm myonuclear domain during mechanical ventilation-induced atrophy. Am J Respir Crit Care Med 2007;175(2):150-159.

12. Levine S, Nguyen T, Taylor N, et al. Rapid disuse atrophy of diaphragm fibers in mechanically ventilated humans. N Engl J Med 2008;358(13):1327-1335.

13. Martin AD. Inspiratrory muscle strength training to facilitate ventilator weaning: a randomized, controlled trial. In. Gainesville, FL: University of Florida; 2009.

14. Ramirez-Sarmiento A, Orozco-Levi M, Guell R, et al. Inspiratory muscle training in patients with chronic obstructive pulmonary disease: structural adaptation and physiologic outcomes. Am J Respir Crit Care Med 2002;166(11):1491-1497.

15. Keens TG, Chen V, Patel P, et al. Cellular adaptations of the ventilatory muscles to a chronic increased respiratory load. J Appl Physiol 1978;44(6):905-908.

16. Tarasiuk A, Scharf SM, Miller MJ. Effect of chronic resistive loading on inspiratory muscles in rats. J Appl Physiol 1991;70(1):216-222.

17. Reid WD, Belcastro AN. Chronic resistive loading induces diaphragm injury and ventilatory failure in the hamster. Respir Physiol 1999;118(2-3):203-218.

18. Thomason DB, Biggs RB, Booth FW. Protein metabolism and beta-myosin heavy-chain mRNA in unweighted soleus muscle. Am J Physiol 1989;257(2 Pt 2):R300-305.

19. Gea J, Hamid Q, Czaika G, et al. Expression of myosin heavy-chain isoforms in the respiratory muscles following inspiratory resistive breathing. Am J Respir Crit Care Med 2000;161(4 Pt 1):1274-1278.

20. Reid WD, MacGowan NA. Respiratory muscle injury in animal models and humans. Mol Cell Biochem 1998;179(1-2):63-80.

21. Bisschop A, Gayan-Ramirez G, Rollier H, et al. Intermittent inspiratory muscle training induces fiber hypertrophy in rat diaphragm. Am J Respir Crit Care Med 1997;155(5):1583-1589.

22. Wilson TA, Boriek AM, Rodarte JR. Mechanical advantage of the canine diaphragm. J Appl Physiol 1998;85(6):2284-2290.

23. Jammes Y, Arbogast S, De Troyer A. Response of the rabbit diaphragm to tendon vibration. Neurosci Lett 2000;290(2):85-88.

24. Pickering M, Jones JF. The diaphragm: two physiological muscles in one. J Anat 2002;201(4):305-312.

25. Sharshar T, Hopkinson NS, Ross ET, et al. Motor control of the costal and crural diaphragm--insights from transcranial magnetic stimulation in man. Respir Physiol Neurobiol 2005;146(1):5-19.

26. Poole DC, Sexton WL, Farkas GA, et al. Diaphragm structure and function in health and disease. Med Sci Sports Exerc 1997;29(6):738-754.

27. Hwang W, Kelly NG, Boriek AM. Passive mechanics of muscle tendinous junction of canine diaphragm. J Appl Physiol 2005;98(4):1328-1333.

28. Sieck GC, Roy RR, Powell P, et al. Muscle fiber type distribution and architecture of the cat diaphragm. J Appl Physiol 1983;55(5):1386-1392.

29. Sieck GC, Zhan WZ, Prakash YS, et al. SDH and actomyosin ATPase activities of different fiber types in rat diaphragm muscle. J Appl Physiol 1995;79(5):1629-1639.

30. Vincent HK, Shanely RA, Stewart DJ, et al. Adaptation of upper airway muscles to chronic endurance exercise. Am J Respir Crit Care Med 2002;166(3):287-293.

31. Laskowski MB, Sanes JR. Topographic mapping of motor pools onto skeletal muscles. J Neurosci 1987;7(1):252-260.

32. Luscher HR, Ruenzel P, Henneman E. How the size of motoneurones determines their susceptibility to discharge. Nature 1979;282(5741):859-861.

33. Sieck GC, Fournier M. Diaphragm motor unit recruitment during ventilatory and nonventilatory behaviors. J Appl Physiol 1989;66(6):2539-2545.

34. Butler JE, Gandevia SC. The output from human inspiratory motoneurone pools. J Physiol 2008;586(5):1257-1264.

35. Gandevia SC, Gorman RB, McKenzie DK, et al. Effects of increased ventilatory drive on motor unit firing rates in human inspiratory muscles. Am J Respir Crit Care Med 1999;160(5 Pt 1):1598-1603.

36. Saboisky JP, Gorman RB, De Troyer A, et al. Differential activation among five human inspiratory motoneuron pools during tidal breathing. J Appl Physiol 2007;102(2):772-780.

37. Arora NS, Rochester DF. Effect of body weight and muscularity on human diaphragm muscle mass, thickness, and area. J Appl Physiol 1982;52(1):64-70.

38. Boriek AM, Rodarte JR, Margulies SS. Zone of apposition in the passive diaphragm of the dog. J Appl Physiol 1996;81(5):1929-1940.

39. Reid WD, Wiggs BR, Pare PD, et al. Fiber type and regional differences in oxidative capacity and glycogen content in the hamster diaphragm. Am Rev Respir Dis 1992;146(5 Pt 1):1266-1271.

40. Sexton WL, Poole DC, Mathieu-Costello O. Microcirculatory structure-function relationships in skeletal muscle of diabetic rats. Am J Physiol 1994;266(4 Pt 2):H1502-1511.

41. Johnson RL, Jr., Hsia CC, Takeda S, et al. Efficient design of the diaphragm: distribution of blood flow relative to mechanical advantage. J Appl Physiol 2002;93(3):925-930.

42. Reid WD, Cairns CL, McRae DJ, et al. Regional and fibre type glycogen utilization patterns in the hamster diaphragm following swimming. Respir Med 1994;88(6):421-427.

43. Wilson TA, De Troyer A. Effect of respiratory muscle tension on lung volume. J Appl Physiol 1992;73(6):2283-2288.

44. Wilson TA, De Troyer A. Respiratory effect of the intercostal muscles in the dog. J Appl Physiol 1993;75(6):2636-2645.

45. Boriek AM, Rodarte JR, Wilson TA. Ratio of active to passive muscle shortening in the canine diaphragm. J Appl Physiol 1999;87(2):561-566.

46. Wilson TA, Angelillo M, Legrand A, et al. Muscle kinematics for minimal work of breathing. J Appl Physiol 1999;87(2):554-560.

47. McKenzie DK, Gandevia SC, Gorman RB, et al. Dynamic changes in the zone of apposition and diaphragm length during maximal respiratory efforts. Thorax 1994;49(7):634-638.

48. Wakai Y, Leevers AM, Road JD. Regional diaphragm shortening measured by sonomicrometry. J Appl Physiol 1994;77(6):2791-2796.

49. Friden J, Lieber RL. Structural and mechanical basis of exercise-induced muscle injury. Med Sci Sports Exerc 1992;24(5):521-530.

50. Vikne H, Refsnes PE, Ekmark M, et al. Muscular performance after concentric and eccentric exercise in trained men. Med Sci Sports Exerc 2006;38(10):1770-1781.

51. Finucane KE, Singh B. Human diaphragm efficiency estimated as power output relative to activation increases with hypercapnic hyperpnea. J Appl Physiol 2009;107(5):1397-1405.

52. Farkas GA, Cerny FJ, Rochester DF. Contractility of the ventilatory pump muscles. Med Sci Sports Exerc 1996;28(9):1106-1114.

53. Schilero GJ, Spungen AM, Bauman WA, et al. Pulmonary function and spinal cord injury. Respir Physiol Neurobiol 2009;166(3):129-141.

54. McKenzie DK, Butler JE, Gandevia SC. Respiratory muscle function and activation in chronic obstructive pulmonary disease. J Appl Physiol 2009;107(2):621-629.

55. De Troyer A, Kirkwood PA, Wilson TA. Respiratory action of the intercostal muscles. Physiol Rev 2005;85(2):717-756.

56. Gandevia SC, Hudson AL, Gorman RB, et al. Spatial distribution of inspiratory drive to the parasternal intercostal muscles in humans. J Physiol 2006;573(Pt 1):263-275.

57. De Troyer A, Legrand A, Wilson TA. Rostrocaudal gradient of mechanical advantage in the parasternal intercostal muscles of the dog. J Physiol 1996;495 (Pt 1):239-246.

58. Mantilla CB, Rowley KL, Fahim MA, et al. Synaptic vesicle cycling at type-identified diaphragm neuromuscular junctions. Muscle Nerve 2004;30(6):774-783.

59. Sharshar T, Ross ET, Hopkinson NS, et al. Depression of diaphragm motor cortex excitability during mechanical ventilation. J Appl Physiol 2004;97(1):3-10.

60. Manchanda S, Leevers AM, Wilson CR, et al. Frequency and volume thresholds for inhibition of inspiratory motor output during mechanical ventilation. Respir Physiol 1996;105(1-2):1-16.

61. Shanely RA, Zergeroglu MA, Lennon SL, et al. Mechanical ventilation-induced diaphragmatic atrophy is associated with oxidative injury and increased proteolytic activity. Am J Respir Crit Care Med 2002;166(10):1369-1374.

62. Maes K, Testelmans D, Powers S, et al. Leupeptin inhibits, ventilator-induced diaphragm dysfunction in rats. American Journal of Respiratory and Critical Care Medicine 2007;175(11):1134-1138.

63. McClung JM, Kavazis AN, Whidden MA, et al. Antioxidant administration attenuates mechanical ventilation-induced rat diaphragm muscle atrophy independent of protein kinase B (PKB-Akt) signalling. Journal of Physiology-London 2007;585(1):203-215.

64. Gayan-Ramirez G, Testelmans D, Maes K, et al. Intermittent spontaneous breathing protects the rat diaphragm from mechanical ventilation effects. Critical Care Medicine 2005;33(12):2804-2809.

65. Shanely RA, Van Gammeren D, Zergeroglu M, et al. Protein synthesis and myosin heavy chain mRNA in the rat diaphragm during mechanical ventilation. Faseb Journal 2003;17(4):A435-A435.

66. DeRuisseau KC, Kavazis AN, Deering MA, et al. Mechanical ventilation induces alterations of the ubiquitin-proteasome pathway in the diaphragm. Journal of Applied Physiology 2005;98(4):1314-1321.

67. Shanely RA, Coombes JS, Zergeroglu AM, et al. Short-duration mechanical ventilation enhances diaphragmatic resistance but impairs fatigue force production. Chest 2003;123(1):195-201.

68. Capdevila X, Lopez S, Bernard N, et al. Effects of controlled mechanical ventilation on respiratory muscle contractile properties in rabbits. Intensive Care Med 2003;29(1):103-110.

69. Huang CH, Martin AD, Davenport PW. Effects of inspiratory strength training on the detection of inspiratory loads. Appl Psychophysiol Biofeedback 2009;34(1):17-26.

70. Kavazis AN, Talbert EE, Smuder AJ, et al. Mechanical ventilation induces diaphragmatic mitochondrial dysfunction and increased oxidant production. Free Radic Biol Med 2009;46(6):842-850.

71. Zhao J, Brault JJ, Schild A, et al. Coordinate activation of autophagy and the proteasome pathway by FoxO transcription factor. Autophagy 2008;4(3):378-380.

72. Favier FB, Benoit H, Freyssenet D. Cellular and molecular events controlling skeletal muscle mass in response to altered use. Pflugers Arch 2008;456(3):587-600.

73. Zhao J, Brault JJ, Schild A, et al. FoxO3 coordinately activates protein degradation by the autophagic/lysosomal and proteasomal pathways in atrophying muscle cells. Cell Metab 2007;6(6):472-483.

74. Masiero E, Agatea L, Mammucari C, et al. Autophagy is required to maintain muscle mass. Cell Metab 2009;10(6):507-515.

75. Anzueto A, Peters JI, Tobin MJ, et al. Effects of prolonged controlled mechanical ventilation on diaphragmatic function in healthy adult baboons. Crit Care Med 1997;25(7):1187-1190.

76. Sassoon CS, Caiozzo VJ, Manka A, et al. Altered diaphragm contractile properties with controlled mechanical ventilation. J Appl Physiol 2002;92(6):2585-2595.

77. Sassoon CS, Zhu E, Caiozzo VJ. Assist-control mechanical ventilation attenuates ventilator-induced diaphragmatic dysfunction. Am J Respir Crit Care Med 2004;170(6):626-632.

78. Zhu E, Sassoon CS, Nelson R, et al. Early effects of mechanical ventilation on isotonic contractile properties and MAF-box gene expression in the diaphragm. J Appl Physiol 2005;99(2):747-756.

79. Racz GZ, Gayan-Ramirez G, Testelmans D, et al. Early changes in rat diaphragm biology with mechanical ventilation. American Journal of Respiratory and Critical Care Medicine 2003;168(3):297-304.

80. Radell PJ, Remahl S, Nichols DG, et al. Effects of prolonged mechanical ventilation and inactivity on piglet diaphragm function. Intensive Care Med 2002;28(3):358-364.

81. Testelmans D, Maes K, Wouters P, et al. Infusions of rocuronium and cisatracurium exert different effects on rat diaphragm function. Intensive Care Medicine 2007;33(5):872-879.

82. Bernard N, Matecki S, Py G, et al. Effects of prolonged mechanical ventilation on respiratory muscle ultrastructure and mitochondrial respiration in rabbits. Intensive Care Med 2003;29(1):111-118.

83. Knisely AS, Leal SM, Singer DB. Abnormalities of diaphragmatic muscle in neonates with ventilated lungs. J Pediatr 1988;113(6):1074-1077.

84. Schweickert WD, Hall J. ICU-acquired weakness. Chest 2007;131(5):1541-1549.

85. Hermans G, De Jonghe B, Bruyninckx F, et al. Interventions for preventing critical illness polyneuropathy and critical illness myopathy. Cochrane Database Syst Rev 2009(1):CD006832.

86. De Jonghe B, Bastuji-Garin S, Durand MC, et al. Respiratory weakness is associated with limb weakness and delayed weaning in critical illness. Crit Care Med 2007;35(9):2007-2015.

87. Powers SK, Kavazis AN, Levine S. Prolonged mechanical ventilation alters diaphragmatic structure and function. Crit Care Med 2009;37(10 Suppl):S347-353.

88. Jubran A. Critical illness and mechanical ventilation: effects on the diaphragm. Respir Care 2006;51(9):1054-1061; discussion 1062-1054.

89. Vassilakopoulos T. Ventilator-induced diaphragm dysfunction: the clinical relevance of animal models. Intensive Care Med 2008;34(1):7-16.

90. Esteban A, Ferguson ND, Meade MO, et al. Evolution of mechanical ventilation in response to clinical research. Am J Respir Crit Care Med 2008;177(2):170-177.

91. Vassilakopoulos T, Zakynthinos S, Roussos C. Bench-to-bedside review: weaning failure--should we rest the respiratory muscles with controlled mechanical ventilation? Crit Care 2006;10(1):204.

92. Epstein SK. Etiology of extubation failure and the predictive value of the rapid shallow breathing index. Am J Respir Crit Care Med 1995;152(2):545-549.

93. Ely EW, Baker AM, Dunagan DP, et al. Effect on the duration of mechanical ventilation of identifying patients capable of breathing spontaneously. N Engl J Med 1996;335(25):1864-1869.

94. Aboussouan LS, Lattin CD, Anne VV. Determinants of time-to-weaning in a specialized respiratory care unit. Chest 2005;128(5):3117-3126.

95. Bien MY, Hseu SS, Yien HW, et al. Breathing pattern variability: a weaning predictor in postoperative patients recovering from systemic inflammatory response syndrome. Intensive Care Med 2004;30(2):241-247.

96. Boles JM, Bion J, Connors A, et al. Weaning from mechanical ventilation. Eur Respir J 2007;29(5):1033-1056.

97. Capdevila X, Perrigault PF, Ramonatxo M, et al. Changes in breathing pattern and respiratory muscle performance parameters during difficult weaning. Crit Care Med 1998;26(1):79-87.

98. Conti G, Montini L, Pennisi MA, et al. A prospective, blinded evaluation of indexes proposed to predict weaning from mechanical ventilation. Intensive Care Med 2004;30(5):830-836.

99. Epstein CD, Peerless JR. Weaning readiness and fluid balance in older critically ill surgical patients. Am J Crit Care 2006;15(1):54-64.

100. Jubran A, Grant BJ, Laghi F, et al. Weaning prediction: esophageal pressure monitoring complements readiness testing. Am J Respir Crit Care Med 2005;171(11):1252-1259.

101. Purro A, Appendini L, De Gaetano A, et al. Physiologic determinants of ventilator dependence in long-term mechanically ventilated patients. Am J Respir Crit Care Med 2000;161(4 Pt 1):1115-1123.

102. Yang KL, Tobin MJ. A prospective study of indexes predicting the outcome of trials of weaning from mechanical ventilation. N Engl J Med 1991;324(21):1445-1450.

103. Gayan-Ramirez G, Decramer M. Effects of mechanical ventilation on diaphragm function and biology. European Respiratory Journal 2002;20(6):1579-1586.

104. Vassilakopoulos T, Routsi C, Sotiropoulou C, et al. The combination of the load/force balance and the frequency/tidal volume can predict weaning outcome. Intensive Care Med 2006;32(5):684-691.

105. Marini JJ. Breathing patterns as integrative weaning predictors: Variations on a theme. Crit Care Med 2006;34(8):2241-2243.

106. Carlucci A, Ceriana P, Prinianakis G, et al. Determinants of weaning success in patients with prolonged mechanical ventilation. Crit Care 2009;13(3):R97.

107. Kallet RH, Hemphill JC, 3rd, Dicker RA, et al. The spontaneous breathing pattern and work of breathing of patients with acute respiratory distress syndrome and acute lung injury. Respir Care 2007;52(8):989-995.

108. Jubran A, Tobin MJ. Passive mechanics of lung and chest wall in patients who failed or succeeded in trials of weaning. Am J Respir Crit Care Med 1997;155(3):916-921.

109. Parthasarathy S, Jubran A, Laghi F, et al. Sternomastoid, rib cage, and expiratory muscle activity during weaning failure. J Appl Physiol 2007;103(1):140-147.

110. Jubran A, Parthasarathy S. Hypercapnic respiratory failure during weaning: neuromuscular capacity versus muscle loads. Respir Care Clin N Am 2000;6(3):385-405;v.

111. Vassilakopoulos T, Zakynthinos S, Roussos C. Respiratory muscles and weaning failure. Eur Respir J 1996;9(11):2383-2400.

112. Harikumar G, Egberongbe Y, Nadel S, et al. Tension-time index as a predictor of extubation outcome in ventilated children. Am J Respir Crit Care Med 2009;180(10):982-988.

113. Ochiai R, Shimada M, Takeda J, et al. Contribution of rib cage and abdominal movement to ventilation for successful weaning from mechanical ventilation. Acta Anaesthesiol Scand 1993;37(2):131-136.

114. Laghi F, Cattapan SE, Jubran A, et al. Is weaning failure caused by low-frequency fatigue of the diaphragm? Am J Respir Crit Care Med 2003;167(2):120-127.

115. Pappens M, Van den Bergh O, De Peuter S, et al. Defense reactions to interoceptive threats: A comparison between loaded breathing and aversive picture viewing. Biol Psychol.

116. Lerman RM, Weiss MS. Progressive resistive exercise in weaning high quadriplegics from the ventilator. Paraplegia 1987;25(2):130-135.

117. Belman MJ. Respiratory failure treated by ventilatory muscle training (VMT). A report of two cases. Eur J Respir Dis 1981;62(6):391-395.

118. Aldrich TK, Karpel JP. Inspiratory muscle resistive training in respiratory failure. Am Rev Respir Dis 1985;131(3):461-462.

119. Aldrich TK, Karpel JP, Uhrlass RM, et al. Weaning from mechanical ventilation: adjunctive use of inspiratory muscle resistive training. Crit Care Med 1989;17(2):143-147.

120. Jederlinic P, Muspratt JA, Miller MJ. Inspiratory muscle training in clinical practice. Physiologic conditioning or habituation to suffocation? Chest 1984;86(6):870-873.

121. Caruso P, Denari SD, Ruiz SA, et al. Inspiratory muscle training is ineffective in mechanically ventilated critically ill patients. Clinics 2005;60(6):479-484.

122. Brochard L, Thille AW. What is the proper approach to liberating the weak from mechanical ventilation? Crit Care Med 2009;37(10 Suppl):S410-415.

123. Johnson PH, Cowley AJ, Kinnear WJ. Evaluation of the THRESHOLD trainer for inspiratory muscle endurance training: comparison with the weighted plunger method. Eur Respir J 1996;9(12):2681-2684.

124. Gosselink R, Wagenaar RC, Decramer M. Reliability of a commercially available threshold loading device in healthy subjects and in patients with chronic obstructive pulmonary disease. Thorax 1996;51(6):601-605.

125. Martin AD, Davenport PD, Franceschi AC, et al. Use of inspiratory muscle strength training to facilitate ventilator weaning: a series of 10 consecutive patients. Chest 2002;122(1):192-196.

126. Chang AT, Boots RJ, Henderson R, et al. Case report: inspiratory muscle training in chronic critically ill patients--a report of two cases. Physiother Res Int 2005;10(4):222-226.

127. Sprague SS, Hopkins PD. Use of inspiratory strength training to wean six patients who were ventilator-dependent. Phys Ther 2003;83(2):171-181.

128. Martin AD. Inspiratrory muscle strength training to facilitate ventilator weaning: a randomized, controlled trial. In. Gainesville, FL: University of Florida; 2008.

129. Kellerman BA, Martin AD, Davenport PW. Inspiratory strengthening effect on resistive load detection and magnitude estimation. Med Sci Sports Exerc 2000;32(11):1859-1867.

130. Witt JD, Guenette JA, Rupert JL, et al. Inspiratory muscle training attenuates the human respiratory muscle metaboreflex. J Physiol 2007;584(Pt 3):1019-1028.

131. Romer LM, McConnell AK. Specificity and reversibility of inspiratory muscle training. Med Sci Sports Exerc 2003;35(2):237-244.

132. Huang CH, Martin AD, Davenport PW. Effect of inspiratory muscle strength training on inspiratory motor drive and RREP early peak components. J Appl Physiol 2003;94(2):462-468.

133. Hulzebos EH, Helders PJ, Favie NJ, et al. Preoperative intensive inspiratory muscle training to prevent postoperative pulmonary complications in high-risk patients undergoing CABG surgery: a randomized clinical trial. Jama 2006;296(15):1851-1857.

134. Nomori H, Kobayashi R, Fuyuno G, et al. Preoperative respiratory muscle training. Assessment in thoracic surgery patients with special reference to postoperative pulmonary complications. Chest 1994;105(6):1782-1788.

135. Weiner P, Zeidan F, Zamir D, et al. Prophylactic inspiratory muscle training in patients undergoing coronary artery bypass graft. World J Surg 1998;22(5):427-431.

136. Darnley GM, Gray AC, McClure SJ, et al. Effects of resistive breathing on exercise capacity and diaphragm function in patients with ischaemic heart disease. Eur J Heart Fail 1999;1(3):297-300.

137. Bickel CS, Slade J, Mahoney E, et al. Time course of molecular responses of human skeletal muscle to acute bouts of resistance exercise. J Appl Physiol 2005;98(2):482-488.

138. Prezant DJ, Aldrich TK, Richner B, et al. Effects of long-term continuous respiratory resistive loading on rat diaphragm function and structure. J Appl Physiol 1993;74(3):1212-1219.

139. Rollier H, Bisschop A, Gayan-Ramirez G, et al. Low load inspiratory muscle training increases diaphragmatic fiber dimensions in rats. Am J Respir Crit Care Med 1998;157(3 Pt 1):833-839.

140. Zhu E, Petrof BJ, Gea J, et al. Diaphragm muscle fiber injury after inspiratory resistive breathing. Am J Respir Crit Care Med 1997;155(3):1110-1116.

141. Schiaffino S, Sandri M, Murgia M. Activity-dependent signaling pathways controlling muscle diversity and plasticity. Physiology (Bethesda) 2007;22:269-278.

142. Quinn LS, Anderson BG, Plymate SR. Muscle-specific overexpression of the type 1 IGF receptor results in myoblast-independent muscle hypertrophy via PI3K, and not calcineurin, signaling. Am J Physiol Endocrinol Metab 2007;293(6):E1538-1551.

143. Blaauw B, Canato M, Agatea L, et al. Inducible activation of Akt increases skeletal muscle mass and force without satellite cell activation. FASEB J 2009;23(11):3896-3905.

144. Rommel C, Bodine SC, Clarke BA, et al. Mediation of IGF-1-induced skeletal myotube hypertrophy by PI(3)K/Akt/mTOR and PI(3)K/Akt/GSK3 pathways. Nat Cell Biol 2001;3(11):1009-1013.

145. Adams GR. Invited Review: Autocrine/paracrine IGF-I and skeletal muscle adaptation. J Appl Physiol 2002;93(3):1159-1167.

146. Spangenburg EE, Le Roith D, Ward CW, et al. A functional insulin-like growth factor receptor is not necessary for load-induced skeletal muscle hypertrophy. J Physiol 2008;586(1):283-291.

147. Phillips SM. Physiologic and molecular bases of muscle hypertrophy and atrophy: impact of resistance exercise on human skeletal muscle (protein and exercise dose effects). Appl Physiol Nutr Metab 2009;34(3):403-410.

148. Adams GR, Caiozzo VJ, Haddad F, et al. Cellular and molecular responses to increased skeletal muscle loading after irradiation. Am J Physiol Cell Physiol 2002;283(4):C1182-1195.

149. Phelan JN, Gonyea WJ. Effect of radiation on satellite cell activity and protein expression in overloaded mammalian skeletal muscle. Anat Rec 1997;247(2):179-188.

150. Rosenblatt JD, Parry DJ. Gamma irradiation prevents compensatory hypertrophy of overloaded mouse extensor digitorum longus muscle. J Appl Physiol 1992;73(6):2538-2543.

151. Petrella JK, Kim JS, Mayhew DL, et al. Potent myofiber hypertrophy during resistance training in humans is associated with satellite cell-mediated myonuclear addition: a cluster analysis. J Appl Physiol 2008;104(6):1736-1742.

152. Kadi F, Schjerling P, Andersen LL, et al. The effects of heavy resistance training and detraining on satellite cells in human skeletal muscles. J Physiol 2004;558(Pt 3):1005-1012.

153. Betters JL, Long JH, Howe KS, et al. Nitric oxide reverses prednisolone-induced inactivation of muscle satellite cells. Muscle Nerve 2008;37(2):203-209.

154. Rennie MJ, Wackerhage H, Spangenburg EE, et al. Control of the size of the human muscle mass. Annu Rev Physiol 2004;66:799-828.

155. Harridge SD. Plasticity of human skeletal muscle: gene expression to in vivo function. Exp Physiol 2007;92(5):783-797.

156. Philippou A, Halapas A, Maridaki M, et al. Type I insulin-like growth factor receptor signaling in skeletal muscle regeneration and hypertrophy. J Musculoskelet Neuronal Interact 2007;7(3):208-218.

157. Ge Y, Wu AL, Warnes C, et al. mTOR regulates skeletal muscle regeneration in vivo through kinase-dependent and kinase-independent mechanisms. Am J Physiol Cell Physiol 2009;297(6):C1434-1444.

158. Trendelenburg AU, Meyer A, Rohner D, et al. Myostatin reduces Akt/TORC1/p70S6K signaling, inhibiting myoblast differentiation and myotube size. Am J Physiol Cell Physiol 2009;296(6):C1258-1270.

159. Roy RR, Talmadge RJ, Fox K, et al. Modulation of MHC isoforms in functionally overloaded and exercised rat plantaris fibers. J Appl Physiol 1997;83(1):280-290.

160. Wanek LJ, Snow MH. Activity-induced fiber regeneration in rat soleus muscle. Anat Rec 2000;258(2):176-185.

161. Kadi F, Eriksson A, Holmner S, et al. Cellular adaptation of the trapezius muscle in strength-trained athletes. Histochem Cell Biol 1999;111(3):189-195.

162. Reid WD, Huang J, Bryson S, et al. Diaphragm injury and myofibrillar structure induced by resistive loading. J Appl Physiol 1994;76(1):176-184.

163. Jiang TX, Reid WD, Belcastro A, et al. Load dependence of secondary diaphragm inflammation and injury after acute inspiratory loading. Am J Respir Crit Care Med 1998;157(1):230-236.

164. Dechman G, Belzberg A, Reid WD. Single-photon emission computed tomography imaging of diaphragm overuse injury in rabbits. Am J Respir Crit Care Med 1996;153(4):A600.

165. Jiang TX, Reid WD, Road JD. Delayed diaphragm injury and diaphragm force production. Am J Respir Crit Care Med 1998;157(3 Pt 1):736-742.

166. Reid WD, Belcastro AN. Time course of diaphragm injury and calpain activity during resistive loading. Am J Respir Crit Care Med 2000;162(5):1801-1806.

167. Wang X, Jiang TX, Road JD, et al. Granulocytosis and increased adhesion molecules after resistive loading of the diaphragm. Eur Respir J 2005;26(5):786-794.

168. Ambrosio F, Kadi F, Lexell J, et al. The effect of muscle loading on skeletal muscle regenerative potential: an update of current research findings relating to aging and neuromuscular pathology. Am J Phys Med Rehabil 2009;88(2):145-155.

169. Jiang TX, Reid WD, Road JD. Free radical scavengers and diaphragm injury following inspiratory resistive loading. Am J Respir Crit Care Med 2001;164(7):1288-1294.

170. Van Gammeren D, Falk DJ, DeRuisseau KC, et al. Reloading the diaphragm following mechanical ventilation does not promote injury. Chest 2005;127(6):2204-2210.

171. Hamer PW, McGeachie JM, Davies MJ, et al. Evans Blue Dye as an in vivo marker of myofibre damage: optimising parameters for detecting initial myofibre membrane permeability. J Anat 2002;200(Pt 1):69-79.

172. Peters D, Barash IA, Burdi M, et al. Asynchronous functional, cellular and transcriptional changes after a bout of eccentric exercise in the rat. J Physiol 2003;553(Pt 3):947-957.

173. Supinski G. Free radical induced respiratory muscle dysfunction. Mol Cell Biochem 1998;179(1-2):99-110.

174. Belcastro AN, Shewchuk LD, Raj DA. Exercise-induced muscle injury: a calpain hypothesis. Mol Cell Biochem 1998;179(1-2):135-145.

175. Proske U, Morgan DL. Muscle damage from eccentric exercise: mechanism, mechanical signs, adaptation and clinical applications. J Physiol 2001;537(Pt 2):333-345.

176. Warren GL, Ingalls CP, Lowe DA, et al. Excitation-contraction uncoupling: major role in contraction-induced muscle injury. Exerc Sport Sci Rev 2001;29(2):82-87.

177. Lieber RL, Thornell LE, Friden J. Muscle cytoskeletal disruption occurs within the first 15 min of cyclic eccentric contraction. J Appl Physiol 1996;80(1):278-284.

178. Kaariainen M, Jarvinen T, Jarvinen M, et al. Relation between myofibers and connective tissue during muscle injury repair. Scand J Med Sci Sports 2000;10(6):332-337.

179. Adams GR, Haddad F, Baldwin KM. Time course of changes in markers of myogenesis in overloaded rat skeletal muscles. J Appl Physiol 1999;87(5):1705-1712.

180. Paoni NF, Peale F, Wang F, et al. Time course of skeletal muscle repair and gene expression following acute hind limb ischemia in mice. Physiol Genomics 2002;11(3):263-272.

181. Pizza FX, Peterson JM, Baas JH, et al. Neutrophils contribute to muscle injury and impair its resolution after lengthening contractions in mice. J Physiol 2005;562(Pt 3):899-913.

182. Ma K, Mallidis C, Bhasin S, et al. Glucocorticoid-induced skeletal muscle atrophy is associated with upregulation of myostatin gene expression. Am J Physiol Endocrinol Metab 2003;285(2):E363-371.

183. Heinemeier KM, Olesen JL, Schjerling P, et al. Short-term strength training and the expression of myostatin and IGF-I isoforms in rat muscle and tendon: differential effects of specific contraction types. J Appl Physiol 2007;102(2):573-581.

184. Warren GL, Summan M, Gao X, et al. Mechanisms of skeletal muscle injury and repair revealed by gene expression studies in mouse models. J Physiol 2007;582(Pt 2):825-841.

185. Dubowitz V, Sewry C. Muscle Biopsy: A Practical Approach. 3rd edition ed. Philadelphia, PA: Saunders; 2007.

186. Ten Broek RW, Grefte S, Von den Hoff JW. Regulatory factors and cell populations involved in skeletal muscle regeneration. J Cell Physiol.

187. Zilberberg MD, de Wit M, Pirone JR, et al. Growth in adult prolonged acute mechanical ventilation: implications for healthcare delivery. Crit Care Med 2008;36(5):1451-1455.

188. Cox CE, Carson SS, Lindquist JH, et al. Differences in one-year health outcomes and resource utilization by definition of prolonged mechanical ventilation: a prospective cohort study. Crit Care 2007;11(1):R9.

189. Angel MJ, Bril V, Shannon P, et al. Neuromuscular function in survivors of the acute respiratory distress syndrome. Can J Neurol Sci 2007;34(4):427-432.

190. Truwit JD, Marini JJ. Validation of a technique to assess maximal inspiratory pressure in poorly cooperative patients. Chest 1992;102(4):1216-1219.

191. Testelmans D, Maes K, Wouters P, et al. Rocuronium exacerbates mechanical ventilation-induced diaphragm dysfunction in rats. Critical Care Medicine 2006;34(12):3018-3023.

192. Sieck GC, Prakash YS. The Diaphragm Muscle. In: Miller AD, Bianchi AL, Bishop BP, editors. Neural Control of the Respiratory Muscles. Boca Raton, FL: CRC Press; 1996. p. 7-20.

193. Hensbergen E, Kernell D. Daily durations of spontaneous activity in cat's ankle muscles. Exp Brain Res 1997;115(2):325-332.

194. Nava S, Ambrosino N, Crotti P, et al. Recruitment of some respiratory muscles during three maximal inspiratory manoeuvres. Thorax 1993;48(7):702-707.

195. Larsson L, Skogsberg C. Effects of the interval between removal and freezing of muscle biopsies on muscle fibre size. J Neurol Sci 1988;85(1):27-38.

196. Scott A, Wang X, Road JD, et al. Increased injury and intramuscular collagen of the diaphragm in COPD: autopsy observations. Eur Respir J 2006;27(1):51-59.

197. Martinez-Llorens J, Casadevall C, Lloreta J, et al. [Activation of satellite cells in the intercostal muscles of patients with chronic obstructive pulmonary disease]. Arch Bronconeumol 2008;44(5):239-244.

198. Smith AG, Urbanits S, Blaivas M, et al. Clinical and pathologic features of focal myositis. Muscle Nerve 2000;23(10):1569-1575.

199. Hanke N, Kubis HP, Scheibe RJ, et al. Passive mechanical forces upregulate the fast myosin heavy chain IId/x via integrin and p38 MAP kinase activation in a primary muscle cell culture. Am J Physiol Cell Physiol;298(4):C910-920.

200. Stauber WT, Miller GR, Grimmett JG, et al. Adaptation of rat soleus muscles to 4 wk of intermittent strain. J Appl Physiol 1994;77(1):58-62.

201. Zhan WZ, Farkas GA, Schroeder MA, et al. Regional adaptations of rabbit diaphragm muscle fibers to unilateral denervation. J Appl Physiol 1995;79(3):941-950.

202. Miyata H, Zhan WZ, Prakash YS, et al. Myoneural interactions affect diaphragm muscle adaptations to inactivity. J Appl Physiol 1995;79(5):1640-1649.

203. Woolstenhulme MT, Conlee RK, Drummond MJ, et al. Temporal response of desmin and dystrophin proteins to progressive resistance exercise in human skeletal muscle. J Appl Physiol 2006;100(6):1876-1882.

204. Yamaguchi A, Ikeda Y, Hirai T, et al. Local changes of IGF-I mRNA, GH receptor mRNA, and fiber size in rat plantaris muscle following compensatory overload. Jpn J Physiol 2003;53(1):53-60.

205. Goldspink G, Ward PS. Changes in rodent muscle fibre types during post-natal growth, undernutrition and exercise. J Physiol 1979;296:453-469.

206. Mantilla CB, Sieck GC. Neuromuscular adaptations to respiratory muscle inactivity. Respir Physiol Neurobiol 2009;169(2):133-140.

207. Hellyer NJ, Mantilla CB, Park EW, et al. Neuregulin-dependent protein synthesis in C2C12 myotubes and rat diaphragm muscle. Am J Physiol Cell Physiol 2006;291(5):C1056-1061.

208. Butler JE, McKenzie DK, Gandevia SC. Discharge properties and recruitment of human diaphragmatic motor units during voluntary inspiratory tasks. J Physiol 1999;518 (Pt 3):907-920.

209. Kumar V, Selby A, Rankin D, et al. Age-related differences in the dose-response relationship of muscle protein synthesis to resistance exercise in young and old men. J Physiol 2009;587(Pt 1):211-217.

210. Mantilla CB, Seven YB, Zhan WZ, et al. Modeling diaphragm motor unit recruitment across ventilatory behaviors. Am J Respir Crit Care Med 2010;181:A3718.

211. Harikumar G, Moxham J, Greenough A, et al. Measurement of maximal inspiratory pressure in ventilated children. Pediatr Pulmonol 2008;43(11):1085-1091.

212. D'Angelo E, Monaco A, Pecchiari M. Motor control of the diaphragm in anesthetized rabbits. Respir Physiol Neurobiol;170(2):141-149.

213. Knight H, Petroll WM, Adams JM, et al. Videofluoroscopic assessment of muscle fiber shortening in the in situ canine diaphragm. J Appl Physiol 1990;68(5):2200-2207.

214. De Troyer A. Interaction between the canine diaphragm and intercostal muscles in lung expansion. J Appl Physiol 2005;98(3):795-803.

215. DiMarco AF, Supinski GS, Budzinska K. Inspiratory muscle interaction in the generation of changes in airway pressure. J Appl Physiol 1989;66(6):2573-2578.

216. Caiozzo VJ, Rourke B. The Muscular System: Structural and Functional Plasticity. In: Tipton CM, editor. ACSM's Advanced Exercise Physiology. Philadelphia, Pa: Lippincott Williams & Wilkins; 2006. p. 144-160.

217. Hershenson MB, Kikuchi Y, Loring SH. Relative strengths of the chest wall muscles. J Appl Physiol 1988;65(2):852-862.

218. Riley DA, Berger AJ. A regional histochemical and electromyographic analysis of the cat respiratory diaphragm. Exp Neurol 1979;66(3):636-649.

219. Powers SK, Lawler J, Criswell D, et al. Regional metabolic differences in the rat diaphragm. J Appl Physiol 1990;69(2):648-650.

220. Sieck GC, Sacks RD, Blanco CE. Absence of regional differences in the size and oxidative capacity of diaphragm muscle fibers. J Appl Physiol 1987;63(3):1076-1082.

221. Sexton WL, Poole DC. Costal diaphragm blood flow heterogeneity at rest and during exercise. Respir Physiol 1995;101(2):171-182.

222. Gayan-Ramirez G, Rollier H, Vanderhoydonc F, et al. Nandrolone decanoate does not enhance training effects but increases IGF-I mRNA in rat diaphragm. J Appl Physiol 2000;88(1):26-34.

223. Sugiura T, Matoba H, Murakami N. Myosin light chain patterns in histochemically typed single fibers of the rat skeletal muscle. Comp Biochem Physiol B 1992;102(3):617-620.

224. Macgowan NA, Evans KG, Road JD, et al. Diaphragm injury in individuals with airflow obstruction. Am J Respir Crit Care Med 2001;163(7):1654-1659.

225. Kariks J. Diaphragmatic muscle fibre necrosis in SIDS. Forensic Sci Int 1989;43(3):281-291.

226. Matecki S, Guibinga GH, Petrof BJ. Regenerative capacity of the dystrophic (mdx) diaphragm after induced injury. Am J Physiol Regul Integr Comp Physiol 2004;287(4):R961-968.

227. Grefte S, Kuijpers-Jagtman AM, Torensma R, et al. Skeletal muscle development and regeneration. Stem Cells Dev 2007;16(5):857-868.

228. Esposito A, Germinario E, Zanin M, et al. Isoform switching in myofibrillar and excitation-contraction coupling proteins contributes to diminished contractile function in regenerating rat soleus muscle. J Appl Physiol 2007;102(4):1640-1648.

229. Kadi F, Thornell LE. Training affects myosin heavy chain phenotype in the trapezius muscle of women. Histochem Cell Biol 1999;112(1):73-78.

230. Cho M, Hughes SM, Karsch-Mizrachi I, et al. Fast myosin heavy chains expressed in secondary mammalian muscle fibers at the time of their inception. J Cell Sci 1994;107 (Pt 9):2361-2371.

231. Allen DL, Leinwand LA. Postnatal myosin heavy chain isoform expression in normal mice and mice null for IIb or IId myosin heavy chains. Dev Biol 2001;229(2):383-395.

232. McKoy G, Leger ME, Bacou F, et al. Differential expression of myosin heavy chain mRNA and protein isoforms in four functionally diverse rabbit skeletal muscles during pre- and postnatal development. Dev Dyn 1998;211(3):193-203.

233. Karsch-Mizrachi I, Travis M, Blau H, et al. Expression and DNA sequence analysis of a human embryonic skeletal muscle myosin heavy chain gene. Nucleic Acids Res 1989;17(15):6167-6179.

234. Beylkin DH, Allen DL, Leinwand LA. MyoD, Myf5, and the calcineurin pathway activate the developmental myosin heavy chain genes. Dev Biol 2006;294(2):541-553.

235. Liu M, Stevens-Lapsley JE, Jayaraman A, et al. Impact of treadmill locomotor training on skeletal muscle IGF1 and myogenic regulatory factors in spinal cord injured rats. Eur J Appl Physiol.

236. Bernhardt V, Denaslow N, Pate K, et al. Tracheal Occlusion Modulation of Gene Expression in the Medial Thalamus. American Journal of Respiratory and Critical Care Medicine 2008;17:A745.

237. Hotchkiss M, Bernhardt V, Pate K, et al. Respiratory related anxiety induced by tracheal obstruction in conscious rats. American Journal of Respiratory and Critical Care Medicine 2008;177:A745.

238. Pacak K. Stressor-specific activation of the hypothalamic-pituitary-adrenocortical axis. Physiol Res 2000;49 Suppl 1:S11-17.

239. Lightman SL. The neuroendocrinology of stress: a never ending story. J Neuroendocrinol 2008;20(6):880-884.

240. Engelbrecht AM, Smith C, Neethling I, et al. Daily brief restraint stress alters signaling pathways and induces atrophy and apoptosis in rat skeletal muscle. Stress;13(2):132-141.

241. Gilson H, Schakman O, Combaret L, et al. Myostatin gene deletion prevents glucocorticoid-induced muscle atrophy. Endocrinology 2007;148(1):452-460.

242. Amthor H, Otto A, Vulin A, et al. Muscle hypertrophy driven by myostatin blockade does not require stem/precursor-cell activity. Proc Natl Acad Sci U S A 2009;106(18):7479-7484.

243. Singleton JR, Baker BL, Thorburn A. Dexamethasone inhibits insulin-like growth factor signaling and potentiates myoblast apoptosis. Endocrinology 2000;141(8):2945-2950.

244. Boriek AM, Miller CC, 3rd, Rodarte JR. Muscle fiber architecture of the dog diaphragm. J Appl Physiol 1998;84(1):318-326.

245. Orozco-Levi M, Lloreta J, Minguella J, et al. Injury of the human diaphragm associated with exertion and chronic obstructive pulmonary disease. Am J Respir Crit Care Med 2001;164(9):1734-1739.

246. Smith BK, Bleiweis MS, Zauhar J, et al. Inspiratory muscle training in a child with nemaline myopathy and organ transplantation. Pediatr Crit Care Med.

247. Deerojanawong J, Chang AB, Eng PA, et al. Pulmonary diseases in children with severe combined immune deficiency and DiGeorge syndrome. Pediatr Pulmonol 1997;24(5):324-330.

248. Carotti A, Digilio MC, Piacentini G, et al. Cardiac defects and results of cardiac surgery in 22q11.2 deletion syndrome. Dev Disabil Res Rev 2008;14(1):35-42.

249. Matsuoka R, Kimura M, Scambler PJ, et al. Molecular and clinical study of 183 patients with conotruncal anomaly face syndrome. Hum Genet 1998;103(1):70-80.

250. Schreiber C, Eicken A, Balling G, et al. Single centre experience on primary correction of common arterial trunk: overall survival and freedom from reoperation after more than 15 years. Eur J Cardiothorac Surg 2000;18(1):68-73.

251. ATS/ERS. ATS/ERS Statement on respiratory muscle testing. Am J Respir Crit Care Med 2002;166(4):518-624.

252. Numa AH, Newth CJ. Anatomic dead space in infants and children. J Appl Physiol 1996;80(5):1485-1489.

253. Aagaard P, Simonsen EB, Andersen JL, et al. Increased rate of force development and neural drive of human skeletal muscle following resistance training. J Appl Physiol 2002;93(4):1318-1326.

254. Andersen LL, Aagaard P. Influence of maximal muscle strength and intrinsic muscle contractile properties on contractile rate of force development. Eur J Appl Physiol 2006;96(1):46-52.

255. Del Balso C, Cafarelli E. Adaptations in the activation of human skeletal muscle induced by short-term isometric resistance training. J Appl Physiol 2007;103(1):402-411.

256. Newth CJ, Venkataraman S, Willson DF, et al. Weaning and extubation readiness in pediatric patients. Pediatr Crit Care Med 2009;10(1):1-11.

257. Vidal Melo MF. Clinical respiratory physiology of the neonate and infant with congenital heart disease. Int Anesthesiol Clin 2004;42(4):29-43.

258. DiCarlo JV, Raphaely RC, Steven JM, et al. Pulmonary mechanics in infants after cardiac surgery. Crit Care Med 1992;20(1):22-27.

259. Shi S, Zhao Z, Liu X, et al. Perioperative risk factors for prolonged mechanical ventilation following cardiac surgery in neonates and young infants. Chest 2008;134(4):768-774.

260. Guyton AC, Lindsey AW, Abernathy B, et al. Venous return at various right atrial pressures and the normal venous return curve. Am J Physiol 1957;189(3):609-615.

261. Simpson JA, Brunt KR, Iscoe S. Repeated inspiratory occlusions acutely impair myocardial function in rats. J Physiol 2008;586(9):2345-2355.

262. Pinsky MR. Cardiovascular issues in respiratory care. Chest 2005;128(5 Suppl 2):592S-597S.

263. Thorsteinsson A, Jonmarker C, Larsson A, et al. Functional residual capacity in anesthetized children: normal values and values in children with cardiac anomalies. Anesthesiology 1990;73(5):876-881.

264. Thorsteinsson A, Werner O, Jonmarker C, et al. Airway closure in anesthetized infants and children: influence of inspiratory pressures and volumes. Acta Anaesthesiol Scand 2002;46(5):529-536.

265. Kosch PC, Hutchinson AA, Wozniak JA, et al. Posterior cricoarytenoid and diaphragm activities during tidal breathing in neonates. J Appl Physiol 1988;64(5):1968-1978.

266. Rehan VK, McCool FD. Diaphragm dimensions of the healthy term infant. Acta Paediatr 2003;92(9):1062-1067.

267. Vazquez RL, Daood M, Watchko JF. Regional distribution of myosin heavy chain isoforms in rib cage muscles as a function of postnatal development. Pediatr Pulmonol 1993;16(5):289-296.

268. Watchko JF, Daood MJ, Sieck GC. Myosin heavy chain transitions during development. Functional implications for the respiratory musculature. Comp Biochem Physiol B Biochem Mol Biol 1998;119(3):459-470.

269. Watchko JF, Sieck GC. Respiratory muscle fatigue resistance relates to myosin phenotype and SDH activity during development. J Appl Physiol 1993;75(3):1341-1347.

270. Grivas TB, Burwell RG, Purdue M, et al. A segmental analysis of thoracic shape in chest radiographs of children. Changes related to spinal level, age, sex, side and significance for lung growth and scoliosis. J Anat 1991;178:21-38.

271. Shardonofsky FR, Perez-Chada D, Carmuega E, et al. Airway pressures during crying in healthy infants. Pediatr Pulmonol 1989;6(1):14-18.

272. Cross KW, Klaus M, Tooley WH, et al. The response of the new-born baby to inflation of the lungs. J Physiol 1960;151:551-565.

273. Al-Hathlol K, Idiong N, Hussain A, et al. A study of breathing pattern and ventilation in newborn infants and adult subjects. Acta Paediatr 2000;89(12):1420-1425.

274. Beck J, Tucci M, Emeriaud G, et al. Prolonged neural expiratory time induced by mechanical ventilation in infants. Pediatr Res 2004;55(5):747-754.

275. Laing IA, Teele RL, Stark AR. Diaphragmatic movement in newborn infants. J Pediatr 1988;112(4):638-643.

276. Tan S, Duara S, Silva Neto G, et al. The effects of respiratory training with inspiratory flow resistive loads in premature infants. Pediatr Res 1992;31(6):613-618.

277. Harkel AD, van der Vorst MM, Hazekamp MG, et al. High mortality rate after extubation failure after pediatric cardiac surgery. Pediatr Cardiol 2005;26(6):756-761.

278. Vida VL, Leon-Wyss J, Rojas M, et al. Pulmonary artery hypertension: is it really a contraindicating factor for early extubation in children after cardiac surgery? Ann Thorac Surg 2006;81(4):1460-1465.

279. Maharasingam M, Ostman-Smith I, Pike MG. A cohort study of neurodevelopmental outcome in children with DiGeorge syndrome following cardiac surgery. Arch Dis Child 2003;88(1):61-64.

BIOGRAPHICAL SKETCH

Barbara Kellerman Smith received a Bachelor of Science Degree in molecular biology from Grove City College, and a Master of Physical Therapy degree from University of Pittsburgh. She has practiced continuously as a physical therapist since 1994, almost exclusively in intensive care and acute cardiopulmonary practice. She studied respiratory sensation and exercise at University of Florida and received a post-entry-level Master of Health Science degree in physical therapy in 1998. In 2007, she returned to the Doctor of Philosophy in rehabilitation science program at University of Florida, studying muscle strength and functional adaptations to inspiratory muscle strength training.